Università degli Studi di Urbino Carlo Bo

Department of Pure and Applied Sciences

Ph.D. Program in: Basic Science and Application

Curriculum: Earth Sciences

XXXIV CYCLE

CHEMICAL NEUTRALIZATION OF INDUSTRIAL BY-PRODUCTS FROM THE SECONDARY ALUMINUM INDUSTRY: RE-USE AS FOAMING AGENTS FOR THE SYNTHESIS OF GEOPOLYMERS AND MONITORING OF THE HYDROGEN-RICH GAS PRODUCTION

The Regione Marche Financially Supported the Entire Research:
"POR Marche FSE 2014/2020 – Progetto Dottorato Innovativo a Caratterizzazione Industriale"

ACADEMIC DISCIPLINE: GEO/09 – MINING RESOURCES, MINERALOGIC AND PETROGRAPHIC APPLICATIONS FOR THE ENVIRONMENT AND CULTURAL HERITAGE

Coordinator: Prof. Alessandro Bogliolo

Supervisor: Prof. Alberto Renzulli

Co-Supervisor: Prof. Eleonora Paris

Ph.D. Student: Roberto Ercoli

ACADEMIC YEAR 2020/21

Acknowledgments

Firstly, I would like to express sincere gratitude to the advisor Prof. Alberto Renzulli for the continuous support of the research for his motivation and knowledge about the argument. His guidance helped me succeed and write articles on scientific journals and the present thesis. I could not have imagined having a better advisor and mentor.

Besides, I would like to thank the rest of the thesis committee, Prof. Eleonora Paris, for their insightful comments and encouragement and the tricky question that incented to widen the research from various perspectives.

A sincere thanks also go to Prof. Ing. Petr Louda and Ing. Katarzyna Ewa Buczkowska. They provided an opportunity to join their research team abroad and allowed me to access the laboratory and research facilities at the Department of Material Science, Technical University of Liberec, Czech Republic. I thank my fellow laboratory mates for the stimulating discussions, for the days we were working together before deadlines, and for all the fun we have had in the last years. In particular, I am grateful to Ing. Le Van Su, Van Vu Nguyen, Dorota Laskowska, and Piotr Łoś for establishing a great collaboration during the study-abroad period.
Without their precious support and experience, completing research would not be possible.

Many thanks to the University of Florence and the National Research Council (Institute of Geosciences and Georesources, Florence) composed by Dr. Andrea Orlando, Dr. Daniele Borrini, Prof. Franco Tassi, and Dr. Gabriele Bicocchi. But also to Karol Pralat and Justyna Ciemnicka, of the Faculty of Civil Engineering, Mechanics and Petrochemistry, Warsaw University of Technology.

Last but not least, I would like to thank my family, girlfriend, and friends for supporting me spiritually throughout completing this research and my life goals in general.

Roberto Ercoli
Urbino, 2022

Abstract

The project, financially supported by the Regione Marche (POR Marche FSE 2014/2020), was assigned to the Ph.D. student Roberto Ercoli (UNIURB) with the supervision of Prof. Alberto Renzulli (UNIURB) and Prof. Eleonora Paris (UNICAM). Several universities and research groups such as the University of Urbino, University of Camerino, Institute of Geosciences and Georesources (IGG-CNR, Florence), University of Florence, Technical University of Liberec, and Warsaw University of Technology collaborated to create a European network working in this innovative and brand-new field. Moreover, the primary aspect of this network is the collaboration between the scientific parts, the regional system, and the industrial system. The involvement of the National Technological Clusters is a proposal of the MIUR in 2012 (Decree No. 257 "Notice for the development and reinforcement of national technological clusters"), as well as national research agencies, such as CNR, INFN, IIT, ENEA, to develop highly qualified scientific research and to support the national development. Considering the policies for the economic development identified by the resolutions of the regional council of the Regione Marche (DGR n.1511/2016, and n. 1035 of 30/7/2018), the present research promotes a more sustainable manufacturing sector. The research focuses on the recovery, re-use, and valorization of industrial by-products from the secondary aluminum industry through their chemical neutralization and synthesis of geopolymer foams.

Valorization of the so-called "industrial by-product" is an actual and discussed theme. The industry stakeholders support the achievement of the environmental targets about resource management efficiency, reducing waste output and gas emissions, and constant industrial processes optimization. The development and activation of demanufacturing logistics are essential for improving relative residual values by specific operations and treatments of raw material derived from end-life products and industrial waste. The chemical neutralization of highly reactive materials that come from the treatment processes of scraps (beverage cans and domestic appliances) was investigated through experiments in aqueous alkaline solutions. These metallic aluminum-rich by-products were classified, according to EU law, as dangerous waste, as they can potentially develop flammable gases capable of forming explosive mixtures with air. In this way, they cannot be disposed of in landfills for non-hazardous wastes if chemical neutralization is not planned and performed beforehand. The first experiments were mainly aimed at unraveling the oxidation rate and quantifying the production of hydrogen-rich gases from the reactions of the metallic aluminum-rich by-products in a water-rich alkaline (liquid or vapor) environment. Reactions were carried out in a stainless-steel batch mini-reactor with metering and sampling valves, with the resulting gases analyzed by gas-chromatography (GC). The experimental runs performed in the mini-reactor proved to be effective for eliminating the reactive metallic aluminum, reaching a maximum hydrogen production of 96% of the total gases. All the obtained results can be transferred and applied to (i) the possible industrialization of the method for the chemical neutralization of these dangerous by-products, increasing sustainability and workplace safety, (ii) the use of the resulting hydrogen as a source of energy for the furnaces of the secondary aluminum industry itself, and (iii) new technological materials, e.g., "geopolymer foams (GFs)," by using hydrogen coupled with aluminosilicate materials as a foaming agent. The special hazardous wastes derived from the entire recycling process in the secondary aluminum industry were trapped into these geopolymers. The experimental study affects a vast reality concerning waste management through the recovery, chemical neutralization, and incorporation of these hazardous substances into the GFs. A geopolymeric matrix composed of metakaolin (MK), silica sand (100 wt.% of MK), and chopped carbon fibers (1% wt.% of MK) was doped, adding the industrial by-products from the screening, pyrolysis, de-dusting, and fusion processes with specific contents (1; 2; 3; 4; 5 wt.% of MK). Several experimental tests were carried out to characterize the GFs by the mechanical (flexural, compressive, and Charpy impact strengths) and thermal properties (thermal conductivity, diffusivity, and specific heat).

Keywords: secondary aluminum industry, industrial by-products, chemical neutralization, hydrogen, geopolymer foams, physical properties, mechanical strengths, thermal conductivity, specific heat, thermal diffusivity

TABLE OF CONTENTS

LIST OF FIGURES

LIST OF TABLES

LIST OF ABBREVIATIONS

Binder Materials Abbreviations

C-A-S-H – Calcium Aluminum Silicate Hydrate
N-A-S-H – Sodium Aluminum Silicate Hydrate
C-S-H – Calcium Silicate Hydrate
GPs – Geopolymers
GFs – Geopolymer Foams
AAMs – Alkali Activated Materials
CSCs – Calcium Sulfoaluminate Cements
OPCs – Ordinary Portland Cements
CEM I – Pure Portland Clinker
CEM II – Cement with the addition of blast furnace slags
CEM III – BFS-OPC Cement
CEM IV – Pozzolanic Cement
CEM V – Composite Cement

Raw Materials Abbreviations

MK – Metakaolin
A – Alkaline Activator
SA – Silica Sand
CFs – Carbon Fibers
UBC – Used Beverage Cans
FG – Scrapes from Coarse-grained Appliances
V – By-product of the Screening Process
D – By-product of the Pyrolysis Process (Bag Filters)
C – By-product of the Abatement Systems (Cyclones)
FF – By-product of the Fusion Process
BFS – Blast Furnace Slags
EOLs – End-of-life Products

Abbreviations of the Experimental Methods

XRD – X-ray diffraction
TG – Thermogravimetric
DTA – Differential Thermal Analysis
DTG – Differential Thermogravimetry
ICP-MS – Inductively Coupled Plasma Mass Spectrometry
ICP-OES – Inductively Coupled Plasma Optical Emission Spectrometry
GC – Gas Chromatography
IR – Infrared Radiation
LOI – Loss of Ignition
VOC – Volatile Organic Compound
DL – Detection Limit

Equation, and Expression Abbreviation

V_g – Gas Volume
n_g – Gas Moles
m_g – Gas Mass
P_i – Partial Pressure
σ_f – Flexural Strength
σ_c – Compressive Strength
σ_i – Impact Strenght
Fmax – Maximum applied load
L – Span length
b – Width of the Sample
h – Depth of the Sample
A_c - Cross-sectional Area of the Sample
E – Absorbed Energy
λ – Thermal Conductivity
C_p – Specific Heat
α – Thermal Diffusivity
V – Sample volume
Q – Amount of Heat Transferred
d – Distance between two Isotherms
A – Surface
ΔT – Temperature Gradient

Other Abbreviations

EWC – European Waste Code
HP – Limits and Hazard Characteristics
LCA – Life Cycle Assessment

CHAPTER 1
INTRODUCTION

1.1 Aims of the Research

The innovative doctoral research is aimed at the chemical neutralization, disposal, and re-use of industrial waste materials (by-products) of the secondary aluminum industry, Profilglass SpA (Bellocchi, Fano, Italy). The industry produces aluminum profiles primarily from the recycling processes of two different plants from the aluminum domestic appliances (FG) and beverage cans collection (UBC).

Solid wastes are generated annually from the secondary aluminum industry in significant amounts. Globally, such waste is recycled and utilized in building materials, essential for sustainable development. No scientific method is followed at the disposal sites, where the industrial by-products from the secondary aluminum industrial processes are disposed of without any processing before being treated.

The present research recover, re-use, and trap secondary aluminum waste through a scientific understanding of the chemical neutralization and geopolymerization processes. The goal is to develop a helpful process to develop new lightweight building materials using the industrial by-products as foaming agents during the geopolymer formation.

Based on waste re-use, this new idea endeavors to change waste as a resource inverting the reliance on limited natural resources. This research is going to provide the (i) re-use of waste materials that would otherwise be landfilled, (ii) decrease in environmental impact, and (iii) significantly reduction of CO_2 emissions by providing alternatives to traditional cement materials.

In the last decades, geopolymers emerged as an alternative and environmentally friend materials compared to the traditional construction materials, such as ordinary Portland cement (OPC). Several advantages are highlighted by using these materials in different fields of application since the environment plays a central role in the worldwide economy. Minimizing the environmental impacts of the treatment and disposal of these materials concern is a crucial key for improving the efficiency of the industries and safeguarding natural resources such as aluminum. The direct effect of re-using industrial waste materials on the industries is to reduce the high costs of their disposal in special landfills. At the same time, the production of binders and old types of cement highly impacts CO_2 production, increasing its concentration in the atmosphere, and the geopolymers can reduce greenhouse emissions by about 95% [1-8].

1.2 Outline of the Thesis

The development of new materials in the area of interest of the circular economy lay the foundations for creating new production and consumption channels through the re-use of industrial waste products and relating to some of the problems of the secondary aluminum industries. Therefore, there is a gradual approach toward the principles of optimization of industrial processes that outline new methods for exploiting secondary raw materials. The experimental work is perfectly interfaced with the current climate, economic, and geopolitical changes. Accordingly, the studies converge on the (i) recovery and process of the material residues and sludges of the secondary aluminum

industry; (ii) development of innovative materials by the synthesis of geopolymer foams (GFs) trapping the hazardous substances; (iii) smartly manage the issues of special dangerous waste disposal (iv) enhance the industrial processes of the secondary aluminum industry, taking into account environmental sustainability.

In the first part of the research, the industrial processes were studied to define suitable materials to re-use. After, the industrial by-products have been chemically and physically classified under the current regulations for waste disposal: (i) CE Reg. 1272/2008 "Classification of hazardous substances" and (ii) CE Reg. 1357/2014 "Limits and hazard characteristics (HP)" as special hazardous wastes. The metallic species found inside the by-products were recognized as highly reactive in water, releasing significant amounts of H_2, which can be inflammable and create explosive mixtures with air. Therefore, the by-products were chemically neutralized, monitoring the laboratory reaction processes by a mini-reactor to quantify the gas production. To make the industrial by-product suitable for the synthesis of new materials, experiments were planned to achieve a complete inertization of the waste. In fact, in the presence of water, metals produce a significative high concentration of hydrogen entailing a non-negligible environmental risk. These by-products were analyzed by ICP-MS through specific digestion techniques (UNI EN 13657:2004 and UNI EN ISO 11885:2009) [9-10] to obtain a quantitative analysis of metals within the sample. XRD and thermogravimetric analysis were also carried out to determine crystal structures and mass loss based on different temperatures.

The second part of the study concerns the re-uses of the aluminum by-products to synthesize geopolymer foams (GFs). These new brand materials are mechanical and atmospheric degradation resistant, and this physical characteristic allows them to trap pollutants and toxic substances inside their hard structure. The synthesis of GFs is made by a chemical process through which alkaline precursors rich in silica and alumina strongly interact with an aqueous alkaline solution. The research defines the mechanical properties of the geopolymers (compressive, flexural, and Charpy impact strengths) and the thermal characteristics related to the microporosity to find new environmental-friendly applications. Geopolymers may have structural and thermomechanical applications such as thermal insulation with resistance to fire and refractory foams in industries as support for structured catalysts or as ceramic filters for high temperatures.

CHAPTER 2
STATE OF THE ART

2.1 The Aluminum Production

The recycling and re-use of industrial by-products from the secondary aluminum industry and using geopolymer materials in the construction industry show several advantages and environmental-economic benefits. Therefore, as previously discussed, the study aims to neutralize the waste materials throughout their incorporation into geopolymer foams (GFs). The main objectives of this research are (i) to study the chemical neutralization processes of the by-products and the behavior that drives the materials to produce gaseous mixtures rich in hydrogen; (ii) to define the chemical composition needed to synthesize geopolymer foams and optimize mechanical and thermal properties.

A real circular economy and sustainable development principle focuses on using industrial by-products and end-of-life (EOL) products to their valorization/transformation for novel/technological applications (materials or renewables) to minimize waste production. The re-use of industrial by-products, which can be addressed for the synthesis of new materials or exploited as an energetic secondary raw material, represents a fundamental answer to the need to develop sustainable economic growth, based on the decrease of the exploitation of natural resources (raw materials) and the minimization of waste output. This approach converts many industrial waste materials into energetic and non-energetic resources (i.e., secondary raw material). In this way, the valorization of the so-called "industrial by-products" is of paramount importance for (i) the sustainability of raw material exploitation and management, (ii) limiting the greenhouse gas emissions, and (iii) reducing the amount of waste to landfills disposal.

This work is focused on the re-use of by-products coming from the industries of secondary aluminum (i.e., using scrap and aluminum-rich EOL products), producing aluminum profiles, pipes, and laminates for different sectors such as construction, automotive, electronics, and mechanics. Secondary aluminum production is sustainable, but some by-products from that process may not be. In particular, being classified as special dangerous waste, some metallic aluminum by-products (European Waste Code 100323*, "Solid wastes from the treatment of fumes containing dangerous substances" and from pre-treatment processes of the scrap and EOL products before their disposal to the melting furnace) need to be appropriately treated (made inert, or inertized) before its utilization for new materials (or landfill disposal). This work will deal with experimental tests to investigate and optimize the neutralization of these highly reactive and dangerous by-products, which are still rich in metallic Al but not enough to be processed in the melting furnace. As they are not suitable for landfill disposal, the neutralization process should be desirable.

A brief description of the different industrial methods of aluminum production is given in the following paragraphs, mainly (i) primary aluminum from bauxite ore mining and alumina extraction and (ii) secondary aluminum from scrap and EOL products.

2.1.1 Primary Aluminum: from Bauxite Ores

Aluminum is the most consumed metal globally and is the third most abundant element on Earth. The aluminum consumption is 65 Mt/y, and 75% of this volume is aluminum exploited and processed from ores [11-12]. Aluminum compounds represent around 8% of the Earth's crust, and mining of the raw material, the bauxite ores, their chemical treatments, and refining allows primary aluminum production. The composition of a bauxite ore ranges from 40 - 60% Al_2O_3, 0.8-17% SiO_2, up to ca. 22% Fe_2O_3, and minor amounts of TiO_2, MnO, Cr_2O_3, V_2O, P_2O_5. Moisture may range between 5 and 30%. The most representative minerals of a bauxite deposit are (i) gibbsite - α-Al_2O_3 $3H_2O$; (ii) boehmite - α-Al_2O_3 H_2O, (iii) diaspore - β-Al_2O_3 H_2O; (iv) hematite - α-Fe_2O_3; (v) goethite - α-FeOOH; (vi) magnetite - Fe_2O_4; (vii) siderite - $FeCO_3$; (viii) ilmenite -$FeTiO_3$; (ix) rutile or anatase - TiO_2; (x) brookite - Al_2O_3 $2SiO_2$ $3H_2O$, (xi) kaolinite - Al_2O_3 $2SiO_2$ $2H_2O$; (xii) quartz - SiO_2 [13]. More than 70% of the world's bauxite ores are exploited in Australia, Guinea, Jamaica, Brazil, and Russia. During the last decades, aluminum production increased at a rate of up to 3% a year, and the increase in energy costs led to the displacements of the primary aluminum industries from the USA, EU, and Japan towards cheaper energy-cost countries such as China, the Middle East, South East Asia, and India. The demand for aluminum significantly spread across the newly industrializing countries, and therefore the aluminum market volatility can quickly grow because of financial dynamics accounting for Al production's sustainability [14].

The primary aluminum production follows the Bayer process (ideated by Karl Bayer in 1888) [15]. It involves digestion of the bauxite at high temperatures (from 140 to 323°C) and pressures (60 to 1000 psi), using NaOH solution, and adding silica to increase the solubility. Setting T-P and NaOH concentration depends on the mineralogical structures of the aluminum oxide. The process generates a sodium aluminate supersaturated solution by removing red muds (silicate and iron oxides impurities). After that, the sodium aluminate is cooled, seeded with alumina trihydrate crystals, washed, and then calcined in a rotary furnace at 1200-1250°C to eliminate the structural water deriving alumina [16]. The calcined alumina generally shows low content of impurities (0.03 wt. wt.% SiO_2; 0.02 wt.% Fe_2O_3; 0.5 wt.%Na_2O; 0.05 wt.% CaO).

Also, nepheline-bearing rocks are valuable raw material sources to extract alumina by mixing nepheline with limestone in rotating furnaces at 1280-1310°C [17]. This process yields dicalcium silicate and sodium aluminate, from which sodium aluminate is converted into sodium carbonate and aluminum hydroxide. Aluminum hydroxide is then calcined to produce the alumina. The electrolysis reduction of alumina (using cryolite - Na_3AlF_6 - as electrolyte) produces primary aluminum. This is a very high energy consumption process (9.30 kWh/kg, varying on the cell voltage and amperage), where the total energy is the sum needed for the cell reaction, electrodes, and connectors. The worldwide process to make Al from alumina was patented by Charles Martin Hall and Paul Lewis Toussaint Héroult, called the "Hall-Hèroult process" [18].

An alternative method to produce primary aluminum is the carbothermic reduction through zone melting furnace processes at high temperatures. The alumina-carbon melt forms an aluminum carbide that reacts to produce Al [19].

2.1.2 Secondary Aluminum: from Scraps and End-of-life Products (EOLs)

The aluminum-rich scraps available worldwide can be approximately predicted, depending on the Life Cycle Assessment (LCA) of products containing aluminum. The classification of aluminum scraps is dictated by the

standards EN 12258-1:2012 and EN 13980:2004 [20-21]: old scraps are primarily derived from used beverage cans (UBCs; containing about 94 wt.% Al, 0.8 wt.% oxides, and 5.2 wt.% other inclusions) [22-23], representing one of the most important sources of secondary aluminum and the most economically recycled material (770-820 €/t) [24]. Currently, recycled aluminum amounts to about 35% of primary aluminum production and requires 10 to 15 times less energy [25]. The total energy saved for each ton of recycled aluminum is estimated to be around 14,000 kWh, and the avoided greenhouse gas emission of CO_2 is ca. 350 kg [26].

Although aluminum is one of the most common elements on Earth, it is too reactive with other elements to occur naturally. Therefore, the natural raw material for primary aluminum production is the bauxite ores, with an average composition of ca. 40–60 wt.% Al_2O_3, 0.8–17 wt.% SiO_2, up to ca. 22 wt.% Fe_2O_3, and minor amounts of TiO_2, MnO, Cr_2O_3, V_2O_5, P_2O_5, and moisture ranges between 5 and 30 wt.%. The most representative minerals of a bauxite deposit are gibbsite—$Al(OH)_3$, boehmite or diaspore—AlO(OH), hematite—Fe_2O_3, goethite—α-FeO(OH), magnetite—$Fe^{2+}Fe^{3+}{}_2O_4$, siderite—$FeCO_3$, ilmenite—$FeTiO_3$, rutile, anatase or brookite—TiO_2, kaolinite—$Al_2Si_2O_5(OH)_4$, and quartz—SiO_2 [27]. The Bayer process, invented and patented in 1887, is the primary process by which alumina is extracted from bauxite ore and separated from red mud [28-29]. The Hall–Héroult process (simultaneously discovered in 1886 by Charles Martin Hall and Paul Héroult) allows aluminum to be refined from alumina through electrolysis. The efforts in recovering (and minimizing) wastes from mining exploitation of bauxite ores to the end of the Bayer process are growing to assure that secondary Al raw materials and by-products would meet all the stakeholder requirements [30]. Nevertheless, the primary aluminum industry is less sustainable than secondary aluminum production, which uses recycled scraps (e.g., beverage cans and domestic appliances) instead of natural raw geomaterial (i.e., the bauxite ores for the primary aluminum industry). The process of secondary aluminum production involves scrap gathering, mixing, comminution, screening, and pyrolysis treatments to produce high-quality Al-rich material that can be subsequently melted, refined, and cast. In this way, secondary aluminum production has increased exponentially in the last few decades to ensure sustainability is applied to optimize reserves, decrease energy consumption, and narrow the gap between supply and demand [31]. Efficient plants have been developed over time, and the processes are constantly improved (Figure 1).

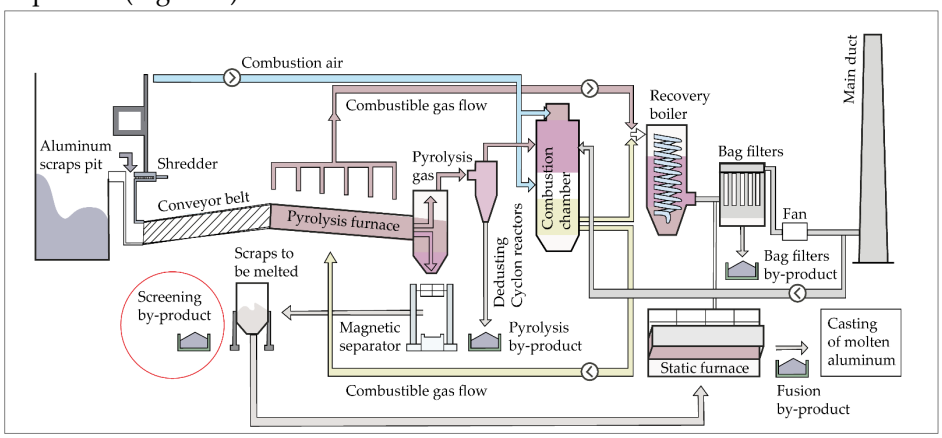

Figure 1. Sketch of a plant for secondary aluminum production. The aluminum scraps pit (on the left) feeds the plant. The by-products investigated in the present work are illustrated (the screening by-product marked by a red circle has been used for the experimental runs of the chemical neutralization – see the text for explanation).

The first step in aluminum recycling concerns the storage, shredding, and handling of the material through the separation of the non-metallic components from the metallic ones [32–34] by applying a combination of various screening techniques, namely: (i) magnetic separation, (ii) Eddy current separation, and (iii) density separation [35–39]. Aluminum scraps are loaded into hoppers by conveyor belt and processed by a pyrolysis combustor at a temperature between 500°C and 580°C. The pyrolysis process provides a significant (95%) reduction of water, oils, paints, and other organic substance contents from the material surface, avoiding possible explosions and oxidation during the subsequent melting [40]. The powders and gases produced are exhausted by two parallel lines of treatment. Gas neutralization occurs at a temperature of 850°C by employing a refractory afterburner (combustion chamber), and exhaust gas is conditioned at 580 °C through a heat exchanger. Gases are then conveyed to (i) the quencher, where the temperature is rapidly brought down (to 220°C) by nebulized water, (ii) the fume purification system, for the abatement of residual dust through bag filters and of SO_x, HCl, and HF gases by lime, and finally, (iii) the post-burner, to remove CO and Total Organic Carbon (TOC). The selected material is subsequently sent to the static melting furnace, employing the minimum possible energy use and, therefore, the minimum oxidation. The melting process occurs using O_2 and low NO_x emission burners, through refining and degassing systems and agitators with inert gases, with Ar/Cl_2 or N_2/Cl_2 mixtures [41] to minimize the energy consumption required to reach the aluminum melting temperature (Tm = 660.3°C). Waste elements, specifically alkali metal impurities, hydrogen, non-metallic inclusions, and alloy elements (Mg), are reduced during the melting stage by refining processes [42]. The compounds derived from the fusion process, such as HCl, Cl_2, and HF, are chemically neutralized, removed through a dedicated plant, and then conveyed to the bag filters for being treated in the cyclone reactor with lime. The lamination and solidification processes are improved to avoid volatile organic compound (VOC) emissions through cyclone fans with a wet scrubber for powders and biofilters. Around 70% of recycled aluminum is transformed into aluminum-silicon alloy castings used for the automotive industry. Aluminum alloys are materials where different elements (up to 15% of the total weight) are added to the pure molten aluminum, increasing properties and efficiency [43].

2.2 Economic Relevance of the Study for the European Industries

In the framework of secondary aluminum production, the present study is of paramount importance because it addresses the problem of the management of by-products from the screening processes of scraps. In fact, due to their physical-chemical features, these by-products cannot be disposed of in landfills for non-hazardous waste if treatments to eliminate environmental impacts are not planned and carried out in advance. Experiments of chemical neutralization of these highly reactive by-products are the main focus of the present paper.

According to European Aluminum data [44-46], there are 220 secondary aluminum recycling plants in Europe, and more than 34 billion aluminum cans were recycled in 2018, representing a total of approximately 0.46 Mt. Post-consumer aluminum available for recycling will be more than double by 2050. However, aluminum recycling treatments generate a large waste amount, such as scraps not suitable to be recycled (separation by the screening process), the fumes abatement collected by the decorator, centrifugal collector dust, and fumes of the melting furnace. The total loss of mass is consequently a substantial part of the entire material recycled.

Nowadays, the three digestion solutions of the not-reusable materials such as the screening scrap, or rather the fraction in small indistinguishable and therefore non-recyclable pieces of waste, are through (i) aerobic/anaerobic bio-oxidation cold systems, (ii) gasification, pyrolysis, or incineration hot systems and (iii) the disposal of in landfills, that designates the main resolution.

Consequently, sustainable recovery and re-use of hazardous industrial waste are achievable only through in-depth knowledge about chemical neutralization processes that drive the metallic parts to produce a gaseous mixture through a multiparametric controlled oxidation process. Therefore, the experimental study affects a vast reality concerning the secondary aluminum industrial waste management through the recovery, inertization, and hazardous substances incorporated into the geopolymer.

Furthermore, the need to re-use industrial waste to be disposed of from other production chains, particularly glass processing residues and fireclays as precursors, dust collected from incinerators as filler, and carbon nanofibers as mechanical reinforcing agents, gives a central role to the geopolymerization process.

In-depth market analysis will evaluate the geopolymer commercialization by creating one or more patents, functionally on the material physicochemical properties: plausible applications are thermally insulated panels, structured catalysts, ceramic industrial filters even at high temperature, and fire resistance capabilities materials of the transport and construction sector. Moreover, the project envisages evaluating the use of hydrogen as a secondary energy source required to produce these foamed materials, consequently supplying a more considerable virtuosity to the entire process.

2.3 Strategic Plan of the European Innovation Partnership on Raw Materials

The European strategy on waste management efficiency, safeguarding resources, and reducing pollutant emissions also impacting human health are relevant topics discussed by all the industrial stakeholders. The E.U. directive on environmental safety and pollution control includes the decree of environmental assessments and authorizations for the industries dealing with hazardous and toxic substances. The goal is to improve environmental and industrial performance, adopting corrective actions continuously. The experimental research outlines the recovery processes through which secondary aluminum waste and end-of-life materials commence a noble re-use path in the circular economy. Further, the aims are to ensure a substantial contribution to several European manufacturing sectors, providing new methodologies of re-using industrial waste materials. Finally, a more efficient waste management achievement combines technological innovation with environmental sustainability by reducing gas emissions and limiting natural resource depletion.

2.4 Secondary Aluminum By-products Trapped in Geopolymers Foams

The disposal of end-of-life and hazardous waste materials represents a severe environmental issue that industries must stand worldwide. Several studies highlighted the disposal of sludges such as uranium-series decay, heavy metals, and various hydrocarbons through (i) ensuring a fast solidification and encapsulation of the contaminants into geopolymer structure, (ii) minimizing the leaching into the ground and drainage water, and (iii) increasing the structural durability during unfavorable environmental conditions. In

particular, aluminum production required a fast response to guarantee clever alternatives on resource management and material re-use, dealing with multiple and still unsolved matters regarding the treatments of special hazardous wastes linked to binding landfills regulations.

Geopolymers display a wide range of characteristics and properties, such as high compressive strength, low shrinkage, excellent freeze-thaw resistance, high-temperature resistance, and acid resistance. The development of geopolymers has become an exciting research subject in recent years because geopolymer binders provide great potential for alternative Portland-cement-based binders. As reported in previous research, the Portland cement manufacturing process demands large amounts of energy and releases significant CO_2 emissions. It is estimated that the cement industry alone is responsible for around 7% of the CO_2 generated globally. Hence, this binder is one of the critical causes of global warming. The introduction of geopolymers not only meets the requirements for mechanical performance but is also interesting as a new green construction material over Portland cement. Foaming methods to reduce the geopolymer density have been investigated, as low-density geopolymers are increasingly being reported in the literature to improve the insulating properties. The macropores can be obtained by releasing hydrogen gas from the aluminum reaction in the alkaline medium [47].

Innovative geopolymer and gypsum composites containing various micro-additives, such as coke dust, microspheres, aerogel, artificial gypsum, and polymers, are often used. Apart from the fact that it is possible to manage waste, their addition allows for obtaining materials with interesting thermal and mechanical properties. So, the ecological profit is double. The resulting innovative composites often show new properties that have not been tested before. It is, therefore, necessary to know and characterize the obtained materials as broadly as possible. As a result of the research, micro-additives in geopolymeric and gypsum composites can significantly improve building material properties.

Thermal conductivity, porosity, compressive strength, flexural strength, and density often improve compared to the reference samples without additives. Examples of actual utilization are foundry molds, insulating panels, fireproof materials for automobiles and airplanes, expanded geopolymer panels for thermal insulation, refractory adhesives, binders, and coatings for high temperatures [48]. Other typical applications are infrared burners, high-temperature filters, lamps, resistors, thermocouples, and heating elements. The versatility comes from their chemical composition: glass and metal oxide powders are used to optimize specific properties such as thermal expansion, thermal conductivity, dielectric strength, and chemical resistance [49].

2.5 Geopolymers: Historical Development

In 1972, for the first time, Davidovits discovered a new material called geopolymer. A geopolymer is a three-dimensional silico-aluminate material constituted by three linear oligomeric units, called polysilanes [50]. However, several studies [51-55] suggest geopolymer technology as an old building material employed in the pyramids of ancient Egypt and other old constructions such as the Moai statues on Easter Island. The evident durability and resistance have oriented the research to study the chemistry and processes of these ancient materials. Joseph Davidovits published the first research on the synthesis of geopolymers in 1979 [56-57]. The first geopolymer was synthesized using kaolinite in a sodium hydroxide solution. Davidovits used kaolinite reacting

with NaOH at 100-150°C and polycondensing into hydrated sodalite to synthesize mineral feldspathoids and zeolites.

Over the last decades, geopolymers have acquired engagement as a valuable new inorganic polymer to replace the ordinary Portland cement (OPC) and other mineral-based products [58]. Ordinary Portland cement uses a significant portion of natural resources and releases a not negligible amount of greenhouse gases [59]. In particular, geopolymers have similar performance to traditional binders and the advantages of reducing gas emissions, increasing the mechanical and thermal properties, and chemical resistance to corrosion and weather degradation.

2.5.1 Chemical Processes to Produce Geopolymers

Alkaline activators and aluminosilicate precursors represent the starting materials involved during the chemical process that leads to the synthesis of geopolymers. Metakaolin is the most studied precursor [60-66], but alkaline activation can involve any materials with high Al_2O_3 and SiO_2 content. The alkaline activation process involves aluminosilicate thermal treatment with a temperature between 500°C and 800°C [67-68], where there is a drop of structural hydroxyl ions in the clay minerals.

The alkaline activation process during the geopolymerization process (Figure 2) is accomplished by mixing the alkaline solution with the aluminosilicate precursor, where Si-O groups dissolution occurs.

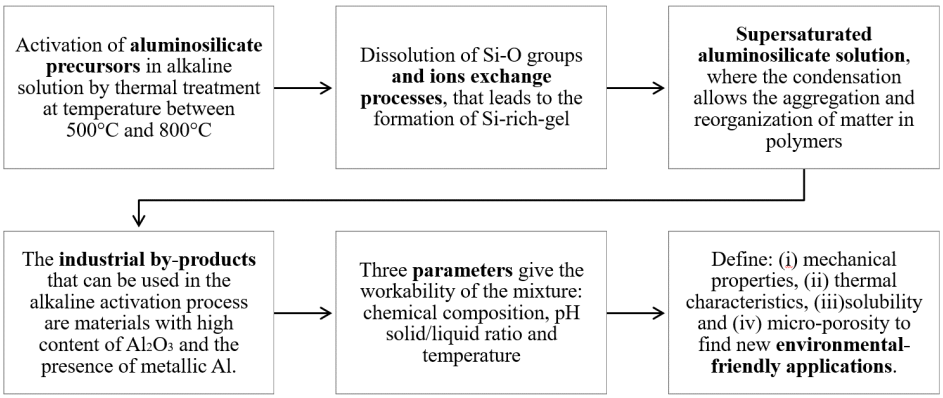

Figure 2. Scheme of the geopolymerization process.

The dissolution of aluminosilicate and bonds breaks through a chemical attack in an alkaline environment. Dissolution processes strongly depend on the pH of the solution. For high values, a fast dissolution rate leads to the formation of supersaturated aluminosilicate solution, where the result condensation of oligomers allows the aggregation and reorganization of matter in polymers. The reaction involves the dissolution of Si-O groups of the initial solid, favoring the formation of a Si-rich gel. The silica gel rearranges and reorganizes during the reaction, building a three-dimensional structure.

After the dissolution, the matter starts to reorganize. The process of condensation allows the formation of polymers that can be classified into two groups based on the calcium concentration: (i) N-A-S-H gel: low Ca content, formed by random silicon and aluminum tetrahedra, where ions can be trapped in the cavities to calibrate the electronegative charge; (ii) C-A-S-H gel: high Ca content, built by a tetrahedral silicate layer [69-72].

Different types of material can be used as fillers in the alkaline activation process. Al and Si are tetrahedrally coordinated, while alkalis balance the electric charge as the substitution of ions Al^{3+} with Si^{4+}. The characteristic slags that can

be used are represented by the material with high content of Al_2O_3 and the presence of small amounts of metallic Al, a foaming agent to make the material more porous and therefore lighter.

Definitively, it is well known that the chemical composition, grain size, solid/liquid ratio, and pH are the main parameters influencing material workability [73-74]. After the geopolymer synthesis, the maturation phase, called curing, is carried out at temperatures between 20°C and 100°C (generally at room temperature) in specific molds and under controlled conditions for specific and different durations.

2.5.2 Summary: Chemistry and Structure of Geopolymers

Inorganic polymers are classified according to the chain structure, polymerization mechanism, and application. Monomers constituted them, including inorganic elements merged by predominantly covalent bonds. A geopolymer material is similar to natural zeolites, with the only difference of amorphous microstructure [75].

Geopolymers are synthesized from an alkaline solution and aluminosilicate-rich materials, achieving an amorphous 3D structure similar to glass. However, GP is formed at low temperatures, incorporating additives as reinforcing during the geopolymerization process. The geopolymerization process involves a fast chemical reaction of Si-Al under alkaline conditions, resulting in three-dimensional polymeric chains (Si-O and Al-O bonds) [76].

In 1950, Glukhovsky conceptualized an early model that gives a general mechanism for the alkali activation of silico-aluminate materials, dividing the process into three main simplified phases [77]: (i) destruction, (ii) condensation, and (iii) stabilization. Later models suggested that the geopolymerization process can be summarized into five steps [78-79]:

(i) ***Dissolution***: Aluminosilicates dissolve into the alkaline solution to produce Si and Al monomers by the reaction (1):

$$\text{Al-Si} + \text{MOH} \rightarrow \text{M} + \text{OSi(OH)}_3 + \text{M} + \text{Al(OH)}_4 \quad (1)$$

(ii) ***Diffusion***: Al and Si species diffuse the aluminosilicate particle surface into the gel. The continuous drop of Al and Si species increases the dissolution rate.

(iii) ***Polymerization***: takes place to form dimers, which react with monomers or dimers or Si-oligomers to build oligomers of varying forms (i.e., linear and cyclic).

$$\text{-OSi(OH)}_3 + \text{M-OSi(OH)}_3 + \text{M+} \rightarrow \text{M-OSi(OH)}_2\text{-O-Si(OH)}_3 + \text{MOH} \quad (2)$$

The polymerization between Al and Si complex will occur in preference to the polymerization between the complex of the same species because the activation energy for forming an Al-O-Si bond is the lowest possible.

(iv) ***Aluminosilicate gel formation***: forming -Al-O-Si- bonds by reacting the M+ and Si-oligomer.

(v) ***Polycondensation and hardening process***: the aluminosilicate gel is then transformed into the final structure by a solid-liquid interaction based on the leaching and diffusion between the particle surface and the gel phase.

The geopolymer is a three-dimensional structure constituted by a network of SiO_4 with aluminate substitution always IV coordinated with oxygen. Within this structure, cations such as Na^+, K^+, and Ca^+ neutralize the negative charge of AlO_4. A modeling structure of the tetrahedral units is proposed in Figure 3:

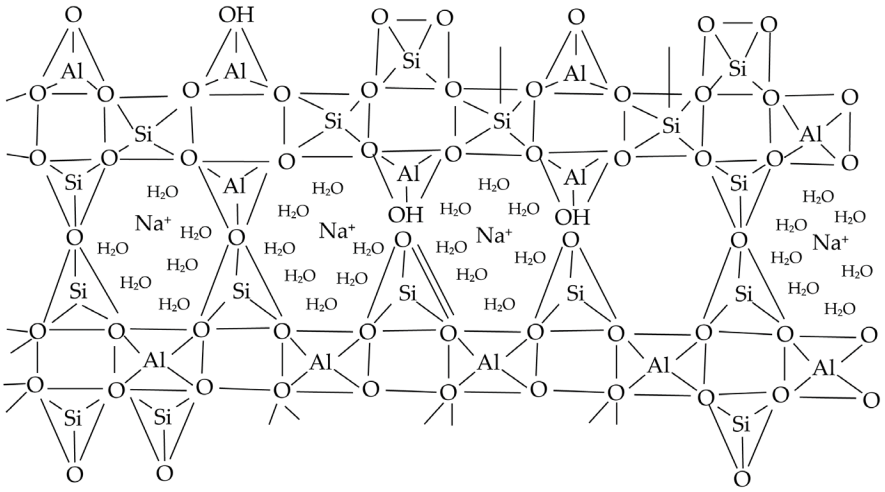

Figure 3. Tetrahedral units of the geopolymer composite [80].

The unit that constitutes the chemical structure is also abbreviated as sialate, or silicon-oxo-aluminate used to describe the silicon bonding. The proposed empirical formula of polysialates is given by the expression 3:

$$Mp\ \{(SiO_2)zAlO_2\}p\ .w\ H_2O \quad (3)$$

where: M = Na^+, K^+, and Ca^+; p is the degree of polycondensation; z is the Si/Al ratio in the oligomers and can be 1 (polysialate - PS: -Si-O-Al-O-), 2 (polysialate-siloxo - PSS: -Si-O-Al-O-Si-O-), or 3 (polysialate-disiloxo - PSDS: Si-O-Al-O-Si-O-Si-O-); and w describes the water content.

The polysialate oligomers are chain and ring polymers characterized by Si^{4+} and Al^{3+} in IV coordination with O_2. The oligomeric building units are illustrated in Figure 4:

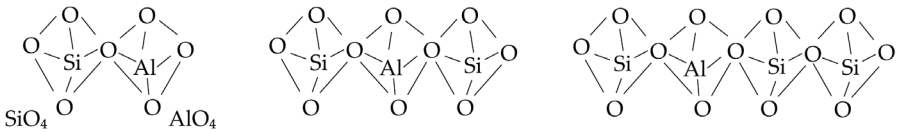

Figure 4. Combination of Si and Al in polysialate oligomers and bonds (tetrahedra) [81].

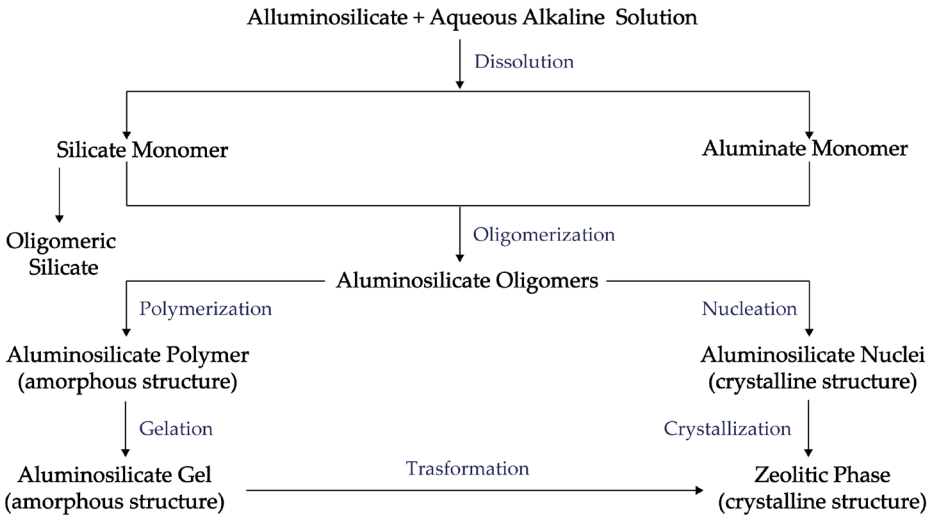

Figure 5. Scheme of the different phases concerning the geopolymerization process [82].

The oligomers of Si and Al units covalently share oxygen atoms to form the larger macromolecules called geopolymers (Figure 5). Si ions are always IV-coordinated, while Al is IV or VI-coordinated to the oxygen.

2.5.3 Properties and Applications of Geopolymers

The continuous exploration and depletion of natural resources cause damage to the environment. During the production processes of cement and other materials, various toxic substances such as CO, CO_2, NO_x, SO_x are emitted into the atmosphere, hardly impacting human and environmental health. Moreover, the price of raw materials for the construction industry increased because of high demand, lack, and the high energy price. For this reason, new environmental solutions were recognized using materials to be disposed of in landfills for synthesizing geopolymers.

It has been discussed how the performances of geopolymer are nearby comparable to OPC, but, on the other hand, the method to synthesize these materials is straightforward and low-energy. As already cited, these properties are of great relevance in research designing geopolymers as materials for new sustainable development [83-86]. Moreover, the primary advantages are the high availability of raw materials, good physical performance such as high mechanical strength, durability, fire resistance, resistance to chemical attack, and trap toxic and hazardous wastes. The chemical composition of the raw materials and the production methods affect the geopolymer physical characteristics, which can be used for different applications. The most common ones are fire and heat-resistant materials, sealants, ceramics, cement, adhesives, coating, insulation, underwater, water-resistant materials, refractory materials, and waste encapsulation [87].

After a curing time of 28 days, the physical properties of the geopolymer are primarily influenced by the chemistry, particularly by the Si/Al ratio (Table 1). The geopolymers structure is three-dimensional for the Si/Al ratio less than 2, suitable as tiles, ceramic, fire-resistant materials, concretes, cement, and waste encapsulating. For a Si/Al ratio above 3, the geopolymer is a crosslinked 2D structure, less rigid and more elastic. For Si/Al ratios up to 35, GP can be employed as adhesive, sealant, or resin with low viscosity [88-89].

Table 1 Applications of the geopolymers on Si/Al ratio.

Si/Al ratio	GP structure	Applications
1	3D	Tiles, ceramic, fire protection
2		Cements, concretes, waste trapping
3	2D	Foundry equipment, fire and heat resistant fiber-glass composites, aeronautics
> 3		Sealants, aeronautics
20-35		Fire and heat resistant fiber composites

In the current research, a Si/Al ratio of around 1.91 is adopted for the geopolymeric matrix suitable for a configuration able to trap toxic and hazardous waste [90].

GPs are responsible for chemical and physical trapping mechanisms for a comprehensive spectrum of inorganic wastes such as cations, heavy metals, or radioactive [91-92]. During the last years, industrial waste materials (fly ash, blast furnace slag, glass waste, ceramics, mine) have been studied as precursors in the alkaline activation process, with an optic of valorization, obtaining

financial and environmental advantages [93]. Nevertheless, the grade of heterogeneity in the raw materials implies that a standard chemical composition guarantees repeatable properties.

Standardization of waste materials for large-scale commercial use is taking place rapidly, even if most of the mixtures being used are based on limited precursors (fly ashes, blast furnace slags). For this reason, synthesizing GPs from industrial by-products of the secondary aluminum or generally new precursors requires an earlier qualitative and quantitative analysis, and specific parameters need to be defined to normalize the processes.

2.6 A Comparison of Geopolymers with Other Binding Materials

It is fundamental to recognize that geopolymers (GPs), alkali-activated materials (AAMs), Calcium Sulfoaluminate Cements (CSCs), and Ordinary Portland Cements (OPCs) are materials with different production processes and chemistry. Figure 6 shows a classification based on the aluminum and calcium content, where geopolymers are binder materials with the highest Al and lowest Ca content.

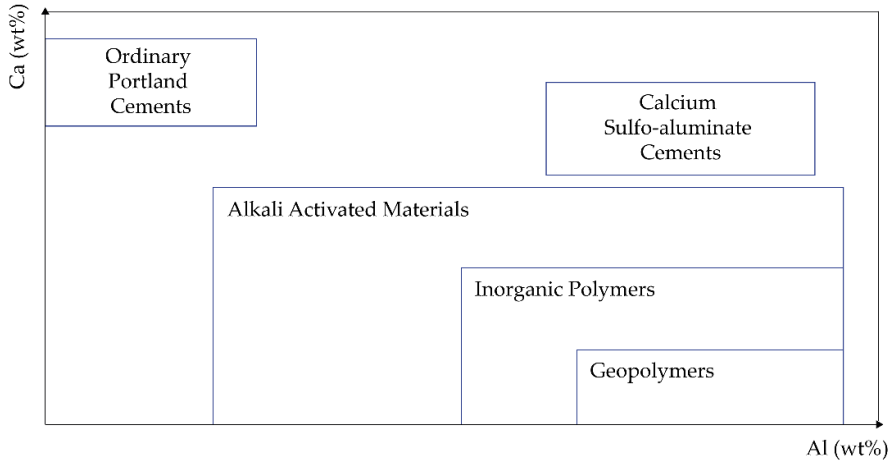

Figure 6. Classification of building materials based on the Al and Ca content.

The main relevant difference between ordinary Portland cement (OPC) and geopolymer cement (GP) is that OPC production is high-energy manufacturing. GPs use materials like fly ashes, slags, and industrial by-products and employ low energy as their production does not involve limestone calcination, such as in OPC [94]. On the other hand, AAMs are cement-like materials formed by calcined clays, and so although they have similar composition compared to GPs, they are not [95-97]. Several studies worldwide recommend the importance of geopolymers conveying attention to their excellent energy-saving and potential to utilize materials such as metakaolin, silica fume, limestone powder, and industrial by-products in geopolymer mortar and concrete development [98].

2.6.1 Ordinary Portland Cement (OPC)

Cement and concretes are the most widely employed building materials. From the beginning of the 19th century, the Ordinary Portland cement (OPC) has become the most used binder in the construction industry. Nowadays, alternative binders, more environment-friendly materials than OPC, have been studied, partially replacing OPC. Worldwide cement production impacts greenhouse gas with at least 5% of the total CO_2 emissions [99-101]. Ordinary Portland cement is usually obtained by combining limestone with secondary raw materials such as clay or other aluminosilicates at a temperature between

1300-1500°C in vertical and continuous rotary ovens. The clay must have the absence of sulfides (pyrite, marcasite), calcium sulfate, organic substances, and heterogeneous nodules. There are two material handling procedures: wet (35-40% H_2O added) and dry (using drum dryers or hot gases). CaO, Al_2O_3, SiO_2, Fe_2O_3 are the main starting components, and after the treatment process, they give rise to the main constituents of Portland cement. The product called clinker, partially melted is mixed with gypsum to control the reaction. It essentially consists of four specific mineral phases: dicalcium silicate or belite (Ca_2SiO_4) - C_2S, tricalcium silicate or alite (Ca_3O_5Si) - C_3S, tricalcium aluminate ($Ca_3Al_2O_6$) - C_3A, and a solid solution of calcium alluminoferrite ($Ca_4Al_2Fe_2O_{10}$) - C_4AF. The hydration process of OPC occurs through the interaction of the clinker, calcium sulfate, and water, leading to the hardening of the material [102].

The UNI EN-197-1, 2007, on the other hand, provides a classification that includes different types of cement such as (i) CEM I: Pure Portland Clinker (OPC), (ii) CEM II: cement with the addition of blast furnace slag (BFS), (iii) CEM III: BFS-OPC cement, (iv) CEM IV: pozzolanic cement, (v) CEM V: composite cement (significant additions of BFS). Each type is further diversified according to the proportions of the listed constituents, present strength classes, and the minimum threshold of compressive strength.

The described processes on Portland cement, particularly during the clinker formation, need high temperatures and, consequently, a high amount of energy.

2.6.2 Hydration Process of OPC

The hydration process is based on the reactions between the clinker, water, and a specific amount of gypsum [103-104]. The process involves dissolution processes and precipitation of colloidal and crystalline hydrates. With the clinker-H_2O interaction, an exchange of species occurs from the solid to the liquid phases, resulting in a rapid increase in the concentration of aluminates, sulfates, and alkalis in the liquid phase.

A significant amount of heat is released during this hydration phase, and a calcium sulfoaluminate ettringite ($3CaO{\cdot}Al_2O_3{\cdot}3CaSO_4{\cdot}32H_2O$) crystalizes. Ca^{2+} and Si^{4+} from the dissolution of alite Ca_3O_5Si pass into the solution: silica content rises until it reaches a saturation point and then decreases rapidly, while calcium and OH^- content continue to increase but not linearly over time. Then, when the reaction velocity with the heat rate decrease, Ca^{2+} ions in the liquid phase reaches a supersaturation point, and the gel nucleation starts, forming $Ca(OH)_2$ crystals (3) [105]:

$$2Ca_3O_5Si + 11H_2O \rightarrow CaO{\cdot}2SiO_2{\cdot}3H_2O + 5Ca(OH)_2 \quad (3)$$

Belite ($Ca_3Al_2O_6$) from the clinker reacts with the gypsum to form ettringite ($C_6Al_2(SO_4)_3(OH)_{12}{\cdot}26H_2O$) (4) that also partially decomposes to form a hydrated calcium mono-sulfoaluminate ($4CaO{\cdot}Al_2O_3{\cdot}CaSO_4{\cdot}12H_2O$):

$$Ca_3Al_2O_6 + 3CaSO_4{\cdot}2H_2O + 26H_2O \rightarrow Ca_6Al_2(SO_4)_3(OH)_{12}{\cdot}26H_2O \quad (4)$$

Definitively, a hydrated calcium silicate gel (C-S-H) is rapidly generated during the hydration process of OPC, and it is considered to give resistance and durable properties to the cement. The Taylor and Richardson and Groves (1993) models [106] suggest that the C-S-H gel has a disorderly layered structure of tetrahedra, considered a solid solution of hydrated calcium silicate and $Ca(OH)_2$.

CHAPTER 3
MATERIALS AND METHODS

3.1 Raw Materials for the Synthesis of Geopolymer Foams (GFs)

3.1.1 By-products from the Secondary Aluminum Industry

The re-use of industrial by-products from the secondary aluminum industry, which can be addressed to new materials or other industrial sectors and thus exploited as an energetic or non-energetic secondary raw material, represents a fundamental answer to the need for developing sustainable economic growth, based on the decrease of natural resource exploitation (primary raw materials) and the minimization of waste output [107]. This approach converts waste materials into energetic or non-energetic resources, valorizing the so-called industrial by-products for (i) enhancing the sustainability of raw material exploitation and management, (ii) limiting greenhouse gas emissions, and (iii) reducing the waste disposal in landfills.

The EU regulations classify these aluminum-rich by-products as special hazardous wastes capable of developing flammable gases and forming explosive mixtures with air (hazard class codes: HP10-HP11-HP12-HP13; European Waste Code, EWC: 100323*, where EWC marked with an asterisk "*" are hazardous waste under the Directive 91/689/EEC). These EWC 100323* by-products are hazardous because they often contain high amounts of metallic aluminum (and other metal species) and are a potential hydrogen release source. The contact with air or water might develop flammable gases. As already pointed out by the literature [108], the chemical process is explained by the reaction (5):

$$2Al + 6H_2O + 2NaOH \rightarrow 2NaAl(OH)_4 + 3H_2 \quad (5)$$

The sodium hydroxide, used as a reaction catalyst, is re-generated from sodium aluminate, as reported in the reaction (6):

$$NaAl(OH)_4 \rightarrow NaOH + Al(OH)_3 \quad (6)$$

The reactions responsible for the material oxidation (7) occur at 575°C and can be expressed by combining aluminum hydroxide molecules that are produced during the previous reaction:

$$2Al(OH)_3 \rightarrow Al_2O_3 + 3H_2O \quad (7)$$

The continuous hydration of the aluminum oxides generates boehmite, which becomes bayerite, again interacting with water. However, the reactions suffer from chemical-physical limitations that prevent a precise quantification of the amount of hydrogen produced by the reaction of metal with the aqueous alkaline solution, compared to the water-splitting contribution in extreme thermodynamic and kinetic contexts.

Other reactions (below) tend to evolve at the operating temperatures of the metallurgical process. Aluminum sulfide can produce hydrogen sulfide (8); aluminum carbide may generate methane (9); whereas aluminum phosphide can produce phosphine (10):

$$Al_2S_3 + 6H_2O \rightarrow 2Al(OH)_3 + 3H_2S_{(g)} \quad (8)$$
$$Al_4C_3 + 6H_2O \rightarrow 3CH_{4(g)} + 2Al_2O_3 \quad (9)$$
$$AlP + 3H_2O \rightarrow Al(OH)_3 + PH_{3(g)} \quad (10)$$

The aluminum by-products were used as additives to foam the geopolymers. The studies of the starting materials were conducted with specific analytical techniques to determine the chemical content subsequently indicated and for the planning of laboratory experiments.

3.1.2 Classification of the Industrial By-products

Before and after the chemical neutralization (i.e., oxidation), analyses of the investigated by-products were carried out to identify the main mineralogical phases of powder X-ray diffraction by a Bruker D8 Advance diffractometer at CRI.ST (centro di servizi di CRIstallografia STrutturale, University of Florence). The grain size of the starting materials was determined through laser beam particle analyses (Hydro 2000MU analyzer, at the University of Milano Bicocca). Mass variation due to thermal treatment and changes concerning thermodynamic conditions were obtained through thermogravimetric analyses with a Netzsch-Gerätebau GmbH-STA 409 CD simultaneous thermal analyzer (MISE-Direzione generale per le risorse minerarie ed energetiche, Rome, Italy).

Chemical analyses (major, minor, and trace elements) were performed by: (i) ICP-OES-MS with near-total multi-acid (hydrofluoric, nitric, and perchloric acids) digestion. After the digestion and dehydration, samples were brought into the solution using aqua regia, solubilizing only certain phases, and analyzed using a Varian ICP and Perkin Elmer Sciex ELAN ICP-MS at the Activation Laboratories Ltd.—Actlabs (Ancaster, Ontario, Canada), with ten sample duplicates and eight reference materials. Loss on Ignition (LOI) was also determined at Actlabs. (ii) IR using an ELTRA instrument to quantify total (graphitic and organic) carbon, CO_2, total sulfur (S), and SO_4 (Actlabs). 0.2 g samples were decomposed in a pure nitrogen environment furnace at 1000°C to determine the CO_2 content. H_2O and other gases were removed before detecting carbon dioxide in the IR cell. For total C, S, and SO_4, the inductive elements of the samples and an accelerator material were coupled with the high-frequency field of induction of a pure oxygen environment furnace. Carbon and sulfur elements were reduced during combustion, forming CO, CO_2, and SO_2. Carbon and sulfur were measured as gases flowed through the IR cells.

Organic compounds were analyzed at the Laboratorio Arca SRL (Fano, PU, Italy) according to UNI EN 14039:2005, EPA 3580A 1992, and EPA 8015C 2007 standard methods [109-111].

The data processing enabled a quantitative assessment of the dangerous compounds (Table 2) in the aluminum processing slags, which are critical when re-used [112-113]. The samples were classified under the normative requirements (Figure 7) on the environmental safety and pollution control required by the European industries to issue the integrated environmental authorization (AIA): the industrial emissions directive 2010/75/EU and Legislative Decree 152/2006 [114-115].

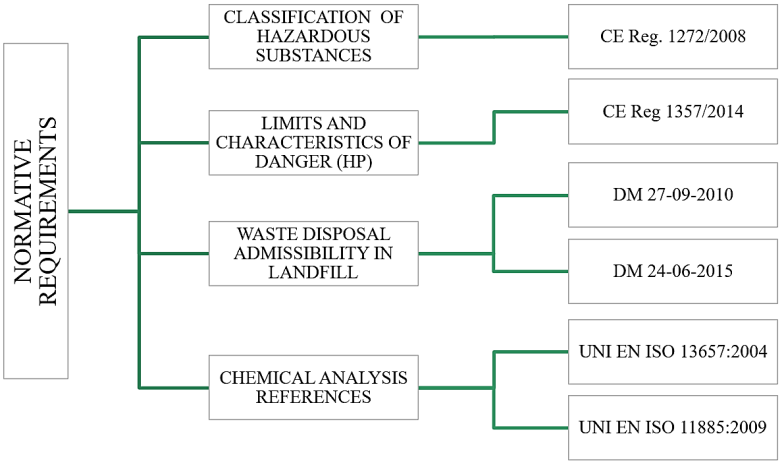

Figure 7. Normative requirements, regulations for classifying hazardous substances, limits, and characteristics of danger (HP), waste disposal admissibility, and chemical analysis references [116-119].

A macroscopic overview of the aluminum-rich by-products is given in Figure 9. The materials used as fillers in the geopolymers derive from the main processes of the secondary aluminum industry: (i) screening process, (ii) pyrolysis process, (iii) fusion process. FG and UBC acronyms are from coarse-grained domestic appliance scrapes and urban beverage cans, the primary materials used for recycling.

V.FG (2.52–893.37 μm) and V.UBC (2.00–893.37 μm) (Figure 8–9a,b) represent by-products from the screening process of the secondary aluminum industry. The mineralogical phases are metallic aluminum and rutile in V.FG, whereas metallic aluminum, quartz, periclase, and carlinite are in V.UBC. The aluminum content is 125,468 ppm and 180,638 ppm, respectively. D.FG (0.40–56.37 μm) and D.UBC (0.40–355.66 μm) (Figure 8–9c,d) are produced during the pyrolysis process. Their aluminum contents are 32,204 ppm and 40,198 ppm. Aluminum, portlandite, rutile, and CaClOH are the main mineralogical phases detected within the two materials. C.FG (0.40–355.66 μm) and C.UBC (0.45–632.46 μm) (Figure 8–9e,f), (dust materials caught from the cyclones) present aluminum contents of 73,296 ppm and 62,333 ppm. The mineralogical phases are aluminum calcite, rutile, graphite, ankerite in C.FG, and zinc in C.UBC. FF.FG (0.40–158.87 μm) and FF.UBC (0.40–63.25 μm) (Figure 8–9g,h), the industrial by-products from the fusion process, have an aluminum content of 14549 ppm and 6636 ppm. The mineralogical pattern is metallic aluminum, halite, sylvite, and portlandite.

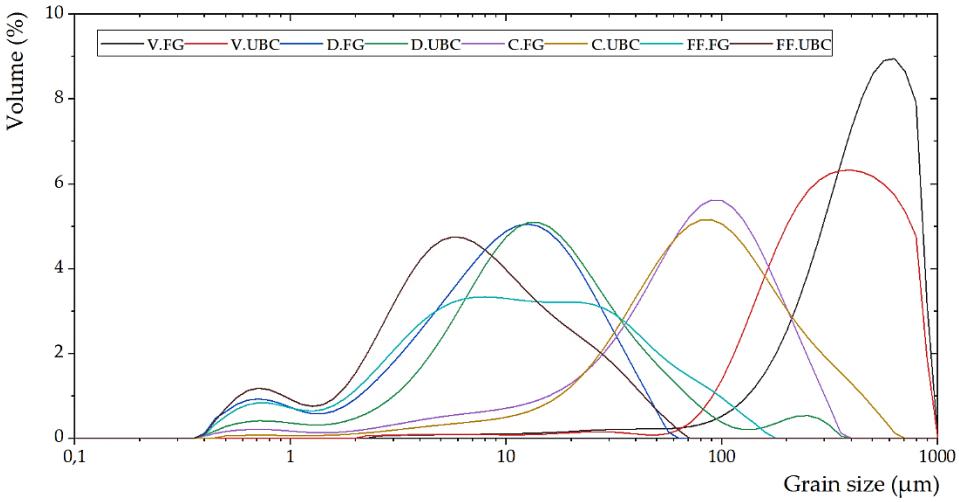

Figure 8. Grain size modal curve of the aluminum-rich by-products.

The organic compounds (in traces) in all the samples are < 5 ppm Hydrocarbons, and < 1 ppm: 4-Methyl-2-Pentanone, Ethyl Acetate, Isobutyl Acetate, N-Butyl Acetate, Acetone, Acetonitrile, Benzyl Alcohol, Ethyl Alcohol, Furfuryl Alcohol, Methyl Alcohol, Isobutyl Alcohol, N-Butyl Alcohol, 2-Butanone, 2-Butoxyethanol, 2-Butossietil Acetate, Cyclohexanol, Cyclohexanone, N-Hexane, Ethylbenzene, 2-Ethylbutanol, 2-Ethylbutanol, 2-Ethoxyethanol, 2-Ethoxyethyl Acetate, Isopropanol, Styrene, Toluene, Toluene, Xylene (O+M+P).

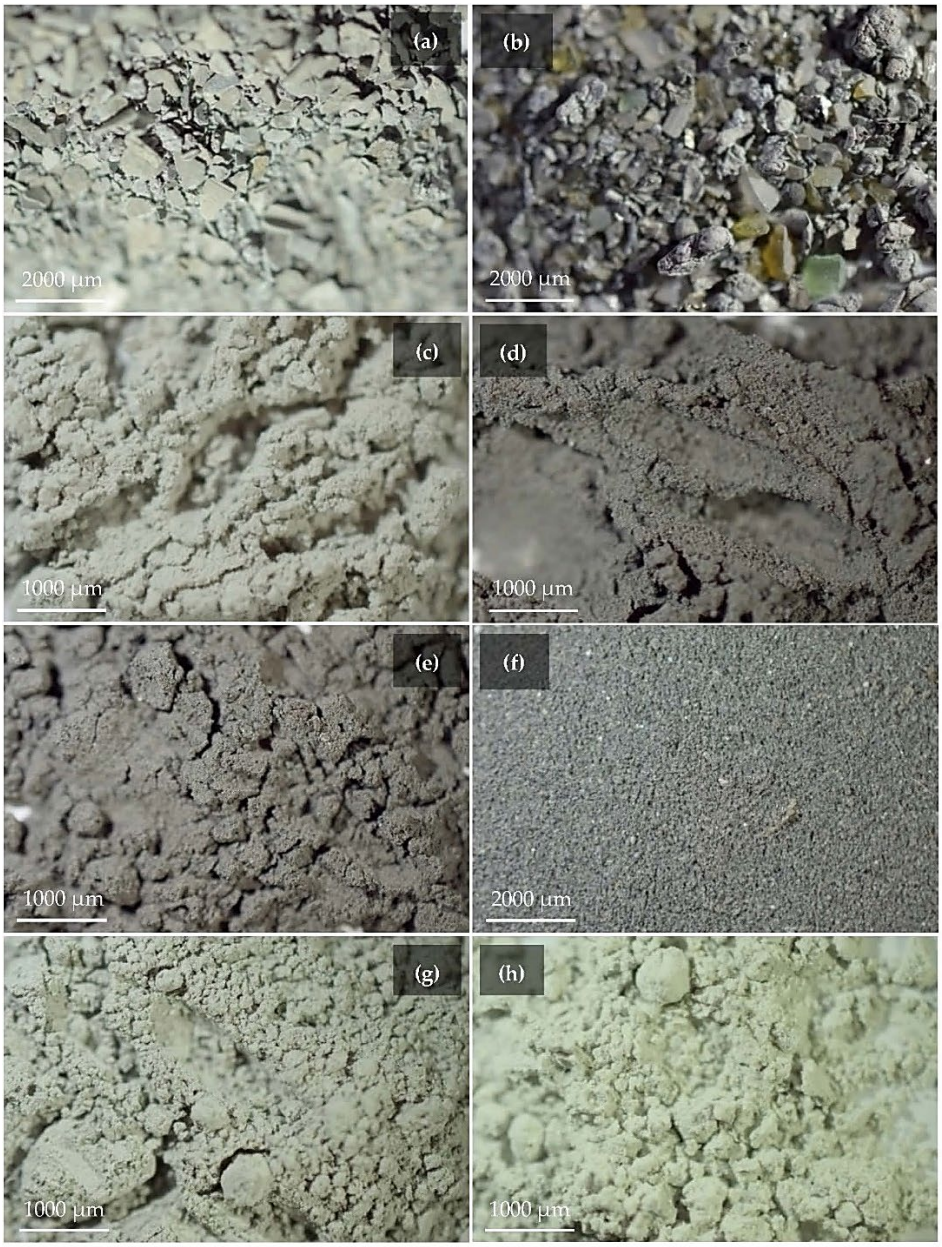

Figure 9. Photos of by-products of the secondary aluminum industry: V.FG (**a**) and V.UBC (**b**): screening; D.FG (**c**) and D.UBC (**d**): pyrolysis; C.FG (**e**) and C.UBC (**f**): abatement dust; FF.FG (**g**) and FF.UBC (**h**): fusion slags.

Table 2. Density (ϱ; g/cc) and metal contents (ppm) of by-products from different processes of the secondary aluminum industry. V.FG and V.UBC: screening; D.FG and D.UBC: pyrolysis; C.FG and C.UBC: dust abatement; FF.FG, and FF.UBC: fusion slags. The hazard class codes are classified according to CE Reg. 1272/2008 and CE Reg. 1357/2014 [116-117].

	V.FG	V.UBC	D.FG	D.UBC	C.FG	C.UBC	FF.FG	FF.UBC	Class. (CE Reg. 1272/2008)	HP (CE Reg. 1357/2014)
ϱ (g/cc)	2.87±0.01	2.69±0.003	2.55±0.09	2.58±0.09	2.34±0.04	2.40±0.09	2.47±0.11	2.52±0.05		

Al (ppm)	125468	180638	32204	40198	73296	62333	14549	6636	H314	50000 HP8
Sb (ppm)	< 5	< 5	6	< 5	< 5	< 5	7.0	11	H314 H314 H411	10000 HP4 50000 HP8 250000 HP 14
As (ppm)	< 5	< 5	< 5	< 5	< 5	< 5	< 5	< 5	H301 H331 H350 H400 H410	50000 HP6 32500 HP6 1000 HP7 250000 HP14 250000 HP14
B (ppm)	36.2	11.1	128.8	137.9	62.4	70.9	77	59	H360FD	3000 HP10
Cd (ppm)	36.2	7.4	25.8	46.1	27.6	70.6	91.3	36.3	H372 H330 H350 H361 H341	10000 HP 5 1000 HP 6 1000 HP 7 30000 HP 10 10000 HP 11
Co (ppm)	28.5	< 5	9.7	31.3	12.3	103.8	< 5	< 5	H317; H334	100000 HP13
Cr^{6+} (ppm)	< 0.5	< 0.5	< 0.5	< 0.5	< 0.5	< 0.5	< 0.5	< 0.5	H340 H361f H317; H334 H350 H302 H410 H335; H372	1000 HP 11 30000 HP 10 100000 HP 13 1000 HP7 250000 HP6 250000 HP 14 10000 HP 5
Cr (ppm)	49.5	107.9	182.3	34.7	326.5	222	94.8	30.3	-	-
Mn (ppm)	930.5	2891	302.4	585.6	671.6	717.8	129.6	29.5	H301; H302; H332 H373	50000 HP6 100000 HP5
Mo (ppm)	< 5	5	< 5	< 5	< 5	< 5	< 5	< 5	H315; H319 H351	200000 HP 4 10000 HP 7
Ni (ppm)	488.7	26.7	66.6	49.8	119.1	134.6	21.5	< 5	H315 H301; H331 H350i H360D H341 H317; H334 H400 H411	200000 HP 4 32500 HP 6 1000 HP 7 3000 HP 10 10000 HP 11 100000 HP 13 250000 HP 14 250000 HP 14
Pb (ppm)	266.1	54.1	2756.4	787.8	3998.0	1378.0	369.5	165.6	H373 H360Df H410 H332	100000 HP 5 3000 HP 10 250000 HP 14 225000 HP 6
Cu (ppm)	2710.3	1287.5	2045.9	640.2	2891.6	744.4	201.2	79.3	H315; H319 H302 H400 H410	200000 HP 4 250000 HP 6 250000 HP 14 250000 HP 14
Se (ppm)	< 5	< 5	< 5	< 5	< 5	< 5	78.8	20	H373 H301; H331	100000 HP5 32500 HP6
Sn (ppm)	102.8	52.4	91.7	15.5	116.2	194.7	39.9	7.2	H314 H412	50000 HP 8 250000 HP 14
V (ppm)	29.6	56.4	24.6	12.6	23.8	23.7	< 5.0	< 5.0	H318 H335 H372 H300; H301; H302; H332 H341 H411	10000 HP4 200000 HP 5 10000 HP 5 1000 HP 6 10000 HP 11 250000 HP 14
Zn (ppm)	14539.0	3501.0	4774.2	3977.2	10109.6	13937.9	2028.6	689.4	H302 H315; H319 H335 H400	250000 HP 6 200000 HP 4 200000 HP 5 250000 HP 14 250000 HP 14

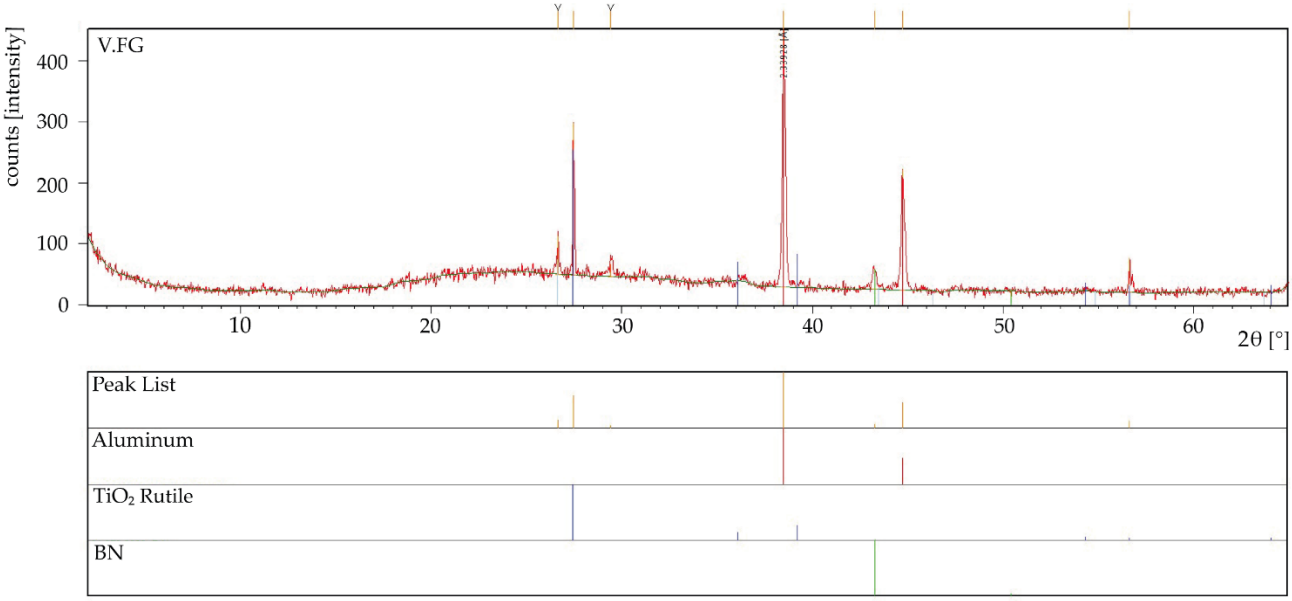

Figure 10. Mineralogical phases of "V.FG": Al; TiO_2; BN.

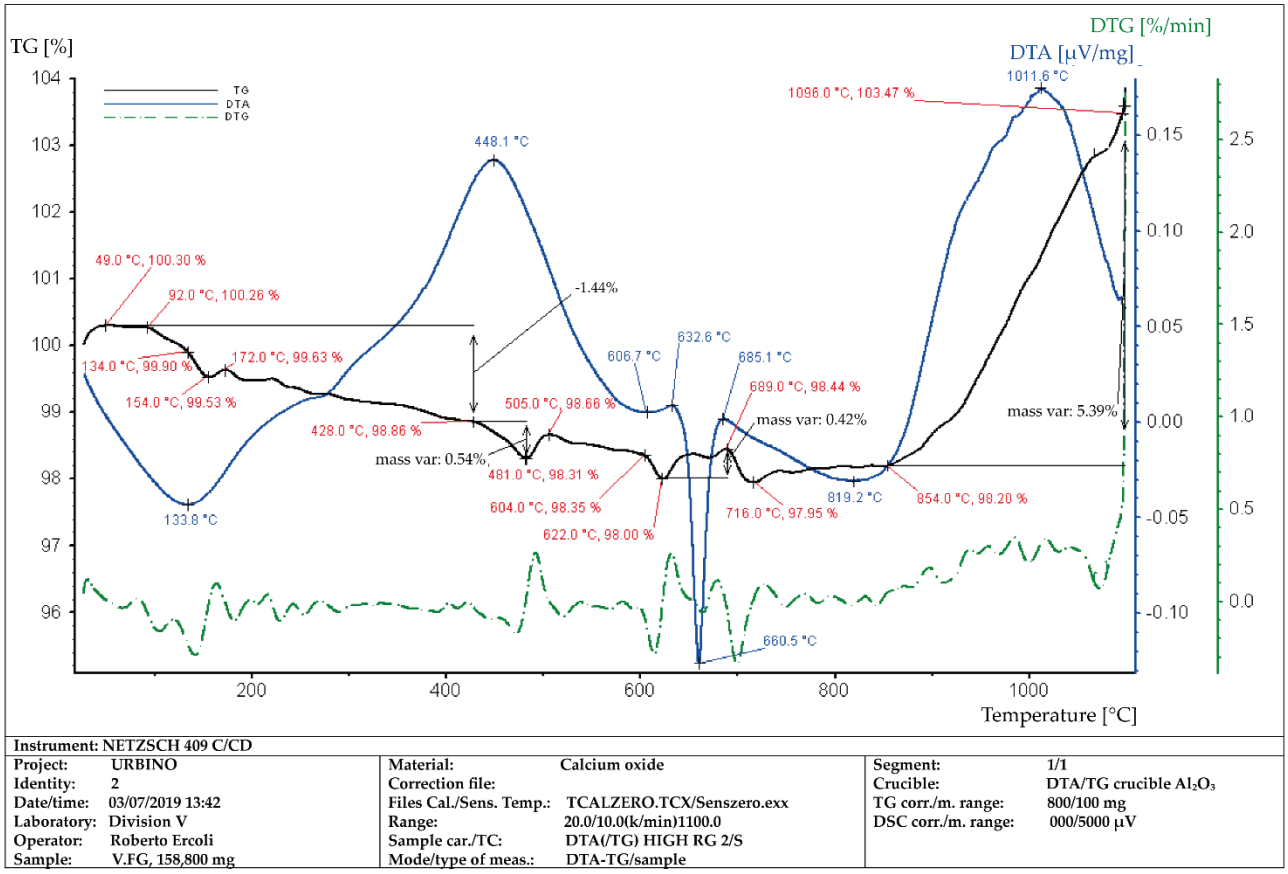

Figure 11. Thermogravimetric analysis of "V.FG". A progressive mass decrease of around 2.3% at 622°C and a mass increase of 5.5% between 716°C and 1096°C are measured.

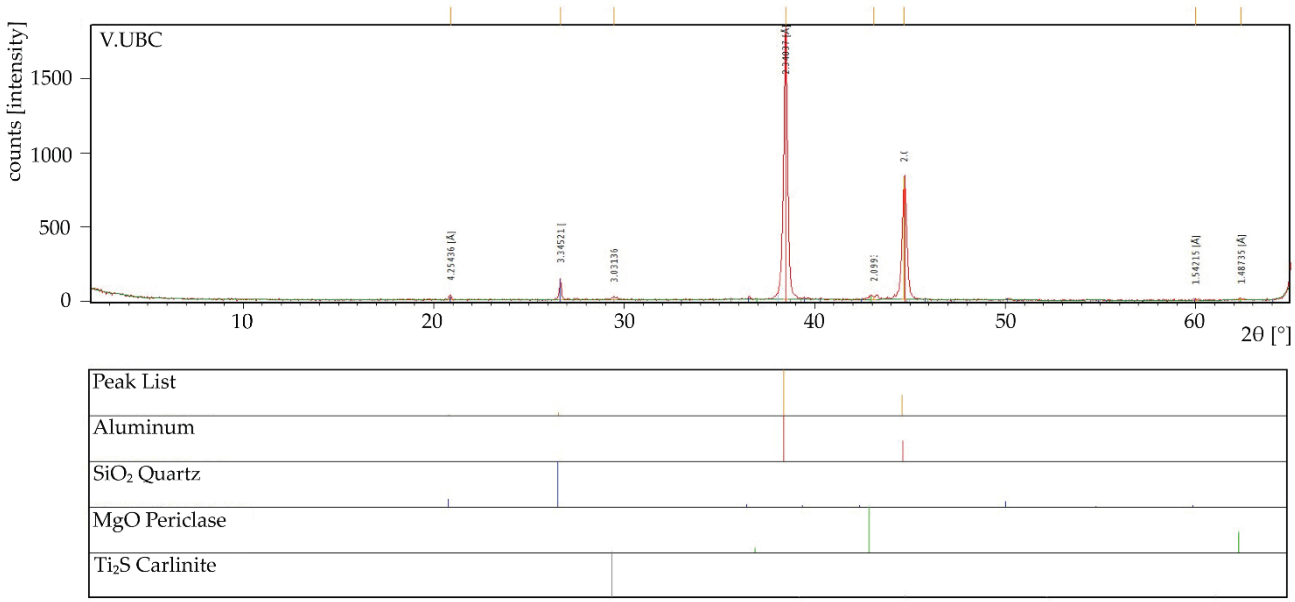

Figure 12. Mineralogical phases of "V.UBC": Metallic Aluminum (Al); Quartz (SiO_2); Periclase (MgO); Carlinite (TI_2S).

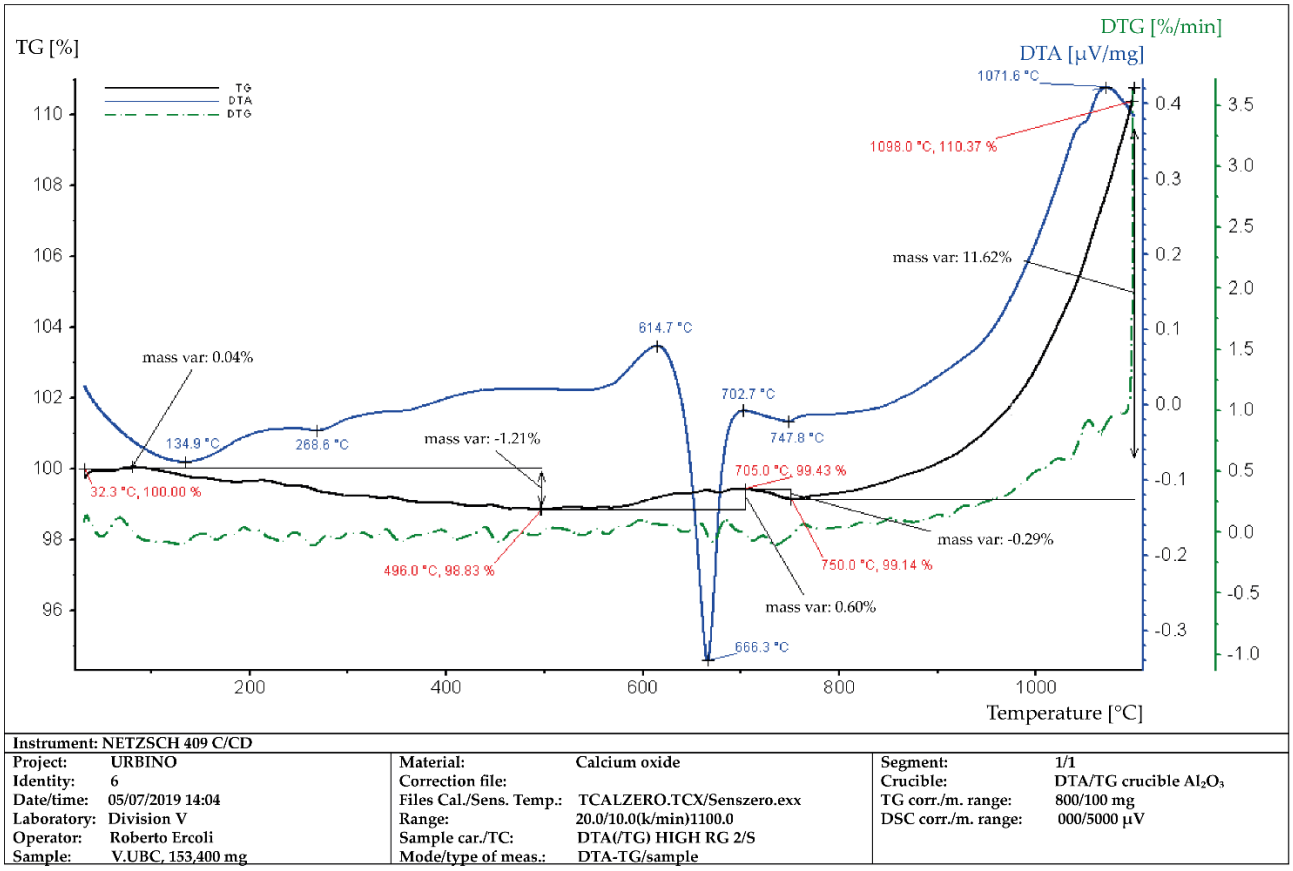

Figure 13. Thermogravimetric analysis of "V.UBC." A decrease of about 1.21% up to 496°C and an increase of 11.62% at 496-1098°C are detected due to the material oxidation. There is a substantial mass increase compared to "V.UBC" as the presence of aluminum is 18.06%, instead of 12.54%.

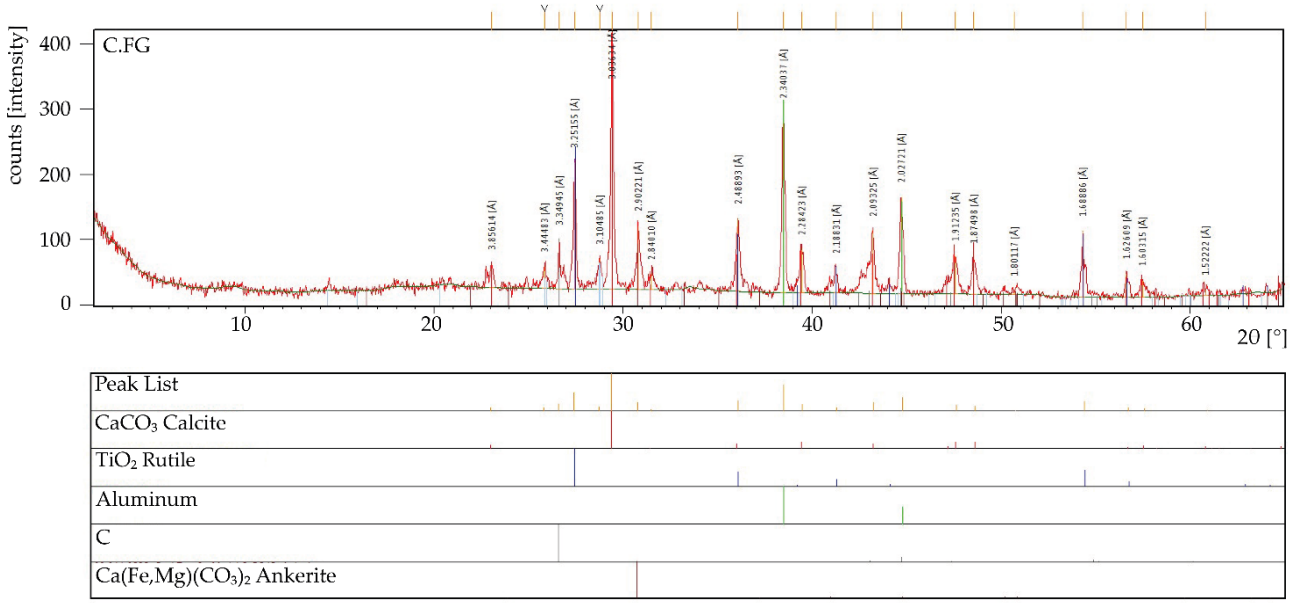

Figure 14. Mineralogical phases in "C.FG": Calcite ($CaCO_3$); Rutile (TiO_2); Al; C; Ankerite $Ca(Fe, Mg)(CO_3)_2$.

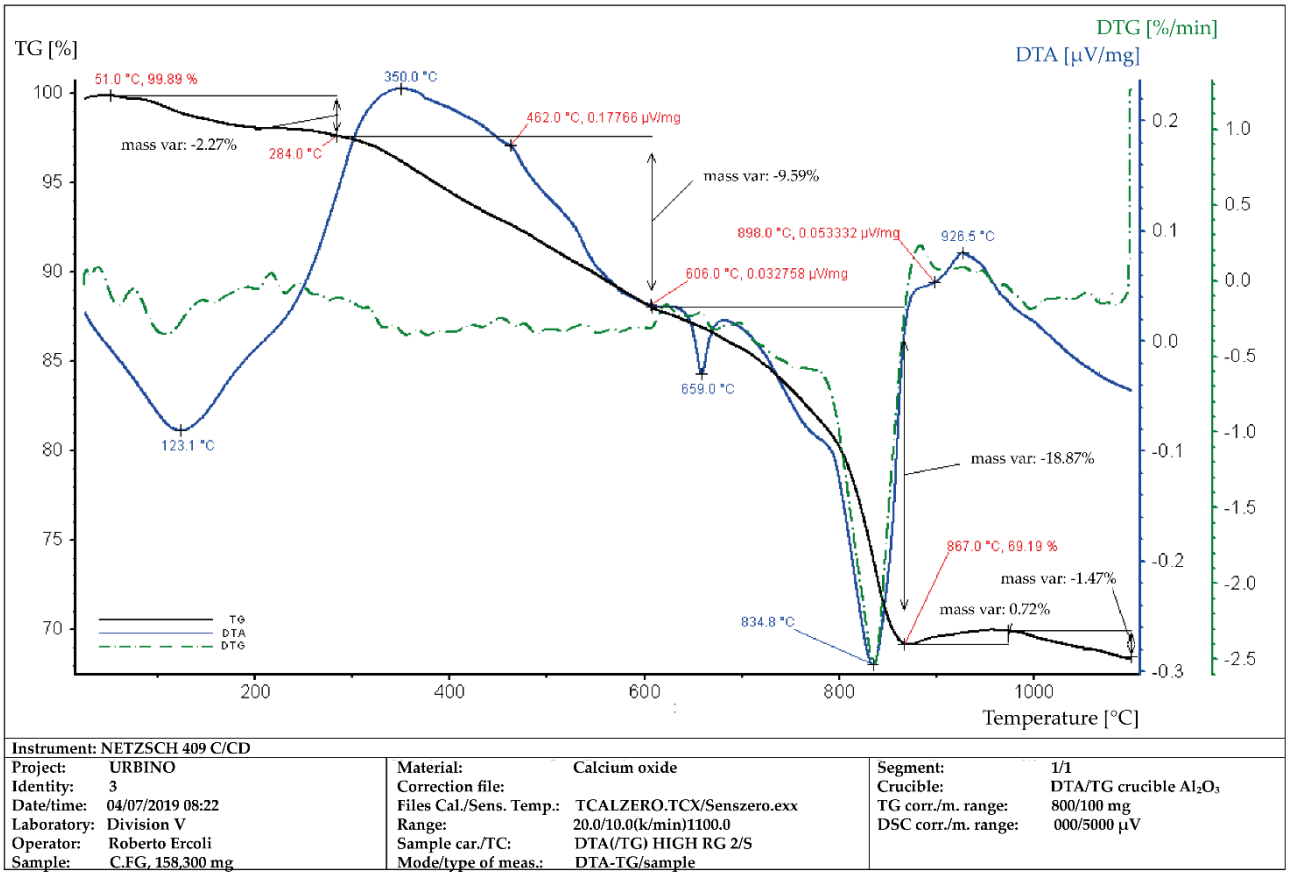

Figure 15. Thermogravimetric analysis of "C.FG" highlights a progressive decrease in weight of about 30.7% up to a temperature of 867°C. Subsequently, there is a slight rise of 0.72% and a negative trend of 1.47%. Unlike the screening, this sample shows a weight loss of 31.45%.

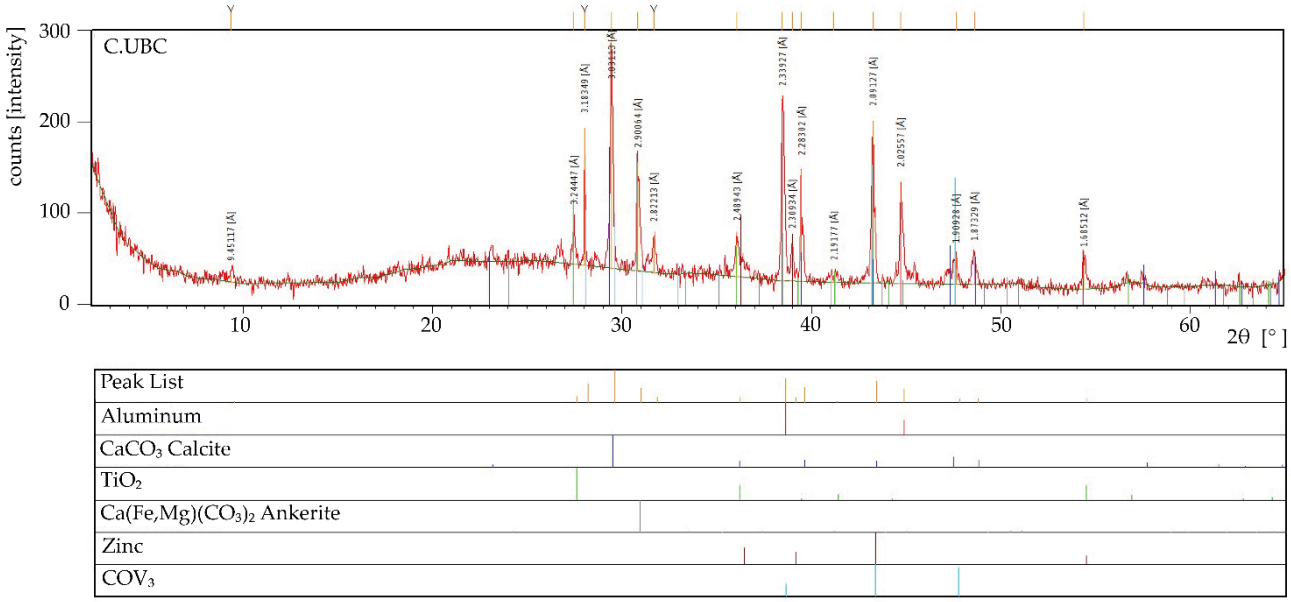

Figure 16. "C.UBC" shows: Aluminum (Al); Calcite ($CaCO_3$); Rutile (TiO_2); Ankerite Ca(Fe, Mg)$(CO_3)_2$; Zinc (Zn); CoV_3.

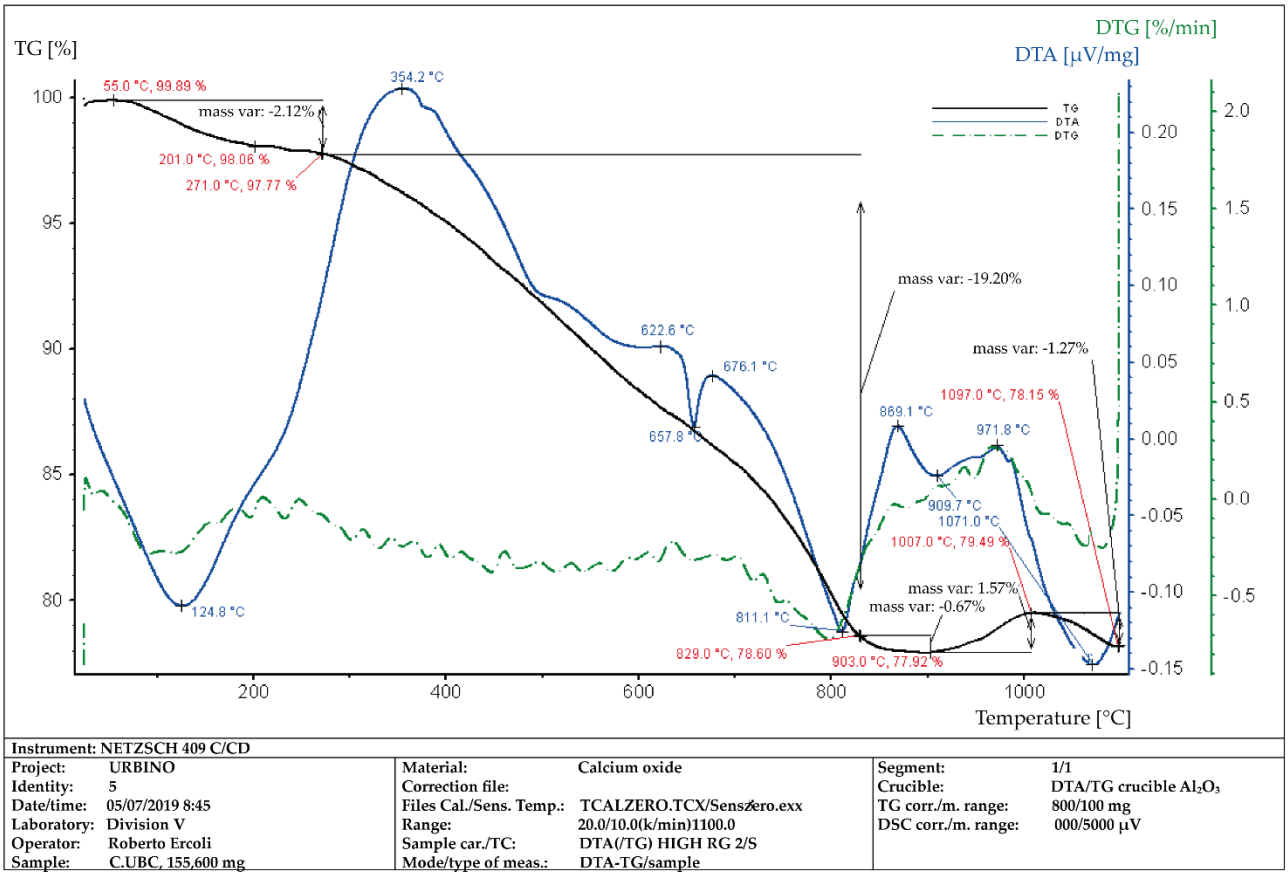

Figure 17. Thermogravimetric analysis of "C.UBC." There is a negative variation of the weight of 21.97% from the TG curve at a temperature range of 55-903°C. As for the "C.FG," there is an increase of 1.57% up to 1007°C and then a negative trend corresponding to 1.47% at 1097°C. Therefore, the cyclone samples probably have a high oxide content and less reactive material.

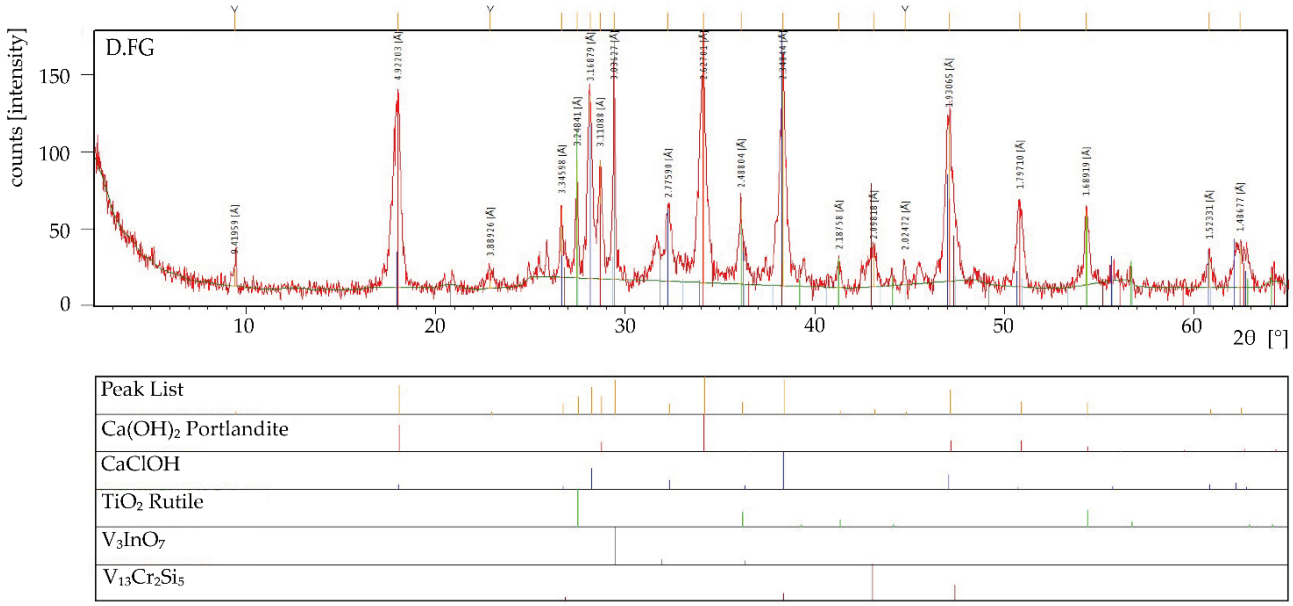

Figure 18. Minerals detected in "D.FG": Portlandite $Ca(OH)_2$; CaClOH; Rutile (TiO_2); and with averse probability V_3InO_7; $V_{13}Cr_2Si_5$.

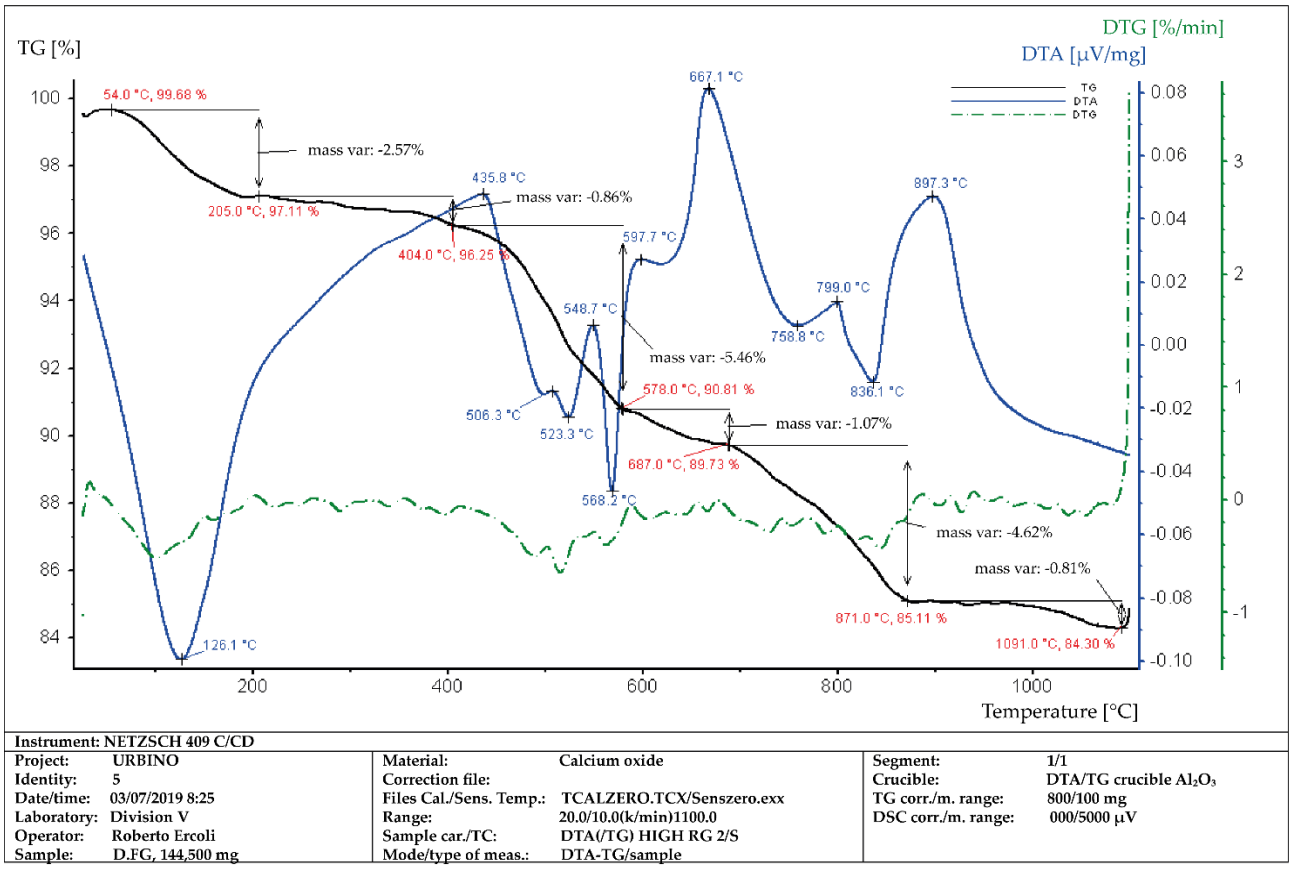

Figure 19. Thermogravimetric analysis of "D.FG" shows a continuous mass decrease without discontinuity of 15.58% through the TG curve.

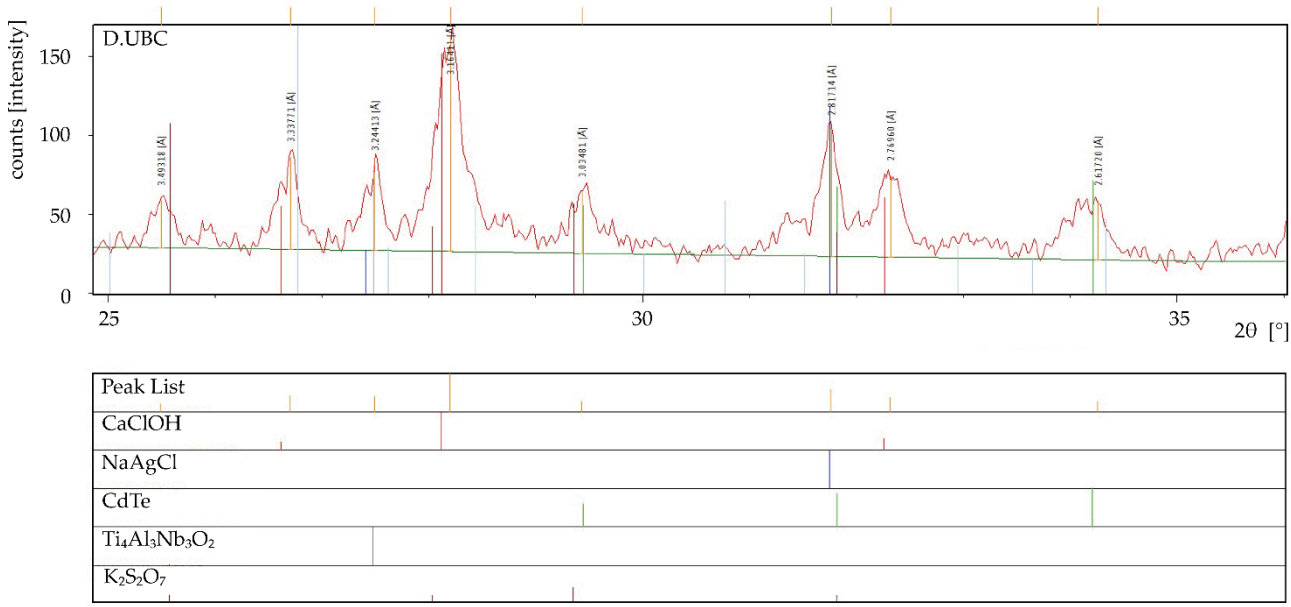

Figure 20. In "D.UBC" there are: CaClOH; $Na_{799}Ag_{201}Cl$; Cadmium Telluride (CdTe); $Ti_4Al_3Nb_3O_2$; Potassium Disulfate $K_2S_2O_7$.

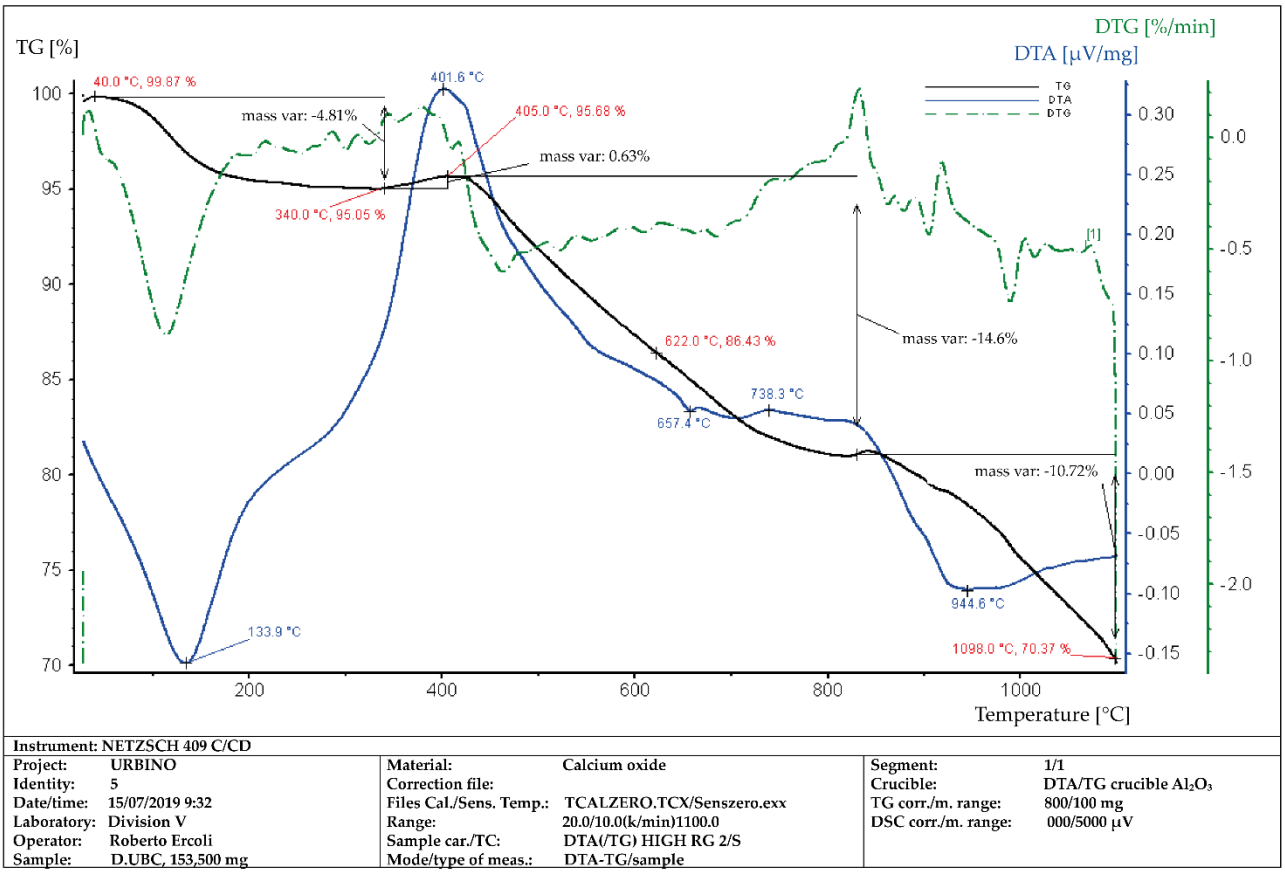

Figure 21. Thermogravimetry shows a negative and discontinuous mass variation of -29.5% at 40-1098°C in "D.UBC."

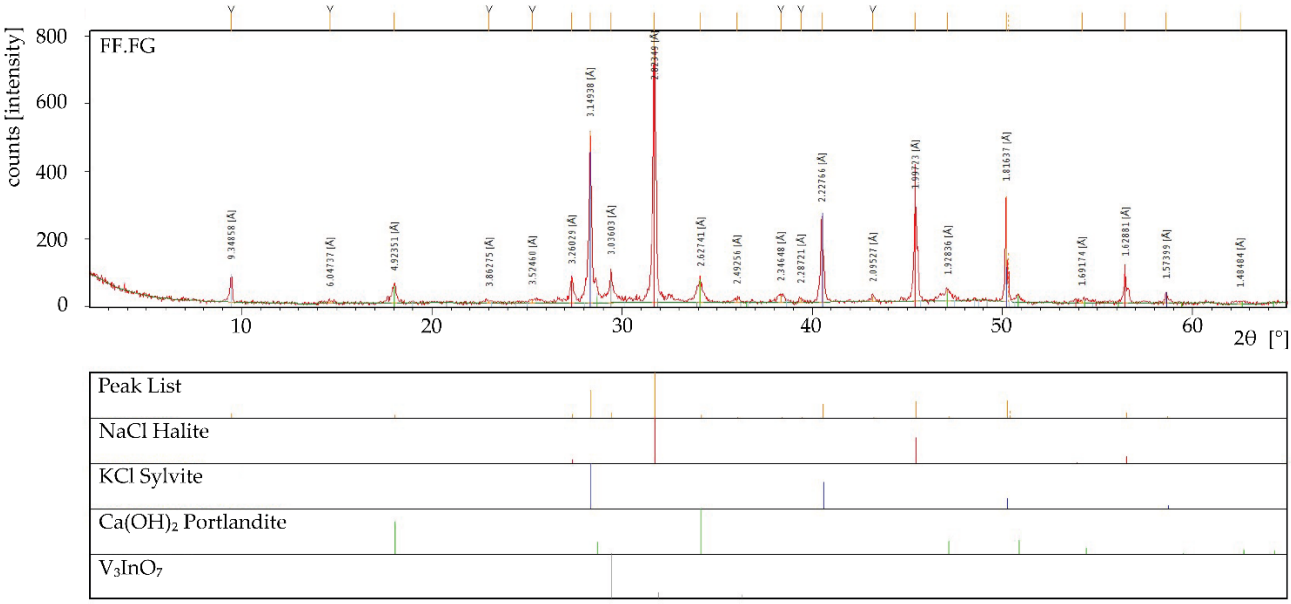

Figure 22. Minerals in "FF.FG" are Halite NaCl; Sylvite $Na_{799}Ag_{201}Cl$; Portlandite $Ca(OH)_2$; V_3InO_7.

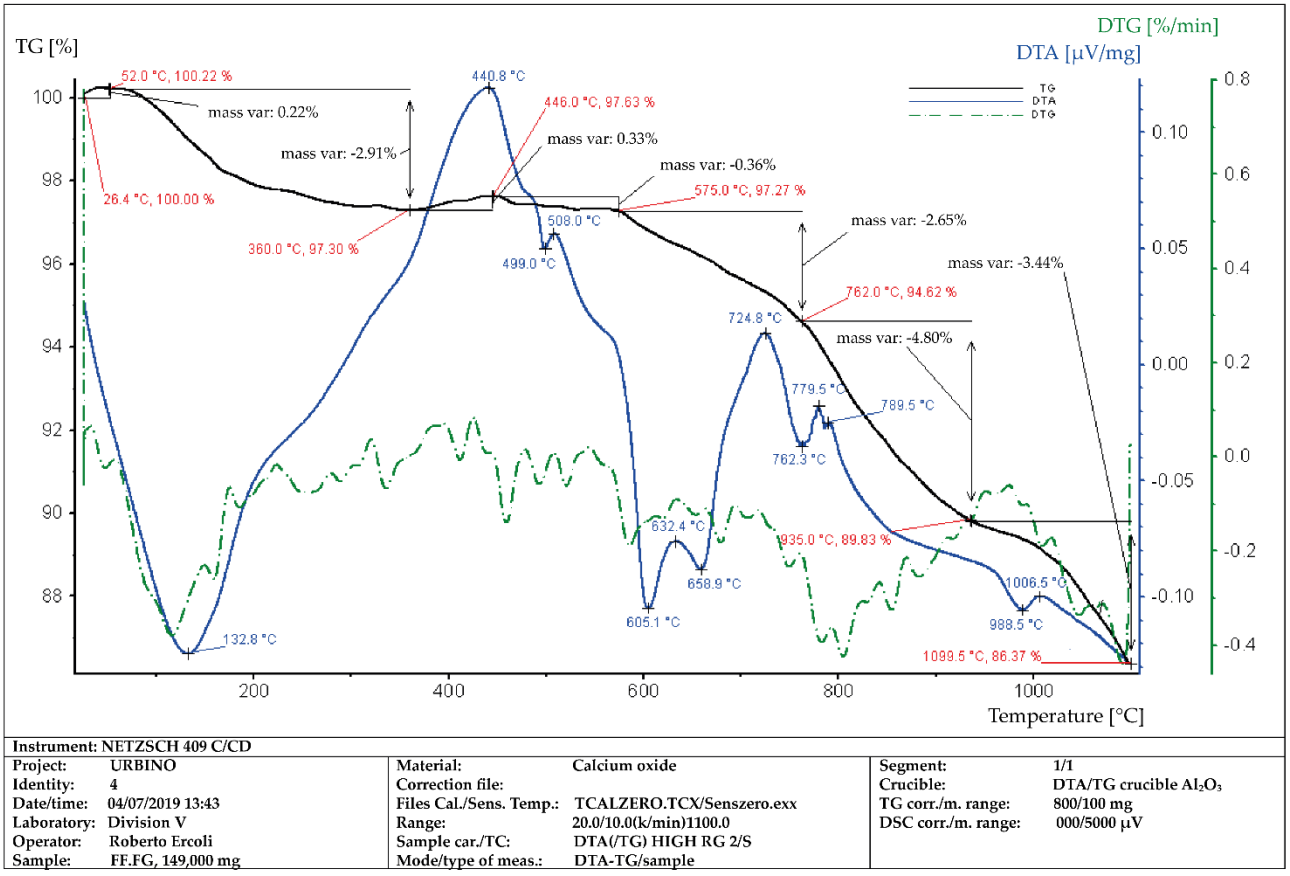

Figure 23. TG curve of "FF.FG" behaves in the same way as D.UBC but has negative mass variation equivalent to 13.85% in the range 52-1099.5°C.

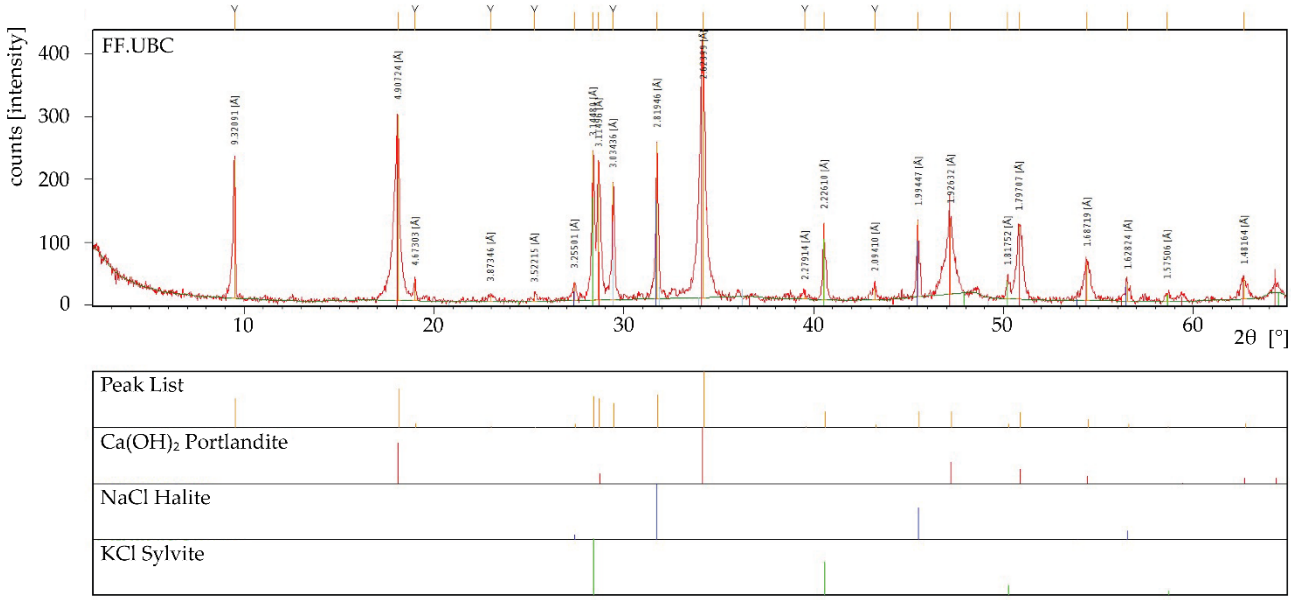

Figure 24. Mineralogical phases of "FF.UBC" are: Portlandite $Ca(OH)_2$; Halite NaCl; Sylvite KCL.

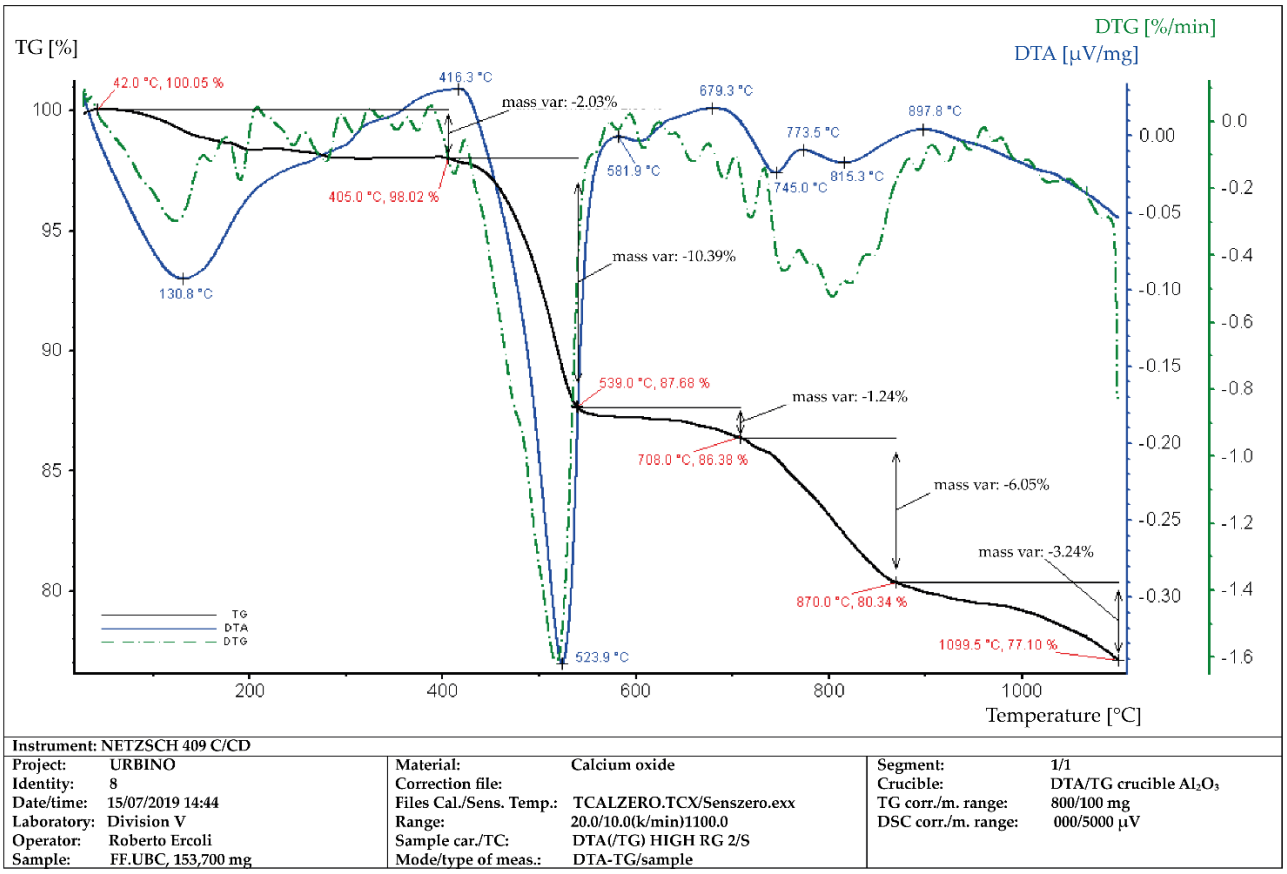

Figure 25. Thermogravimetry of "FF.UBC" shows a fast mass variation due to a negative enthalpy change in the peak at 523.9°C. There is a loss of 10.34% at 405-539°C and a total loss weight of 22.95%.

3.1.3 Chemical Neutralization Process of the Industrial By-products

The industrial by-products of the secondary aluminum industry used as fillers into the geopolymers derive from the (i) screening process, (ii) pyrolysis process, and (iii) fusion process. FG and UBC typologies are from coarse-grained appliance scrapes and municipal waste, the primary materials used for recycling [120]. In particular, the first framework of the research focused on the by-products from the screening processes of the aluminum scraps (by-products with the highest aluminum content) to evaluate the chemical neutralization process and the gas generation. Experiments were planned to completely neutralize the dangerous metallic aluminum-rich by-products, which are highly water-reactive and release significant amounts of gases, including H_2, CH_4, and possibly, minor amounts of CO from the organic components that are still present on the particle surfaces. As they are not suitable for non-hazardous waste landfill disposal, the neutralization process of these by-products from the secondary aluminum industry is mandatory through the appropriate treatments for safe storage and utilization as secondary raw material. The experiments to obtain chemical neutralization were performed by mixing the aluminum-rich by-products with an aqueous alkaline solution in a stainless-steel compact mini-reactor equipped with gas inlet and outlet valves, a liquid sampling valve, and an internal thermocouple. All the experimental runs were carried out at the Istituto di Geoscienze e Georisorse (IGG) of the National Research Council (CNR) and the Dipartimento di Scienze della Terra of the University of Florence.

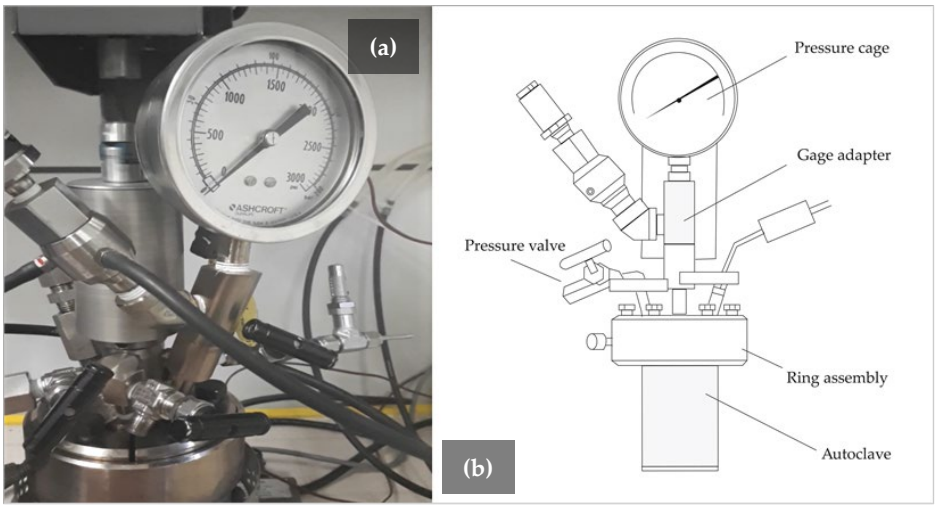

Figure 26. Photo of the mini-reactor used for the experimental runs (**a**). A sketch of the main parts of the mini-reactor assemblage is also shown (**b**).

The mini-reactor assemblage (series 5500 HP T316, Parr Instrument Company; Figure 26) consists of a vessel (autoclave) of ca. 25 mL of volume (ca. 5 cm^2 section area and ca. 4.5 cm height) equipped with a compact and variable-speed stirrer drive, capable of assuring the adequate mixing of the fluid-solid slurry at viscosities up to 10,000 PI (Pa·s). The instrument has gas inlet and outlet valves, a liquid sampling valve, a pressure gauge, a safety rupture disc, and an internal thermocouple. The vessel support also acts as a heater for the reactor. An aluminum block provides an excellent thermal uniformity (a stainless-steel heat shield is mounted for safety around the whole heating block). The maximum working pressure of this reactor reaches 200 bars, while the actual maximum operating temperature (ranging from 225 up to 350°C) depends on the type of gasket seal selected.

To quantify the volume of gases produced by metal oxidation within a specific time frame and to analyze its composition, experimental runs were performed in a mini-reactor by reacting solid metallic aluminum-rich by-products (50% domestic appliances V.FG and 50% beverage cans from urban waste collection materials V.UBC) with an aqueous alkaline solution. Among the experimental parameters, a pH of 11 for the alkaline solution, and a solid-liquid mass ratio of 1.27 were maintained constant during the four different experiments (Parr 174, 202, 204, 212). In contrast, grain size (< 63 μm or 125-250 μm), liquid volume (4 or 8 mL), temperature (40 or 70°C), and durations (24-25 or 94 h) of the experimental runs were varied in order to investigate the influence of these physical parameters on the gas production reactions. The solid samples (mass 10.17-10.18 or 5.10 g; density 2.78 g/mL) and the aqueous alkaline solution were continuously mixed inside the vessel using a magnetic stirrer set to 400-600 rounds per minute (Table 3). The temperature was kept constant during each run until the material residues and gases were sampled and analyzed. In particular, the pressure variation due to gas production was a direct and essential parameter taken into consideration.

Table 3. Physical-chemical parameters of the experimental tests in the mini-reactor.

Tests	Solid Grain Size (μm)	Solid Density (g/mL)	Solid Mass (g)	Liquid Volume (mL)	Liquid (pH)	Solid/Liquid (g/mL)	T (°C)	Stirrer (rpm)	Time (h)
Parr 174	125-250	2.78	10.18	8	11	1.27	70	400	24
Parr 202	125-250	2.78	10.17	8	11	1.27	40	400	24
Parr 204	< 63	2.78	5.10	4	11	1.27	40	400	25
Parr 212	125-250	2.78	10.17	8	11	1.27	70	600	94

3.1.4 Quantification of the Gas Production by G.C. Analysis

Gas sampling was obtained through a needle inserted into the gas-out valve. When sampling the gas, the out valve was slowly opened and, after 2 s, the needle was injected into an Exetainer® vial sealed with a porous membrane. The vial was initially filled with de-aired (by N_2 bubbling for at least 4 h) Milli-Q® water, and, finally, the gas species were analyzed through the gas chromatographic method. The gas that came from the reaction was analyzed for N_2, Ar, O_2, CO, and H_2 contents by using a Shimadzu 15A and a Thermo Focus gas chromatograph equipped with Thermal Conductivity Detectors (TCD), whereas CH_4 was analyzed by using a Shimadzu 14A gas chromatograph equipped with a Flame Ionization Detector (FID).

Before starting the runs, (except for the experiment Parr 174), the aqueous alkaline solutions were degassed through nitrogen "bubbling" for 24 h, whereas the free volume of air inside the vessel of the mini-reactor was displaced by flushing N_2 for 3 min. This gas-displacement or "degassing" procedure was applied to reduce to a minimum any oxygen contamination from the air to constrain the gas production processes. However, effective reactions are theoretical, given the extreme experimental settings: relatively low T, high dynamic pressure, and significantly reduced redox conditions.

The ideal gas law was adopted as a theoretical model to quantify the moles of gases generated during the reaction. The free volume inside the experimental setup was estimated by subtracting the reactant's volume from the vessel's known total capacity.

It was possible to relate each partial pressure of the gas species to the mass amount of gas produced. The reference model (11) developed to quantify gas

moles produced inside the vessel, based on the pressure that is generated, can be expressed by the following expressions:

$$n_g = \frac{P\left(V - V_l - \frac{m_S}{\rho_S}\right)}{0.01\ RT} V_g \quad (11)$$

where: n_g—moles of each gas produced (mol); P—pressure inside the vessel (atm); V—volume of the vessel corresponding to 0.025 (L); V_l—volume of the aqueous solution (L); m_S—mass of the starting material (g); ρ_S—density of the starting material (g/L); V_g—gas percentage quantified by GC analyses (%); R—gas constant (L atm/K mol) = 0.082057; T—temperature (K).

Concerning the way the gases fill the volume inside the vessel, as the gas generation process during the chemical neutralization reaction was progressively optimized, the saturation point was reached more rapidly. The pressure-time curve depends on the metal oxidation rate that reaches its maximum when at least one reagent is wholly consumed.

3.2 Procedure and Binder Materials for the Synthesis of GFs

Several geopolymers were synthesized to investigate the influence of the aluminum-rich by-products and the gas generation on several physical properties: flexural strength, compressive strength, Charpy impact strength, thermal conductivity, specific heat, and thermal diffusivity. The previously described aluminum-rich by-products would play the role of foaming agent, generating H_2-enriched gas pockets inside the geopolymer structure and making the material more porous and therefore lighter.

For this purpose, metakaolin (MK), (Al_2O_3 40.1 wt.%; SiO_2: 54.1 wt.%) has been used during the alkaline activation process as precursor materials, using a potassium hydroxide aqueous solution (pH 11) [121-122]. The reference geopolymer REF-1 consists of MK and silica sand (SA), thus obtaining 76.7 wt.% SiO_2, 20.2 wt.% Al_2O_3, 0.065 wt.% CaO, 0.09 wt% MgO, 0.4 wt.% K_2O, 0.55 wt.% Fe_2O_3, and 0.9 wt.% TiO_2. In addition, chopped carbon fibers are used in the REF-2 material and in all the other geopolymers where aluminum waste materials are used as additives and foaming agents to increase the mechanical properties of the materials.

First, as reported in Figure 27, metakaolin (MK) and alkaline activator (A) were mixed for about 5 min to obtain the homogenous mortar. Next, chopped carbon fibers (CFs) were added to the mortar, mixing for 2 min. After that, silica sand (SA) was added and mixed for 3 min. Finally, each industrial by-products (marked as V.FG, V.UBC, D.FG, D.UBC, C.FG, C.UBC, FF.FG, or FF.UBC) were mixed for 2 min to prepare different geopolymeric foams (Table 4).

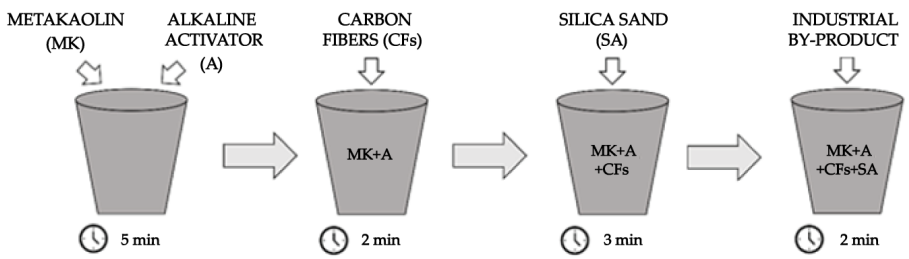

Figure 27. The preparation process of the geopolymer foams.

After the mixing, the geopolymer mortar was decanted into molds with the dimension of 30 × 30 × 150 mm (for the three-point bending test and compression

test), 19 × 20 × 60 mm (for the Charpy impact test), and 100 x 100 x 100 mm (for thermal analysis). These samples were covered using a polypropylene film and cured at room temperature. After 24 h, the samples were pulled out of the molds, wrapped again using a polypropylene film, and kept at room temperature for 28 days before being analyzed.

Table 4. Ratio of the main components used to synthesize the geopolymer foams.

By Weight Ratio (-)				
Metakaolin (MK)	**Alkaline activator (A)**	**Carbon fibers (CFs)**	**Silica sand (SA)**	**Industrial by-products**
1	0.9 MK	0.01 MK	1 MK	0.01 MK 0.02 MK 0.03 MK 0.05 MK 0.1 MK

The inorganic two-component aluminosilicate binder (commercial name: Bausik LK), (České lupkové závody, a.s., Czech Republic) [123] is a two-component aluminosilicate binder based on metakaolin (hereafter MK, part A), (commercial name: Mephisto L05), (grain size D_{50}= 3 μm, D_{90} = 10 μm) activated by an aqueous alkaline activator (part B). The mixing ratio of these two components was taken out according to the manufacturer's requirements. In preparing the binder mixture based on the inorganic polymer, five parts by weight of part A and four parts of B (activator) are usually used. The silica sand (hereafter SA, ST 01/06), (Sklopísek Střeleč, a.s., Czech Republic), (D_{50} = 0.44 mm, D_{90} = 0.63) [124] was used as aggregate. Chopped carbon fibers with an elastic module up to 230 GPa and tensile strength of 3500 MPa [125-129] were used as reinforcing materials. Table 5 shows the chemical composition of the raw materials used in this experiment to produce the geopolymer-based matrix.

Table 5. Density and chemical composition of metakaolin (MK), silica sand (SA), and chopped carbon fibers (CFs).

	ϱ g/cc	**SiO_2 (wt.%)**	**Al_2O_3 (wt.%)**	**TiO_2 (wt.%)**	**Fe_2O_3 (wt.%)**	**K_2O (wt.%)**	**MgO (wt.%)**	**CaO (wt.%)**	**C (wt.%)**
MK	1.95	54.1	40.1	1.80	1.10	0.80	0.18	0.13	-
SA	2.65	99.4	-	-	0.04	-	-	-	-
CFs	1.8	-	-	-	-	-	-	-	>95%

3.3 Methods for the Mechanical Tests

The samples were cured for 28 days before being tested to characterize the mechanical properties of the GFs and the influence of the different by-products used as foaming agents. Figure 28 shows the three main laboratory instruments (at the Department of Material Science, University of Liberec, Czech Republic) and techniques to carry out analyses for mechanical properties: (a) three-point bending test, (b) compressive strength test, (c) Charpy impact test,

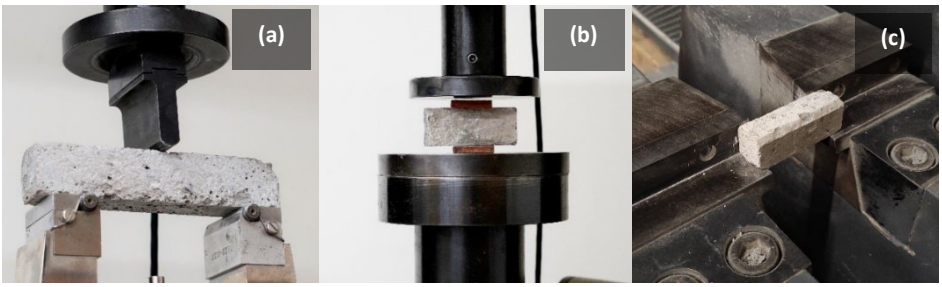

Figure 28. Laboratory techniques to carry out the three-point bending test **(a),** the compressive strength test **(b),** and the Charpy impact test **(c)**.

3.3.1 Three-point Bending Strength

The three-point bending tests were conducted using a universal Testing Mechanical INSTRON Model 4202. Six 30 × 30 × 150 mm samples were tested (Figure 28a). The tests were carried out at room temperature with a crosshead speed of 6.0 mm/min and a span length of 100 mm. The flexural strength (σ_f) was calculated by the equation 12:

$$\sigma_f = 3L \frac{F_{max}}{2bh^2} \ (MPa) \tag{12}$$

where: F_{max} – the maximum applied load indicated by the machine (N); L – the span length (mm); b – the width of the sample (mm); h – the depth of the sample (mm).

3.3.2 Compressive Strength

The compressive tests were performed employing a universal Testing Mechanical INSTRON Model 4202. The broken parts from the samples used in the bending test were used (Figure 28b). In this way, a series of 12 samples with dimensions 30 × 30 × 30 mm were obtained for each composition. The tests were conducted at room temperature with a 6.0 mm/min crosshead speed. The compressive strength (σ_c) was obtained by the equation 13:

$$\sigma_c = \frac{F_{max}}{A_c} \ (MPa) \tag{13}$$

where: A_c – the cross-sectional area of the sample (mm^2).

3.3.3 Charpy Impact Strength

The impact tests were carried out using a PIT-C Series Pendulum Impact Testing Machine (Standards: ISO 148 EN10045) with a pendulum capacity of 150 J, energy losses compensation of 0.23 J, and estimated absorbed energy of 150 J. Six samples with the dimensions 19 × 20 × 60 (mm) were tested (Figure 28c). The tests were performed at room temperature. The impact strength (σ_i) was calculated by the equation 14:

$$\sigma_i = \frac{E}{V} \ (MPa) \tag{14}$$

where: E – the absorbed energy indicated by the machine (J); V – the sample volume (mm^3).

3.4 Methods of the Thermal Measurements

The thermal analyses were performed at the Faculty of Civil Engineering, Mechanics and Petrochemistry, Warsaw University of Technology, Poland, by a microprocessor-controlled commercial instrument with interchangeable probes. A known heat source produced a wave propagating radially into the specimen. The dissipation of electrical energy generates the heat flow through the probes in direct contact with the material, and a serial port RS232C records the signal. The temperature rises linearly with the logarithm of time [130-133]. Semiconductor sensors at specific points on the materials sampled the temperature change in function of time.

According to the 2nd law of thermodynamics, the thermal conductivity (λ) was determined by equation 15:

$$\lambda = \frac{\mathrm{Qd}}{\mathrm{A}\Delta\mathrm{T}}\left(\frac{W}{mK}\right) \tag{15}$$

where: Q – the amount of heat transferred, d – the distance between the two isotherms, A – the surface, and ΔT – the temperature gradient.

The specific heat capacity (C_p) is the heat needed to increase the temperature of 1 gram of a substance by 1°C and is given by:

$$\mathrm{C_p} = \frac{\mathrm{Q}}{\mathrm{m}\Delta\mathrm{T}}\left(\frac{J}{KgK}\right) \tag{16}$$

where: m – the mass.

The thermal diffusivity (α) quantifies the heat transfer rate of the material from the hot side to the cold side, and it was computed by the equation 17:

$$\alpha = \frac{\lambda}{\rho \mathrm{C_p}}\left(\frac{mm^2}{sec}\right) \tag{17}$$

where: ρ – the density of the geopolymer.

CHAPTER 4
RESULTS AND DISCUSSION

4.1 The Experimental Runs in the Mini-Reactor

The chemical neutralization involves the complete oxidation of metals, as it was already known that the interaction of metallic aluminum with an alkaline aqueous solution gives rise to the release of flammable and toxic gases [134]. The current experimental tests were developed to investigate the efficiency of the oxidation of the solid material during reactions to recover hazardous aluminum-rich by-products and to obtain laboratory data for the possible industrialization of a method capable of improving sustainability and workplace safety in secondary aluminum plants. In the experimental tests performed with the mini-reactor, we exactly quantified gas production at a constant solid–aqueous alkaline (pH 11) solution mass ratio of 1.27, allowing for a comparison of the different experimental procedures.

The laser beam analyses that were carried out to characterize the sample grain size (Figure 29) emphasize a unimodal distribution with a surface moment mean D (3, 2) of 17.7 μm, a volume moment mean D (4, 3) of 373 μm, a specific surface area of 0.34 m^2/g, and a uniformity coefficient (Cu) of 0.566.

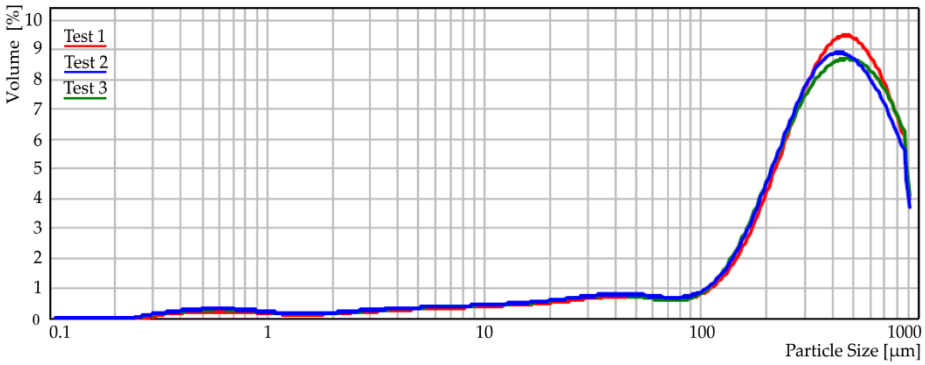

Figure 29. Histogram representing the grain size of the reference sample (50% V.FG and 50% V.UBC). The colored curves (red, blue, and green) represent three different laser beam analyses on the same sample, showing accurate results and low variability.

The XRD analyses of the investigated mixture of by-products, taken as the starting material for the experimental runs, emphasize the presence of aluminum, both in the grain size < 63 μm and 125–250 μm range (Figure 29). Quartz, rutile, cuprite, spinel, and zinc are present in both the above-mentioned granulometric fractions, whereas jamborite and Pb-rich barite were only detected in the sample with a grain size < 63 μm. By contrast, Mg-calcite and chromite only appear in the coarser grain size X-ray diffractogram.

ICP-OES-MS analyses using near-total multi-acid digestion (Table 6) show the presence of aluminum (14 wt.%), Ca (1.15 wt.%), Ti (1.19 wt.%), Fe (1.08 wt.%), Na (1.08 wt.%), Zn (> 1 wt%), Ba (0.92 wt.%), Mg (0.62 wt.%), Cu (> 1 wt.%), Pb (0.26 wt.%), Mn (0.12 wt.%), and K (0.11 wt.%) as major and minor elements. In addition, trace elements, such as Cr (456 ppm), Ni (378 ppm), P (190 ppm), S (200 ppm), Sn (89 ppm), Bi (69 ppm), Co (37 ppm), and Cd (17 ppm) were also detected. The analysis does not report some major elements of the by-products, such as Si.

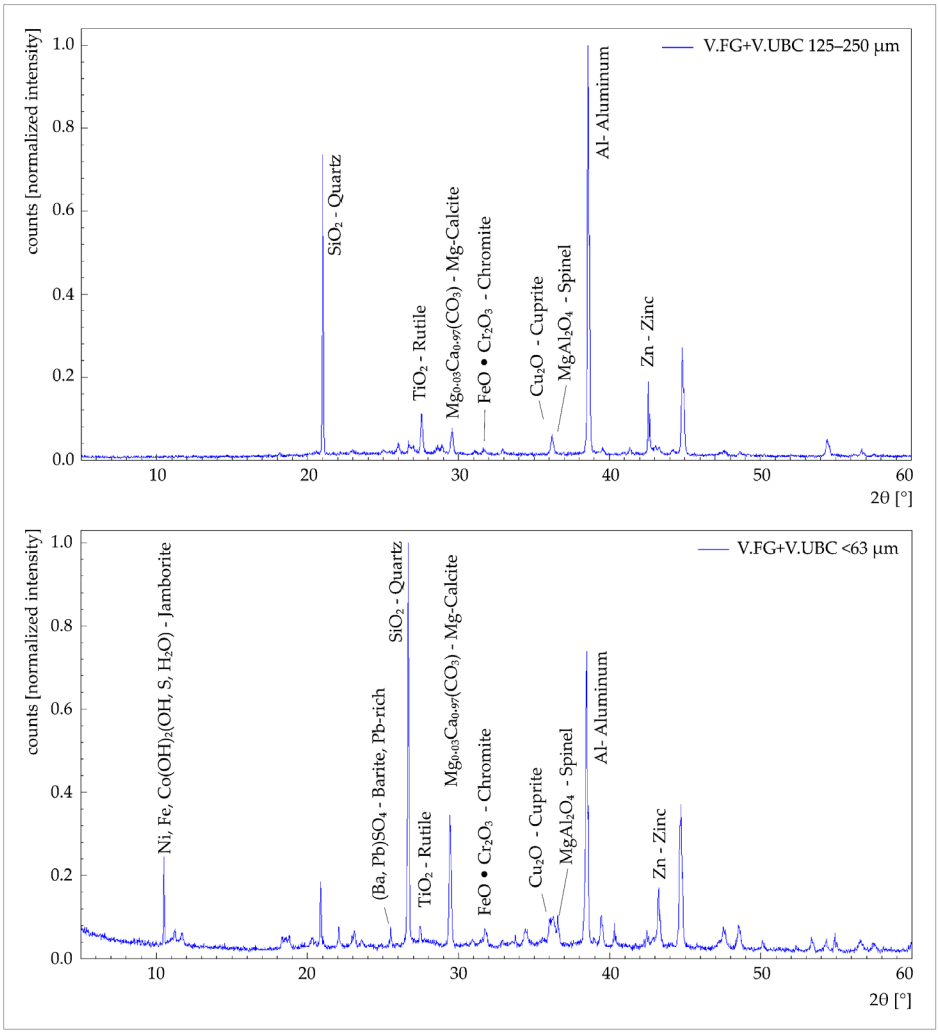

Figure 30. X-Ray diffractograms of the investigated by-products were used for the experimental runs. Grain size < 63 µm (bottom) and the 125-250 µm granulometric range (top) were analyzed. Secondary peaks of the recognized phases are not labeled.

Table 6. ICP-OES-MS chemical composition of the Al-rich by-products mixture used for the experimental runs, using near-total multi-acids digestion. DL—detection limit.

Analyte	ICP-OES (ppm)	DL (ppm)	Analyte	ICP-MS (ppm)	DL (ppm)	Analyte	ICP-MS (ppm)	DL (ppm)
Al	140000	100	Cu	>10000	0.2	As	1.6	0.2
Ti	11900	50	Pb	2640	0.5	W	1.4	0.1
Ca	11500	100	Ni	378	0.2	La	1.1	0.5
Fe	10800	100	Zr	148	0.5	Se	1	1
Na	10800	100	Sn	89.5	0.2	Rb	0.9	0.1
Zn	>10000	2	Bi	68.6	0.01	Y	0.8	0.1
Ba	9240	10	Co	36.7	0.1	Be	0.73	0.05
Mg	6200	100	Ag	28.4	0.01	U	0.6	0.1
Mn	1160	5	Sb	18.7	0.05	Ta	0.48	0.05
K	1100	100	Cd	17.4	0.02	Sc	0.3	0.3
Cr	456	1	Li	12	0.2	In	0.279	0.005
S	200	100	Nb	5.3	0.1	Cs	0.25	0.05
P	190	10	Mo	4.72	0.05	Th	0.2	0.2
Sr	166	0.2	Ce	4.01	0.01	Tl	0.18	0.02
V	33	1	Hf	3	0.1	Ge	0.15	0.05

Total carbon (4.7 wt.%), graphitic carbon (2.5 wt.%), CO_2 (1.5 wt.%), organic carbon (1.6 wt.%), total sulfur (0.32 wt.%), and SO_4 (0.49 wt.%), analyzed by IR, are reported in Table 7. Other organic components (not reported as tables) are negligible, i.e., < 5 ppm for hydrocarbons and < 1 ppm for all the other compounds (VOC included), and measured according to UNI EN 14039:2005, EPA 3580A:1992, and EPA 8015C:2007 [109- 111].

Table 7. IR analysis of total carbon, organic and inorganic carbon, carbon dioxide, total sulfur, and sulfate ion contents of the Al-rich by-products. DL—detection limit.

Analyte	IR (wt.%)	DL (wt.%)
C-Total	4.65	0.01
C-Graphitic	2.5	0.05
C-Organic	1.6	0.5
CO_2	1.48	0.01
Total S	0.32	0.01
SO_4	0.49	0.05

The starting sample contains a nominal amount of 14 wt.% of metallic aluminum, also representing the main crystalline phase recognized by XRD (Figure 30) in the sample before the chemical neutralization.

As pointed out in Figure 31, the oxidation rate of the experiment was monitored for 24 h. During the first experiment, Parr 174, 10.18 g of the sample were used for the reaction at 70°C. Therefore, according to the stoichiometric calculations and assuming that the raw material was not oxidized, the maximum theoretical metallic aluminum content is 1.42 g.

The amount of gas on the total free volume comprises 81.1% H_2, that is, partial pressure of 19.46 bar on the total 24 bar (Table 8), and a mass of 1.83 x 10-2 g; a total of 0.09 bar of methane (7.02 x 10-4g) and 0.01 bar of carbon monoxide (7.86 x 10-5g) were also produced, while O_2, Ar, and N_2 are partially considered as air component gases.

Table 8. Gas chromatography analyses of gas sampled in situ, V_g = volume of each gas produced (%), n_g = moles number of gas, m_g = gas mass (g), P_i = partial pressure of the gas components (bar). The "degassing procedure" reduces O_2 in the experiments Parr 202, 204, and 212.

Experiments		H_2	O_2	Ar	N_2	CH_4	CO	Tot.
Parr 174	V_g (%)	81.1	2.71	0.19	15.6	0.39	0.025	100
	n_g	9.10×10^{-3}	3.04×10^{-4}	2.13×10^{-5}	1.75×10^{-3}	4.38×10^{-5}	2.80×10^{-6}	1.12×10^{-2}
	m_g (g)	1.83×10^{-2}	9.73×10^{-3}	8.52×10^{-4}	4.9×10^{-2}	7.02×10^{-4}	7.86×10^{-5}	7.87×10^{-2}
	P_i (bar)	19.46	0.65	0.05	3.74	0.09	0.01	24
Parr 202	V_g (%)	95.84	0.041	0.056	4.03	0.029	0.005	100
	n_g	2.95×10^{-3}	1.26×10^{-6}	1.72×10^{-6}	1.24×10^{-4}	8.92×10^{-7}	1.54×10^{-7}	3.07×10^{-3}
	m_g (g)	5.94×10^{-3}	4.03×10^{-5}	6.88×10^{-5}	3.47×10^{-3}	1.43×10^{-5}	4.31×10^{-6}	9.54×10^{-3}
	P_i (bar)	5.75	0.002	0.003	0.24	0.002	0.0003	6
Parr 204	V_g (%)	72.53	1.55	0.31	25.6	0.015	0.005	100
	n_g	2.14×10^{-3}	4.56×10^{-5}	9.13×10^{-6}	7.54×10^{-4}	4.42×10^{-7}	1.47×10^{-7}	2.94×10^{-3}
	m_g (g)	4.3×10^{-3}	1.46×10^{-3}	3.65×10^{-4}	2.11×10^{-2}	7.08×10^{-6}	4.12×10^{-6}	2.73×10^{-2}
	P_i (bar)	2.9	0.06	0.01	1.02	0.001	0.0002	4
Parr 212	V_g (%)	95.95	0.031	0.012	3.99	0.021	0.005	100
	n_g	2.6×10^{-2}	8.41×10^{-6}	3.25×10^{-6}	1.08×10^{-3}	5.70×10^{-6}	1.36×10^{-6}	2.71×10^{-2}
	m_g (g)	5.25×10^{-2}	2.69×10^{-4}	1.30×10^{-4}	3.03×10^{-2}	9.14×10^{-5}	3.80×10^{-5}	8.33×10^{-2}
	P_i (bar)	55.65	0.018	0.007	2.31	0.012	0.003	58

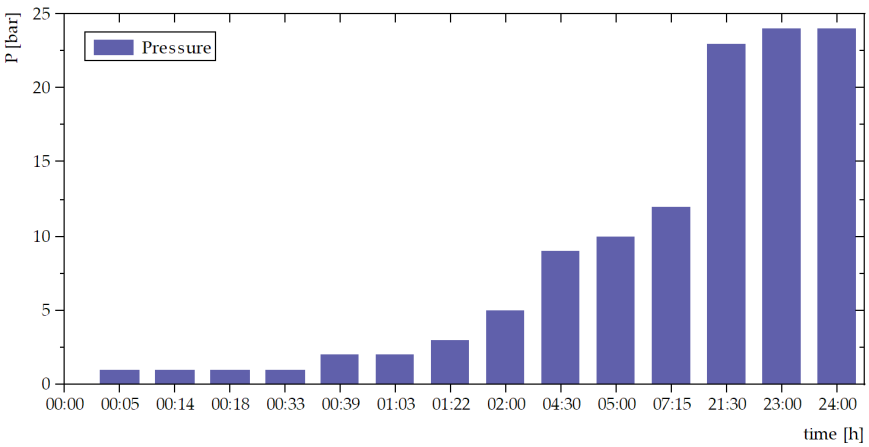

Figure 31. The pressure-time relationship was monitored in the experiment Parr 174. The oxygen content in the air allowed for more rapid exhaustion of the reaction (Al oxidation) than that of the Parr 212 experiment, which took place over a more extended time and developed a more significant pressure.

Parr 202 was run by keeping all experimental parameters constant, except for the temperature, which was lowered to 40°C. By N_2 degassing, less CH_4 and CO were expected to be produced due to the drastic O_2 activity reduction in the vessel free volume. The oxygen concentration in the gas products decreased by 0.9 compared to Parr 174, and 0.002 bar of CH_4 and 0.0003 bar of CO were produced. Thereby, H_2 shows an even higher concentration than Parr 174, contributing to 95.84% of the gas mixture with a partial pressure of 5.75 bar and a mass of 5.94 x 10^{-3}g (Table 8). On the other hand, the hydrogen mass value of the experiment Parr 202 makes it clear that the chemical neutralization decreased as the oxidation rate diminished due to the lower amount of O_2 dissolved.

To test the particle size influence on the reactions, the grain size and the sample mass of the experiment Parr 204 were changed to <63 μm grain size and 5.1 g, respectively, maintaining the temperature at 40°C and employing the same solid-liquid mass ratio as in the previous runs. The measurement reveals a relative decrease in the gas-generation volume. However, assuming that the same sample mass was used during the experiment Parr 202, an increase of 1.44 times the H_2 mass was observed.

A summary of the gas mixtures (mass) generated during all the experimental runs is reported in Figure 32.

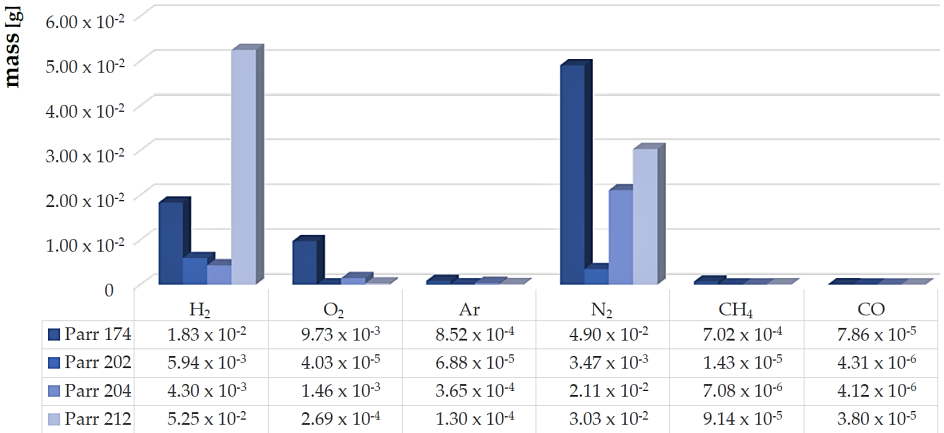

	H_2	O_2	Ar	N_2	CH_4	CO
Parr 174	1.83 x 10^{-2}	9.73 x 10^{-3}	8.52 x 10^{-4}	4.90 x 10^{-2}	7.02 x 10^{-4}	7.86 x 10^{-5}
Parr 202	5.94 x 10^{-3}	4.03 x 10^{-5}	6.88 x 10^{-5}	3.47 x 10^{-3}	1.43 x 10^{-5}	4.31 x 10^{-6}
Parr 204	4.30 x 10^{-3}	1.46 x 10^{-3}	3.65 x 10^{-4}	2.11 x 10^{-2}	7.08 x 10^{-6}	4.12 x 10^{-6}
Parr 212	5.25 x 10^{-2}	2.69 x 10^{-4}	1.30 x 10^{-4}	3.03 x 10^{-2}	9.14 x 10^{-5}	3.80 x 10^{-5}

Figure 32. Graphical view of the gas mixture generated for each of the four experimental runs (Parr 174, 202, 204, and 212) performed in the mini-reactor, separated for the different species.

Experiment 212 produced the highest moles of gas, reaching a pressure of 58 bar. The reaction duration was raised to 94 h (at 70°C) to evaluate the influence of run duration. A more efficient yield shows a partial pressure of 55.65 bar and a gas mass production of 5.25 x 10^{-2} g of hydrogen (Table 8).

Thermogravimetric analysis on the starting material showed a mass increase compared to that obtained by the experimental runs, such as the Parr 174 (Figure 33), and perfectly agrees with the hydrogen production results. The reference by-product from the screening processes underwent a mass increase of 1.07 times, whereas the mass increase for its correspondent experimental residuals was only 98.54 wt.% out of 150.3 mg. Definitively, this difference between the starting sample and the experimental residue can be ascribed mainly to the oxidation that occurred during the reactions in the mini-reactor during the experimental test. As seen in the thermogravimetric analysis, moisture and structural water are released at a temperature of 59°C and 133.5°C, respectively. The system releases energy into the environment at higher temperatures while losing mass. At the temperature of 460.1°C, the system shifts to endothermic after the pyrolysis of organic compounds, and at 572.9°C, approaching the melting temperature of aluminum, the material becomes more reactive. At 657.2°C, around 7.50% of the initial mass is lost, and there is enough energy to start melting. The system gives energy until 906.9°C, where it reverses its behavior. The oxidation process (18) is, until 1099°C, according to the primary reaction:

$$2Al + 1.5O_2 \rightarrow Al_2O_3 \qquad (18)$$

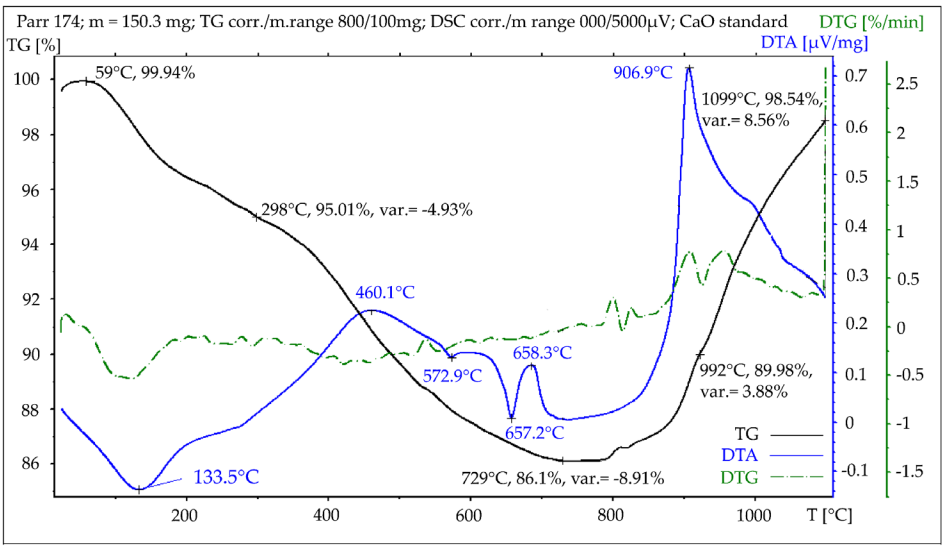

Figure 33. The temperature-time curve monitored the oxidation rate of the experiment Parr 174 residual material. By recording the weight of the sample as a function of temperature (or time), a step thermogravimetric (TG) curve is obtained. The differential thermal curve (DTA) provides exothermic and endothermic reactions. The differential thermogravimetric (DTG) curve allows the highlighting of slight variations of the TG slope, that is, the variation of transformation speed that the TG cannot detect.

The XRD analysis performed on the residual material after the Parr 204 experimental test shows the absence of metallic aluminum, emphasizing the completion of the oxidative processes (Figure 34). The main phases detected by XRD are represented by rutile, magnesium calcite, jamborite, chromite, barite, quartz, zinc, cuprite, and spinel.

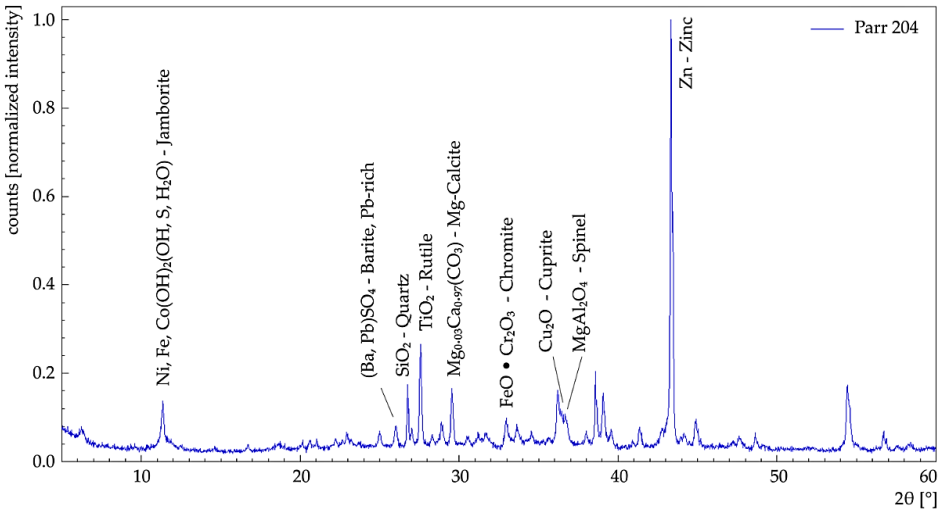

Figure 34. X-ray diffractogram of the residual (chemically neutralized) product after the Parr 204 experiment. Secondary peaks of the detected phases are not labeled.

The total C, S, and C-graphitic contents of the residual material of the Parr 212 experiment are lower than those of the initial starting material: i.e., 97% of the C-total, 61.6% of the C-graphitic, and 87.5% of the total S (Table 9). By contrast, the C-organic increased (137.5%), as did CO_2 and SO_4 (179% and 171.4%, respectively). Therefore, the increase of the organic components CO_2 and SO_4 is remarkable during the chemical neutralization procedure.

Table 9. Comparative IR analyses of carbon and sulfur species between the starting material by-products and residual material after the Parr 212 experiment.

Analyte	V. FG + V. UBC (wt.%)	Parr 212 (wt.%)	DL (wt.%)
C-total	4.65	4.44	0.01
C-graphitic	2.5	1.54	0.05
C-organic	1.6	2.2	0.5
CO_2	1.48	2.65	0.01
Total S	0.32	0.28	0.01
SO_4	0.49	0.84	0.05

The generated mixture of gas during the experiments at the mini-reactor was primarily identified as hydrogen and minor components that are represented by methane and carbon monoxide, with the temperature, pH, and time of the experiments being the main relevant driving factors of the neutralization reaction of the metallic aluminum-rich industrial by-products [135]. Experimental results show a pretty efficient reaction leads to the highest gas production at 70°C, with a coarse grain size starting material (125–250 μm; Parr 212 run), using a high-stirring speed and a run duration of 94 h. Nevertheless, according to the XRD analysis, the complete chemical neutralization is reached in the experiment Parr 204 with a grain size of < 63 μm, thus emphasizing the strong influence of particle size on the reaction process.

The present discussion will also address the relationship between the Loss on Ignition (LOI) of the aluminum-rich by-products sample and the residual materials after the chemical neutralization in the mini-reactor. The LOI value is obtained as the mass variation of the sample after heating at 1000°C for 2 h. This process involves losing volatile components (H_2O, hydrates, CO, and CO_2 groups). Therefore, the mass increase represented by negative LOI values is a strong indication of the presence of metallic content that can be evaluated by separating the contribution of different components, such as (i) hygroscopic water (H_2O, at 105°C), (ii) the contribution of water to the crystalline structure

of the mineral phases (H_2O^+, at 700–950°C), (iii) the decomposition of organic matter (at 400°C), and (iv) the decarbonization of the carbonates (at 350°C for magnesium carbonates and 825°C for calcium carbonates). Indeed, it can be inferred that the most significant increase of the mass by LOI is due to the oxidation process of metallic aluminum. At a temperature higher than its melting point (660.3°C), Al becomes more reactive with O_2 as a phase state change occurs. LOI values of (i) the by-products sample of the screening processes and (ii) the observed residues of the four experimental runs have been compared in Figure 35.

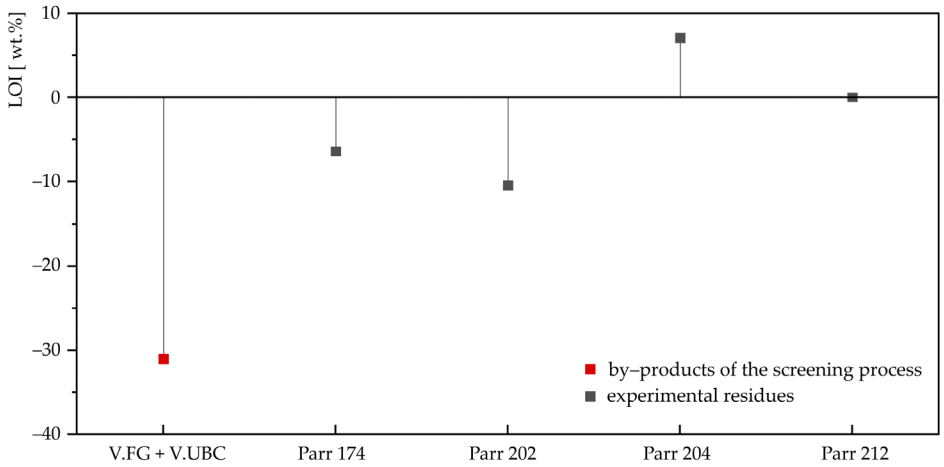

Figure 35. LOI values of the industrial by-products of the screening processes and residues from the experimental runs.

The starting material (50% V.FG + 50% V.UBC), having an aluminum content of 14 wt.% and an Al phase detected by XRD, shows a negative Loss on Ignition −31.05 wt.%. By contrast, the residual products from the experimental runs (Parr 174, 202, 204, 212) have LOI of −6.4 wt.%, −10.4 wt.%, 7.0 wt.%, and 0.04 wt.%, respectively. It is worth noting that the experiments Parr 204 and 212, which produced the highest amount of gas, do not show negative LOIs. The highest positive LOI value (7.0 wt.%) of the Parr 204 residue also matches the absence of metallic aluminum, as proven by XRD phase composition (Figure 34). Despite the loss of volatiles, mainly H_2O and CO_2, the starting by-products sample (V.FG + V.UBC) increases its mass due to oxidation (very high negative LOI; Figure 35), whereas when the more chemical neutralization during the experiments occurs, the more final by-product residues show positive LOI values. LOI ≥ zero seems to represent a good indicator of by-products that have virtually become non-reactive due to the absence of metallic aluminum.

The present experimental research emphasizes the feasibility of hydrogen production (that could be potentially stored and/or reused as fuel) from the secondary aluminum by-products (waste) coming from the screening processes of scraps, mainly beverage cans and domestic appliances. The hydrogen recovery could represent an essential energetic (fuel) integration for the melting furnaces in the same secondary aluminum plants. Alternatively, the gaseous mixture production from the metallic aluminum by-products could be mixed with a silica component (e.g., from the glass industry), allowing for the production of foamed geopolymers, with pockets of hydrogen trapped in pores throughout the body of a material with high strength and hardness, which is suitable not only as an insulation material but also for industrial applications. It is worth noting that a fundamental physical characteristic of geopolymers is their resistance to mechanical, thermal, and atmospheric degradation, and they are also suitable for entrapping polluting and toxic substances [136].

The creation and implementation of registries of Al-rich wastes and by-products [137], coupled with platforms such as the Bureau of International

Recycling [138], will enormously help the possibility of acting as matchmaking between (i) producers/holders and (ii) potential industries seeking secondary Al raw materials to enhance the sustainability and performance of their products (e.g., as filler or for cement binders). Suppose the present laboratory procedure of chemical neutralizing the metallic aluminum-rich by-products will be transferred to an industrialized process. In that case, the recovered residual material could undoubtedly be recorded in such registries, and therefore the most appropriate use and synergies between different industrial sectors and chains could be easily found.

4.2 Physical Properties of Geopolymer Foams

The reactivity of the industrial by-products used as fillers and foaming agents during the geopolimerization can be mainly attributed to the chemical composition (metallic aluminum content), mineralogy, and grain size [139-140]. These features influence the physical characteristics of the geopolymers thanks to the porosity formed during the metallic aluminum oxidation [141-145].

4.2.1 Mechanical Properties of GFs

Mechanical properties are the most relevant parameters for evaluating geopolymer performances and understanding the applications [146-147]. It is highlighted that the aluminum-rich by-products decrease the flexural and tensile strengths of geopolymers during the consolidation process. On the other hand, the impact strengths mainly increase.

We can observe a decrease in the bending and compressive strengths of REF-2 (with respect REF-1) where σ_f and σ_c are 6.25 ± 0.20 MPa and 44.02 ± 2.08 MPa, respectively. On the other hand, the Charpy impact strength value of REF-2 increases two times the REF-1 because of the use of chopped carbon fibers, which, as mentioned, reinforce the geopolymer structure.

Figure 36a,b illustrates the gas bubbles distribution of the geopolymer foam: FF.UBC-3 appears not homogeneous and characterized by different size holes. The areas of these bubbles were quantitatively estimated on the breaking section after the three-point bending tests by an open-source software analysis (ImageJ), applying a color threshold for the analysis. 13.2% of the total surface (900 mm^2) consists of bubbles that, of course, define the overall geopolymer structure and shape the surface along which the break occurs.

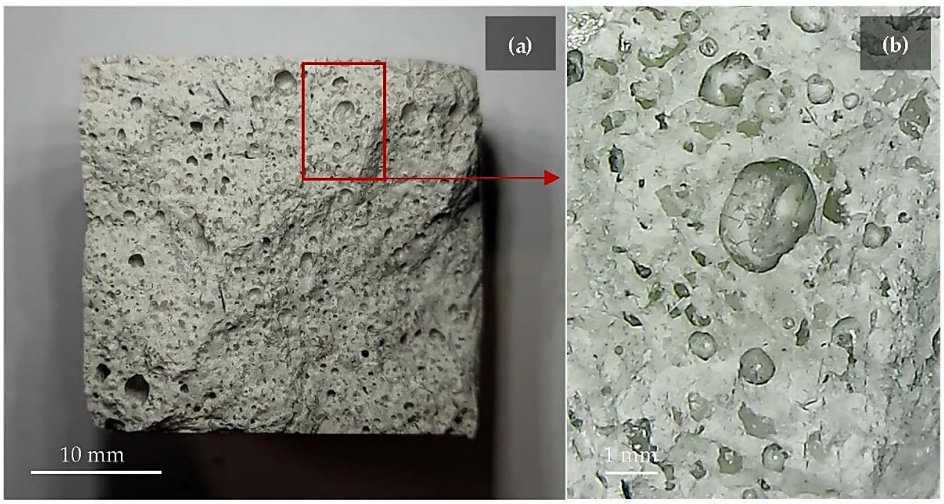

Figure 36. (**a**) FF.UBC-3 section (30 × 30 mm) and (**b**) magnified image of bubbles.

Table 10. Summary of the mechanical properties (Three-point bending test, σ_f; Compressive strength test, σ_c; Charpy impact test, σ_i) of the synthesized geopolymer foams, with the addition of various percentages (1, 2, 3, 5, 10 wt% to MK) of different by-products of the secondary aluminum industry coming from the screening (V.FG and V.UBC), pyrolysis (D.FG and D.UBC), abatement dust (C.FG and C.UBC) and fusion (FF.FG and FF.UBC) processes.

	Geopolymers	**Three-point bending strength**	**Compressive strength**	**Charpy impact strength**
	By-products wt.%*(MK)	**σ_f (MPa)**	**σ_c (MPa)**	**σ_i (MPa)**
REF-1	-	7.04 ± 0.31	46.24 ± 1.84	0.17 ± 0.01
REF-2	-	6.25 ± 0.20	44.02 ± 2.08	0.35 ± 0.02
V.FG-	1	4.41 ± 0.11	16.56 ± 0.71	0.32 ± 0.01
	2	3.87 ± 0.19	15.75 ± 0.85	0.44 ± 0.01
	3	3.61 ± 0.17	10.98 ± 0.54	0.35 ± 0.02
	5	2.62 ± 0.12	7.44 ± 0.34	0.28 ± 0.01
	10	1.78 ± 0.08	5.73 ± 0.13	0.29 ± 0.01
V.UBC-	1	4.25 ± 0.13	8.08 ± 0.22	0.39 ± 0.01
	2	3.05 ± 0.13	5.96 ± 0.26	0.36 ± 0.02
	3	2.26 ± 0.11	5.19 ± 0.24	0.30 ± 0.01
	5	2.59 ± 0.08	3.95 ± 0.08	0.30 ± 0.01
	10	1.55 ± 0.08	3.56 ± 0.05	0.26 ± 0.01
D.FG-	1	6.04 ± 0.19	22.96 ± 0.96	0.69 ± 0.03
	2	4.81 ± 0.22	17.57 ± 0.06	0.61 ± 0.02
	3	4.05 ± 0.20	12.00 ± 0.50	0.50 ± 0.03
	5	2.69 ± 0.12	9.39 ± 0.32	0.36 ± 0.01
	10	3.14 ± 0.12	10.28 ± 0.40	0.38 ± 0.004
D.UBC-	1	5.78 ± 0.28	26.58 ± 1.32	0.63 ± 0.02
	2	5.31 ± 0.24	23.35 ± 0.63	0.71 ± 0.03
	3	4.46 ± 0.19	16.99 ± 0.80	0.53 ± 0.01
	5	3.25 ± 0.05	9.08 ± 0.36	0.51 ± 0.01
	10	2.24 ± 0.11	4.27 ± 0.19	0.30 ± 0.01
C.FG-	1	2.09 ± 0.08	6.67 ± 0.30	0.28 ± 0.01
	2	2.18 ± 0.08	5.90 ± 0.25	0.26 ± 0.01
	3	1.71 ± 0.08	3.27 ± 0.06	0.29 ± 0.002
	5	2.58 ± 0.07	4.94 ± 0.19	0.31 ± 0.01
	10	2.23 ± 0.01	4.05 ± 0.09	0.35 ± 0.02
C.UBC-	1	3.09 ± 0.09	6.35 ± 0.18	0.29 ± 0.001
	2	2.17 ± 0.09	4.24 ± 0.17	0.26 ± 0.01
	3	1.99 ± 0.08	3.66 ± 0.16	0.19 ± 0.003
	5	1.96 ± 0.07	3.46 ± 0.13	0.26 ± 0.01
	10	1.74 ± 0.08	2.96 ± 0.13	0.31 ± 0.01
FF.FG-	1	6.18 ± 0.25	27.03 ± 1.03	0.20 ± 0.01
	2	5.03 ± 0.20	20.60 ± 0.88	0.35 ± 0.02
	3	3.91 ± 0.15	14.44 ± 0.65	0.42 ± 0.01
	5	3.71 ± 0.07	10.64 ± 0.49	0.35 ± 0.01
	10	2.15 ± 0.10	6.40 ± 0.27	0.31 ± 0.005
FF.UBC-	1	7.48 ± 0.22	44.67 ± 0.31	0.54 ± 0.02
	2	6.21 ± 0.23	42.05 ± 2.07	0.31 ± 0.004
	3	6.24 ± 0.31	40.53 ± 1.85	0.30 ± 0.01
	5	6.77 ± 0.16	39.47 ± 1.88	0.34 ± 0.004
	10	5.01 ± 0.23	27.92 ± 0.84	0.44 ± 0.003

4.2.2 GFs from the Aluminum-rich By-products of the Screening Processes

The maximum detected values of the three-point bending and compressive strengths are identified in V.FG-1 (σ_f = 4.41 ± 0.11 MPa; σ_c = 16.56 ± 0.71 MPa) and V.UBC-1(σ_f = 4.25 ± 0.13 MPa; σ_c = 8.08 ± 0.2 MPa), following a decreasing trend by adding higher filler contents. The Charpy impact strength is improved than the reference geopolymers by adding 2 and 3 wt.% MK of V.FG (σ_i = 0.44 ± 0.01 MPa; 0.35 ± 0.02 MPa) and 1 and 2 wt% MK of V.UBC (σ_i = 0.32 ± 0.01 MPa; 0.4 ± 0.01 MPa) (Figure 37).

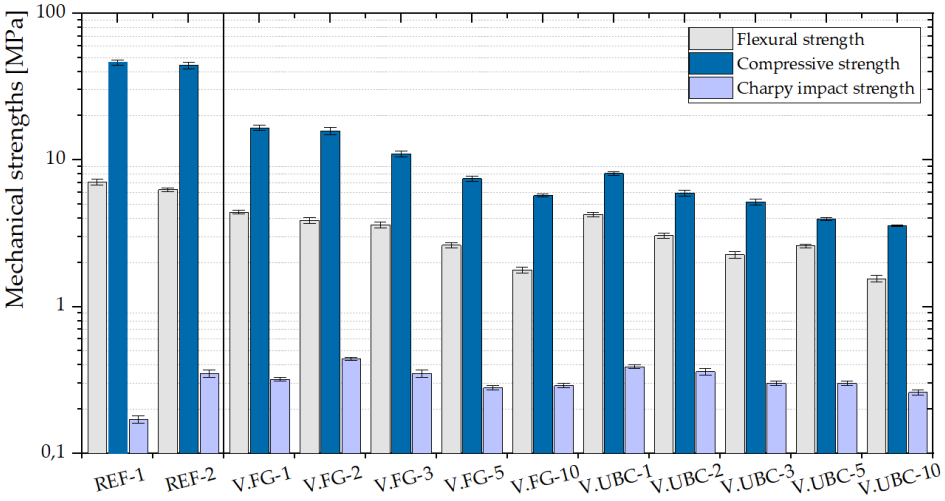

Figure 37. Mechanical properties of the GFs, V.FG, and V.UBC, with the addition of various percentages of these aluminum-rich by-products (1, 2, 3, 5, 10 wt.% of MK). Reference standard geopolymers (REF-1 and REF-2) are also shown.

4.2.3 GFs from the Aluminum-rich By-products of the Pyrolysis Processes

The aluminum contents of the pyrolysis by-products D.FG and D.UBC are 32204 and 40198 ppm, respectively. As shown in Figure 38, the mechanical strengths are better performed than the scraps of the screening processes. In this case, the impact strength of D.FG-1 is around four times higher than the reference sample REF-1 and two times more than REF-2. Moreover, also D.UBC-2 shows the same behavior with a σ_i of 0.71 MPa. This increase in performance is directly related to the aluminum content and finer-grained and more homogeneous particles of this kind of aluminum-rich by-products.

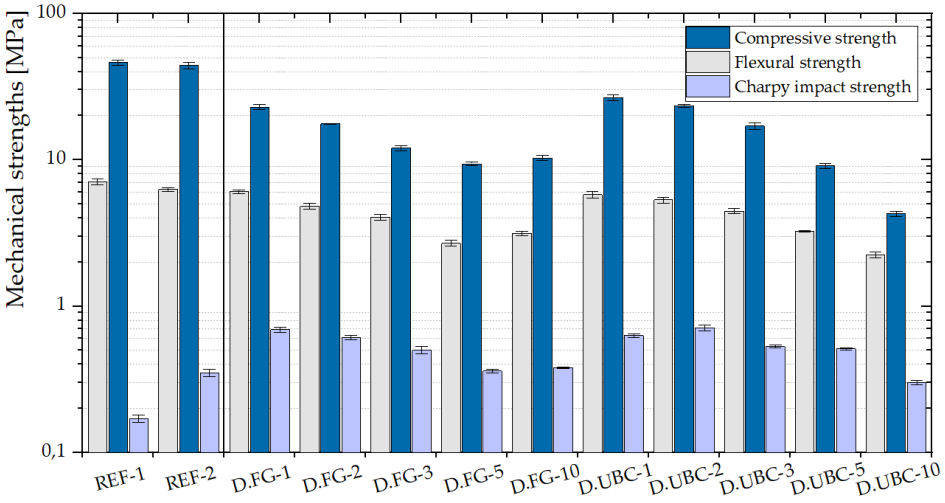

Figure 38. Mechanical properties of the GFs, D.FG, and D.UBC, with the addition of various percentages of these aluminum-rich by-products (1, 2, 3, 5, 10 wt.% of MK). Reference standard geopolymers (REF-1 and REF-2) are also shown.

4.2.4 GFs from the Aluminum-rich By-products of the Dust Abatement Systems

C.FG and C.UBC raw materials have an aluminum content of 73296 and 62333 ppm. It is observable a conspicuous decrease of the flexural and compressive strengths (Figure 39) against the reference materials (REF-1, and REF-2), and also the impact strength compared to the standard with chopped carbon fibers, being the aluminum content around two times the one within geopolymers synthesized by the foaming agents D.FG – D.UBC.

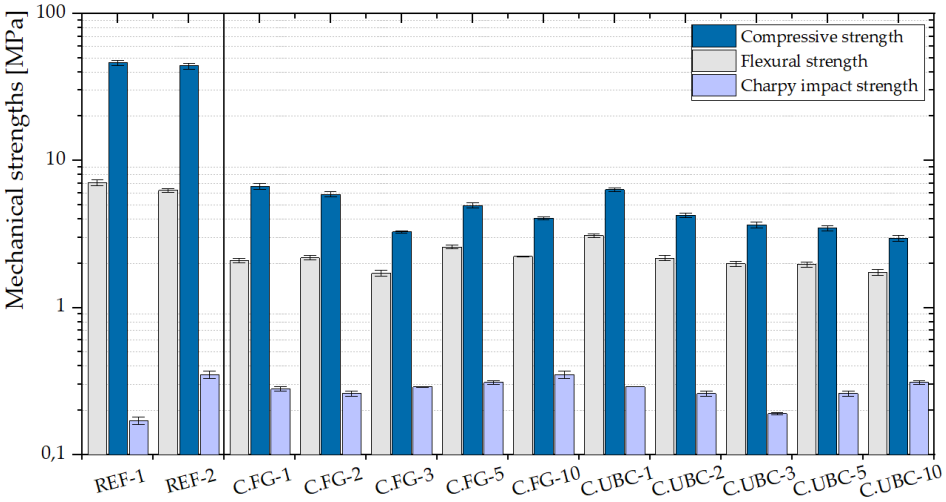

Figure 39. Mechanical properties of the GFs, C.FG, and C.UBC, with the addition of various percentages of these aluminum-rich by-products (1, 2, 3, 5, 10 wt.% of MK). Reference standard geopolymers (REF-1 and REF-2) are also shown.

4.2.5 GFs from the Aluminum-rich By-products of the Fusion Processes

The best mechanical performances for the geopolymers obtained with the addition of the by-products of the fusion processes (Figure 40) are found in FF.UBC where compressive, flexural, and Charpy impact strengths are almost similar to the reference samples. In particular, FF.UBC-1 is the best GF in term of mechanical performance with $\sigma_f = 7.48 \pm 0.22$ MPa; $\sigma_c = 44.67 \pm 0.31$ MPa; $\sigma_i = 0.54 \pm 0.02$ MPa. We can conclude that FF.UBC slag, having the lowest aluminum content (6636 ppm) is the most suitable by-product to be trapped in the geopolymeric structure keeping unchanged the fundamental mechanical properties of the reference geopolymers.

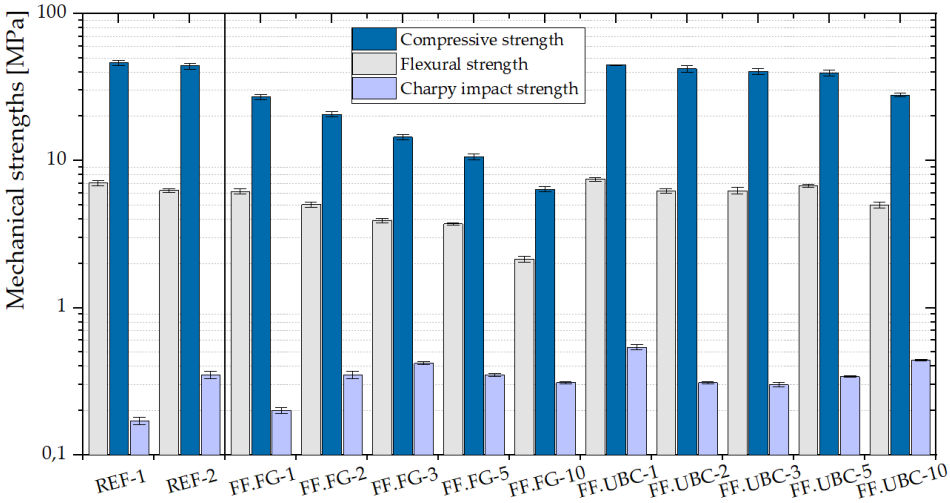

Figure 40. Mechanical properties of the GFs, FF.FG, and FF.UBC, with the addition of various percentages of these aluminum-rich by-products (1, 2, 3, 5, 10 wt.% of MK). Reference standard geopolymers (REF-1 and REF-2) are also shown.

4.2.6 Densities versus Thermal Conductivity, Diffusivity, and Specific Heat

The density (ρ) and the thermal conductivity (λ), diffusivity (α), and specific heat (C_p) of the obtained geopolymer foams are reported in Table 11. A clear relationship between the density and the thermal properties can be observed.

Table 11. Summary of density (ρ, g/cc) and thermal properties (thermal conductivity, λ; specific heat, C_p; diffusivity, α) of the GFs, with the addition of various percentages (1, 2, 3, 5, 10 wt% of MK) of by-products from the screening (V.FG and V.UBC), pyrolysis (D.FG and D.UBC), dust abatement (C.FG and C.UBC) and fusion (FF.FG and FF.UBC) processes

Geopolymer	By-products wt.%*(MK)	ρ (g/cc)	λ (W/mK)	C_p (J/KgK)	α (mm^2/sec)
REF-1	-	1.81 ± 0.06	1.2981 ± 0.0606	1.8518 ± 0.0855	0.7056 ± 0.0295
REF-2	-	2.00 ± 0.08	1.4607 ± 0.0167	1.9078 ± 0.0194	0.7667 ± 0.0124
V.FG-	1	1.75 ± 0.03	0.8740 ± 0.0414	1.5828 ± 0.0206	0.5447 ± 0.0256
	2	1.78 ± 0.05	0.8330 ± 0.0050	1.4794 ± 0.0649	0.5639 ± 0.0216
	3	1.62 ± 0.06	0.6947 ± 0.0345	1.4758 ± 0.0065	0.4709 ± 0.021
	5	1.44 ± 0.01	0.5239 ± 0.0039	1.5815 ± 0.0166	0.3302 ± 0.0058
	10	1.30 ± 0.02	0.5249 ± 0.0190	1.5446 ± 0.0495	0.3426 ± 0.0145
V.UBC-	1	1.73 ± 0.03	0.8304 ± 0.0199	1.5828 ± 0.0692	0.5264 ± 0.0277
	2	1.38 ± 0.05	0.4424 ± 0.0183	1.5195 ± 0.0219	0.2969 ± 0.0139
	3	1.46 ± 0.07	0.5723 ± 0.0237	1.5245 ± 0.0179	0.3735 ± 0.0114
	5	1.29 ± 0.04	0.5533 ± 0.0273	1.5168 ± 0.0108	0.3544 ± 0.0186
	10	1.16 ± 0.05	0.3864 ± 0.0131	1.4043 ± 0.0073	0.2752 ± 0.0079
D.FG-	1	1.99 ± 0.08	1.1351 ± 0.0065	1.8014 ± 0.0016	0.6383 ± 0.0093
	2	1.86 ± 0.08	0.9585 ± 0.0255	1.7580 ± 0.0114	0.5453 ± 0.0181
	3	1.79 ± 0.05	0.8056 ± 0.0091	1.6898 ± 0.0293	0.5203 ± 0.1047
	5	1.70 ± 0.03	0.8150 ± 0.0134	1.7186 ± 0.0318	0.5745 ± 0.0164
	10	1.53 ± 0.04	0.5666 ± 0.0164	1.5385 ± 0.0357	0.3683 ± 0.0026
D.UBC-	1	1.70 ± 0.06	1.0742 ± 0.0510	1.5547 ± 0.0751	0.7246 ± 0.0319
	2	1.64 ± 0.06	0.9446 ± 0.0073	1.7715 ± 0.0411	0.5336 ± 0.0164
	3	1.77 ± 0.05	0.7761 ± 0.0291	1.6812 ± 0.0466	0.4624 ± 0.0231
	5	1.64 ± 0.04	0.7012 ± 0.0097	1.6448 ± 0.0090	0.4263 ± 0.0037
	10	1.24 ± 0.05	0.6841 ± 0.0320	1.5549 ± 0.0353	0.3597 ± 0.0158
C.FG-	1	1.25 ± 0.05	0.5222 ± 0.0038	1.5815 ± 0.0166	0.3302 ± 0.0058
	2	1.20 ± 0.04	0.4568 ± 0.0074	1.5125 ± 0.0102	0.2999 ± 0.0066
	3	1.05 ± 0.08	0.3306 ± 0.0069	1.5235 ± 0.0583	0.2194 ± 0.0008
	5	1.06 ± 0.05	0.4154 ± 0.0190	1.5079 ± 0.0145	0.2754 ± 0.0099
	10	1.11 ± 0.04	0.4444 ± 0.0212	1.4302 ± 0.0167	0.2903 ± 0.0135
C.UBC-	1	1.50 ± 0.04	0.6539 ± 0.0239	1.6092 ± 0.0230	0.4064 ± 0.0150
	2	1.41 ± 0.04	0.3829 ± 0.0191	1.5076 ± 0.0173	0.2542 ± 0.0218
	3	1.11 ± 0.05	0.4443 ± 0.0076	1.5359 ± 0.0096	0.2892 ± 0.0032
	5	0.95 ± 0.04	0.4217 ± 0.0205	1.5390 ± 0.0103	0.2741 ± 0.0132
	10	1.08 ± 0.05	0.3265 ± 0.0150	1.4678 ± 0.0558	0.2220 ± 0.0113
FF.FG-	1	1.98 ± 0.05	1.0599 ± 0.0528	1.8263 ± 0.0520	0.5892 ± 0.0288
	2	1.96 ± 0.04	0.9873 ± 0.0130	1.7583 ± 0.0226	0.5643 ± 0.0024
	3	1.75 ± 0.01	0.8694 ± 0.0134	1.6577 ± 0.0717	0.5250 ± 0.0147
	5	1.47 ± 0.05	0.7647 ± 0.0071	1.6716 ± 0.0445	0.4577 ± 0.0112
	10	1.15 ± 0.02	0.6655 ± 0.0178	1.5719 ± 0.0540	0.3564 ± 0.0094
FF.UBC-	1	1.95 ± 0.11	1.3399 ± 0.0153	1.8743 ± 0.0613	0.7152 ± 0.0152
	2	1.99 ± 0.04	1.2267 ± 0.0531	1.7256 ± 0.0564	0.7127 ± 0.0656
	3	1.82 ± 0.04	1.2116 ± 0.0126	1.8506 ± 0.0628	0.6551 ± 0.0155
	5	1.80 ± 0.04	1.1462 ± 0.0245	1.8472 ± 0.0090	0.6197 ± 0.0168
	10	1.71 ± 0.05	1.0018 ± 0.0119	1.8159 ± 0.0154	0.5700 ± 0.0452

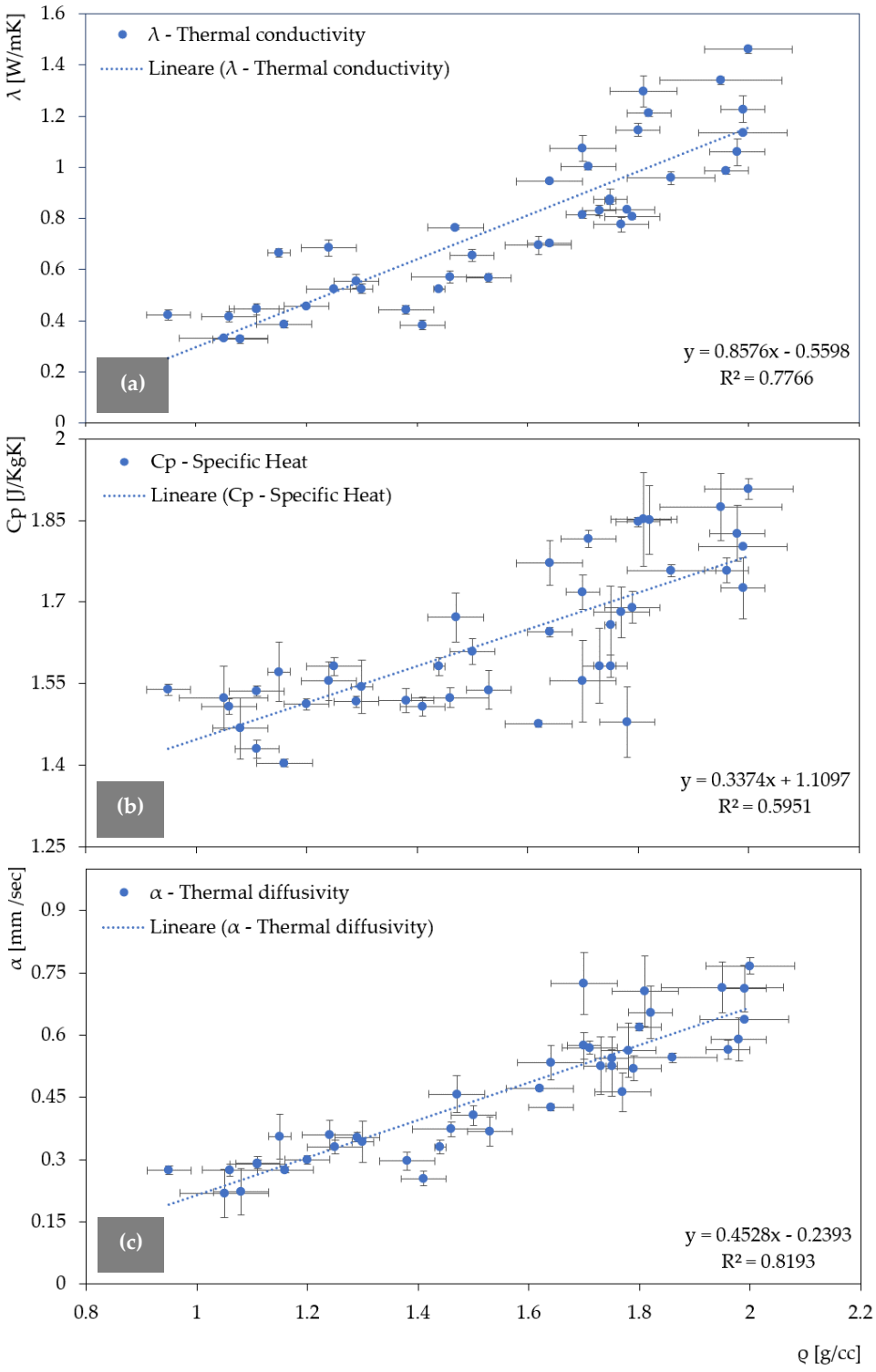

Figure 41. Thermal conductivity **(a)**, specific heat **(b),** and thermal diffusivity **(c)** versus density for all the obtained geopolymer foams.

The linear regression of λ with ρ shows a R^2 of 0.7766 (Figure 41a), so the thermal conductivity depends on the density of the geopolymers. Moreover, also C_p (Figure 41b) and α (Figure 41c) are strongly related to the density with R^2 of 0.5951 and 0.8193, respectively. For low densities, the porosity of the GFs increases, and consequently λ, C_p and α significantly decreases. Definitively, the lower densities of these materials are a great advantage compared to the traditional building materials such as Portland cement. They are lightweight

materials, and the thermal insulation properties are better performed. λ, C_p and α decrease by adding the industrial by-products which act as foaming agents.

REF-1 and REF-2, with a density of 1.81 ± 0.06, and 2 ± 0.08 g/cc show a λ of 1.2981 ± 0.0606, and 1.4607 ± 0.0167 W/mK, a C_p of 1.8518 ± 0.0855, and 1.9078 ± 0.0194 J/KgK, an α of 0.7056 ± 0.0295, and 0.7667 ± 0.0124 mm^2/sec, respectively. The higher values in the REF-2 are due to the chopped carbon fibers (CFs), which improve the mechanical properties, but on the other hand, increase the thermal properties by around 5-10%.

The densities of the GFs decrease because of the foaming agents and range from 0.95 ± 0.04 g/cc (C.UBC-5) up to 1.99 ± 0.08 g/cc (D.FG-1). The lowest thermal conductivity (Tab 11) was measured with the industrial by-products C.FG and C.UBC from the dust abatement collectors (cyclones). The geopolymer foam C.FG-3 (Figure 42a) recorded a thermal conductivity of 0.3306 ± 0.0069 W/mK and a density of 1.05 ± 0.08 g/cc. C.UBC-10 (Figure 42b) has an even lower λ of 0.3265 ± 0.0150 W/mK, and a density of 1.08 ± 0.05 g/cc.

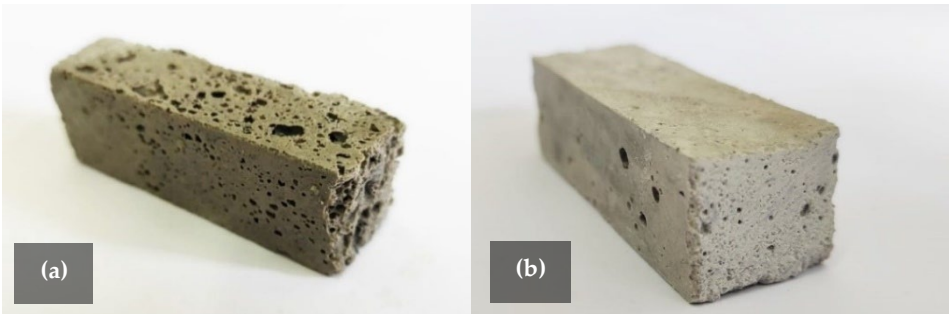

Figure 42. C.FG-3 **(a)** and C.UBC-10 (**b**) represent the GFs characterized by the lowest thermal conductivity.

4.3 Classification of GFs

The GFs were classified into six groups following the physical parameter of density versus compressive strength and thermal conductivity (Figure 43) to highlight which material has the best thermal insulation and mechanical properties.

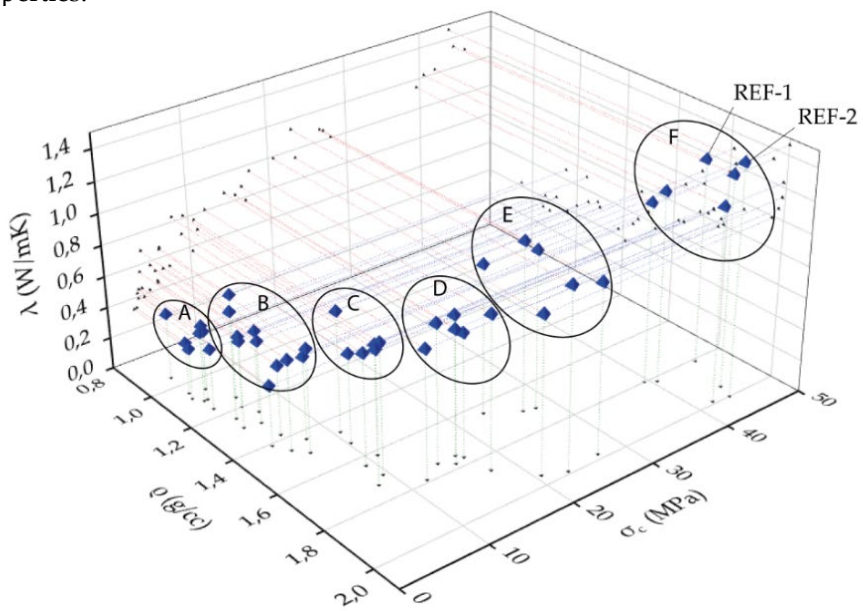

Figure 43. 3D scatter plot of the density (ρ), compressive strength (σ_c) and thermal conductivity (λ) of the geopolymer foams (GFs).

Group A shows the lowest thermal conductivity values and the lowest densities from 0.95 to 1.16 g/cc. This population of data shows relatively low σ_c ranging between 2.96 and 4.05 MPa. Group B has relatively higher densities than group A and, consequently, higher thermal conductivities. The compressive strengths are slightly higher, with an average value of around 5 MPa. Group C is characterized by σ_c at around 10 MPa and λ which corresponds to 0.7 W/mK. The compressive strength of Group D range between 10 and 20 MPa, with thermal conductivity with an average value of 0.9 W/mK and a mean density of around 1.8 g/cc. Group E (density between 1.6 and 2 g/cc) is between 20 and 30 MPa for the compressive strength, with thermal conductivity of 1.1 W/mK. Finally, group F exhibits similar performance to the reference standard geopolymers (REF-1 and REF-2) concerning mechanical and thermal properties due to its higher density. The group F population shows a density between 1.8 and 2.0 g/cc, a mean λ of 1.3 W/mK, and mean σ_c of around 42 MPa.

CHAPTER 5
CONCLUSIONS

5.1 General Conclusion and Perspectives

The investigated industrial by-products from the beverage cans and domestic appliances recycling treatments in secondary aluminum production are generally classified by EU law as solid wastes containing dangerous substances that can potentially develop flammable gases and explosive mixtures. This hazard mainly comes from the metallic aluminum still present in these by-products, which are highly reactive in water-rich environments, facilitating hydrogen-rich gas production. The different experimental phases will therefore have as requirements: (i) the enhancement, recovery, and reuse of products and processing residues of the aluminum industry, (ii) the definition of the chemical reactions and dynamics for which it is possible to synthesize the new materials subjecting them simultaneously to chemical neutralization processes, (iii) experimentation for improvement in terms of physical performance of geopolymer foams.

The experiments in the mini-reactor between by-products and aqueous alkaline solutions at pH 11 determined the composition of the hydrogen-rich gas (up to 96% of the total gases) and the oxidation rate, leading to the elimination of the highly reactive (and dangerous) metallic aluminum. Although only four experimental runs were carried out (at a constant solid-aqueous alkaline solution mass ratio of 1.27), the results clearly emphasize the efficiency of transforming the by-products into non-reactive material. However, further laboratory investigations should be addressed to fit the various physical conditions (solid grain size, pH, temperature, stirring speed, and time), only partially controlled.

In the framework of a circular economy and sustainability, we believe the metallic aluminum-rich by-products could potentially become a new secondary raw material resource addressed to the energetic (i.e., hydrogen as fuel) or non-energetic (e.g., “geopolymer foams”) use. The secondary aluminum industry must increase workplace safety by reducing the risks of storing metallic aluminum-rich hazardous by-products. In this way, it will be of paramount importance that the knowledge acquired from the chemical process of neutralization performed in the mini-reactor could be deepened further and, finally, transferred from the laboratory to the prototyping and industrialization phases.

The final geopolymer foams are mainly low-density materials with good physical performances. The research investigates the physical properties of GFs through mechanical (flexural, compressive, Charpy impact strengths) and thermal measurements (thermal conductivity, specific heat, thermal diffusivity). We demonstrated that the industrial by-products collected from the secondary aluminum industry could modify the structure of the reference REF-1, REF-2, which does not contain foaming agents. In particular, the work proved that FF.UBC is the most suitable material for improving mechanical properties compared to REF-1 and REF-2, and it is an appropriate raw material to foam lightweight geopolymers. However, significant decreases in thermal conductivity, specific heat, and thermal diffusivity are observable in the GFs using the waste materials C.FG and C.UBC.

5.2 Recommendations for Future Works

The valorization of raw materials from the secondary aluminum industry can be achieved through their use as fillers for alkali-activated binders such as geopolymers. Moreover, designing new materials or procedures for large-scale deployment demands a conspicuous supply and repeatability with a standard binder formulation. Several types of research explaining the principles for re-using industrial by-products have already been performed [148-166]. The production of geopolymers based on a considerable volume of waste need standard-performance concrete to encourage their usage in a functional and fruitful context. Environment and cost benefits can emerge from using specific industrial by-products, avoiding the disposal of materials in the landfill [167].

The evaluation of new resource use mechanisms leads to the development of solutions, increasing awareness of the organization of a new strategic industrial plan and waste management at a regional and national level by creating an Industry 4.0 with technologies new and innovation. Furthermore, the purpose of the research is closely related to environmental sustainability and the socio-economic growth of the Marche region. As previously discussed, the Marche Foundation cluster has the prerogative of identifying the strategic sectors in which funds for research and development should be invested to increase innovation.

The study led to the publication of relevant scientific articles: (**i**) "Hydrogen-Rich Gas Produced by the Chemical Neutralization of Reactive By-Products from the Screening Processes of the Secondary Aluminum Industry" in Sustainability Journal [168], (**ii**) "Low-Density Geopolymer Composites for the Construction Industry" in Polymers Journal [169], and (**iii**) "Mechanical and Thermal Properties of Geopolymer Foams (GFs) Doped with By-Products of the Secondary Aluminum Industry" in Polymers Journal [170]. It revealed that using geopolymer foams as an alternative material for the construction industry finds an intelligent compromise to balance the physical properties and guarantee the usability of the composite materials. Such properties include mechanical, thermal, and chemical resistance and toxic substances encapsulation, leading these materials over traditional products. For this reason, future studies will focus on mixing the three industrial by-products (FF.UBC, C.FG, C.UBC), trying to improve the physical properties to keep the mechanical performance unvaried and lower the thermal properties.

Finally, implementing these studies on the chemical neutralization of the industrial by-products will see a possible collaboration with Profilglass SpA in the recovery and use of hydrogen as a secondary energy source for the energy sustenance of the plants.

REFERENCES

1. Ramesh, G. Geopolymer Concrete: A review. IJSE 2021, PP: 5-8, Volume-1 Issue-2.
2. Swagato Das; Purna Saha; Swatee Prajna Jena; Pratyush Panda. Geopolymer concrete: Sustainable green concrete for reduced greenhouse gas emission – A review. Materials Today: Proceedings 2021.
3. Leandro B. de Oliveira; Afonso R.G. de Azevedo; Markssuel T.Marvila; Elaine C. Pereira; Roman Fediuk; Carlos Mauricio F. Vieira. Durability of geopolymers with industrial waste. Case Studies in Construction Materials Volume 16, June 2022, e00839.
4. Kiran Kumar Poloju. Geopolymer Concrete 2021, Advanced Materials and Sustainability in Civil Engineering pp 43-51.
5. Ahmad L.Almutairi; Bassam A.Tayeh; Adeyemi Adesina; Haytham F.Isleem; Abdullah M.Zeyad. Potential applications of geopolymer concrete in construction: A review. Case Studies in Construction Materials, Volume 15, December 2021, e00733.
6. Furqan Farooq; JinXin; Muhammad Faisal Javed; Arslan Akbar; Muhammad Izhar Shah; FahidAslam; RayedAlyousef. Geopolymer concrete as sustainable material: A state of the art review. Construction and Building Materials, Volume 306, 1 November 2021, 124762.
7. Srividya T.; Kannan Rajkumar P.R.Sivasakthi M.; Sujitha A.; Jeyalakshmi R. A state-of-the-art on development of geopolymer concrete and its field applications. Case Studies in Construction Materials. Volume 16, June 2022, e00812.
8. Hengels Castillo, Humberto Collado, Thomas Droguett, Mario Vesely, Pamela Garrido and Sergio Palma. State of the art of geopolymers: A review. e-Polymers 2022, https://doi.org/10.1515/epoly-2022-0015.
9. UNI. Available online: https://store.uni.com/catalogo/uni-en-13657:2004 (accessed on 31 January 2022).
10. UNI. Available online: https://store.uni.com/catalogo/uni-en-iso-11885-2009 (accessed on 31 January 2022).
11. International Minerals Statistics and Information (USGS). Available online: https://www.usgs.gov/energy-and-minerals/mineral-resources-program (accessed on 31 January 2022).
12. International aluminum. Available online: https://international-aluminium.org/statistics/primary-aluminium-production/ (accessed on 31 January 2022).
13. Totten G. E.; MacKenzie D.S. Handbook of Aluminum: Vol. 1. Physical Metallurgy and processes. Marcel Dekker, Inc: New York, NY, USA, 2003.
14. Nappi C. The Global Aluminium Industry 40 years from 1972, London, UK, 2013.
15. Donaldson D.J. Energy Savings in the Bayer Process. JOM 2013, 33 (9), 37-41.
16. Kondoh K.; Kosuge T.; Takeda Y. Lubrication Pump Made of Rapidly Solidiced Aluminum Alloy for High Performance Engine. SAE International Congress and Exposition, Detroit, MI, USA, 1990.
17. Reverdy M.; Potocnik V. History of Inventions and Innovations for Aluminum Production. TMS 2020 149th Annual Meeting & Exhibition Supplemental Proceedings, 2020.
18. Gesing A.; Wolanski R. Recycling Light Metals from End-of-Life Vehicles. JOM 2001, 53 (11), 21-23.
19. Wrigley A. Aluminum in Family Vehicles; The Recent History and a Forecast, Powder Metallurgy Aluminum and Light Alloys for Automotive Applications Conference, Troy, MI, 1998, pp. 135-145.
20. European standards. Accessed online: https://www.en-standard.eu/bs-en-12258-1-2012-aluminium-and-aluminium-alloys-terms-and-definitions-general-terms/ (accessed on 31 January 2022).
21. UNI. Accessed online: https://store.uni.com/catalogo/uni-en-13980-2004 (accessed on 31 January 2022).
22. Rabah, M. Preparation of aluminium-magnesium alloys and some valuable salts from used beverage cans. Waste Manag. 2003, 23, 173–182.
23. Boin, U.M.J.; Bertram, M. Melting standardized aluminum scrap: A mass balance model for europe. JOM 2005, 57, 26–33.
24. Blomberg, J.; Söderholm, P. The economics of secondary aluminium supply: An econometric analysis based on European data. Resour. Conserv. Recycl. 2009, 53, 455–463.
25. Green, J.A. Aluminum Recycling and Processing for Energy Conservationa and Sustainability; Green, J.P., Ed.; ASM International: Novelty, OH, USA, 2007; p. 220.
26. Antrekowitsch, H.; Hanko, G.; Ebner, P. Recycling of different types of magnesium scrap. In Magnesium Technology, 1st ed.; Kaplan, H.I., Ed.; TMS: Pittsburgh, PA, USA, 2002; pp. 43–48.
27. Totten, G.E.; MacKenzie, D.S. Physical Metallurgy and Processes. In Handbook of Aluminum, 1st ed.; CRC Press: New York, NY, USA, 2003; Volume 1, pp. 1–33.
28. Metson, J. Production of Alumina. In Fundamentals of Aluminum Metallurgy, 1st ed.; Lumley, R., Ed.; Woodhead Publishing: Cambridge, UK, 2011; pp. 23–28.
29. Kvande, H. Production, Processing and Applications. In Fundamentals of Aluminum Metallurgy; Lumley, R., Ed.; Woodhead Publishing: Cambridge, UK, 2011; pp. 49–69.

30. Žibret, G.; Teran, K.; Žibret, L.; Šter, K.; Dolenec, S. Building of the Al-Containing Secondary Raw Materials Registry for the Production of Low CO2 Mineral Binders in South-Eastern European Region. Sustainability 2021, 13, 1535.
31. Choate, W.T.; Green, J.A.S. U.S. Energy Requirements for Aluminum Production: Historical Perspective, Theoretical Limits and Current Practices; Energy Efficiency and Renewable Energy, U.S. Department of Energy: Washington, DC, USA, 2007.
32. Capuzzi, S.; Timelli, G. Preparation and Melting of Scrap in Aluminum Recycling: A Review. Metals 2018, 8, 249.
33. Padamata, S.K.; Yasinskiy, A.; Poliakov, P.A. Review of Secondary Aluminum Production and its Byproducts. JOM 2021, 73, 9. https://doi.org/10.1007/s11837-021-04802-y.
34. Bell, S.; Davis, B.; Javaid, A.; Essadiqi, E. Final Report on Scrap Management, Sorting and Classification of Aluminum. In Natural Resources Canada Report; 2003; Volume 22.
35. Smith, Y.R.; Nagel, J.R.; Rajamani, R.K. Eddy current separation for recovery of non-ferrous metallic particles: A comprehensive review. Miner. Eng. 2019, 133, 149–159.
36. Schlesinger, M.E. Aluminum Recycling, 1st ed.; CRC Press: Boca Raton, FL, USA, 2007; pp. 63–65, 71–75.
37. Mesina, M.B.; De Jong, T.P.R.; Dalmijn, W.L. Improvements in separation of non-ferrous scrap metals using an electromagnetic sensor. Phys. Sep. Sci. Eng. 2003, 12, 87–101.
38. Coates, G.; Rahimifard, S. Modelling of post-fragmentation waste stream processing within UK shredder facilities. Waste Manag. 2009, 29, 44–53.
39. Rao B.V.; Kapur P.C.; Konnur R. Modeling the size–density partition surface of dense-medium separators. Int. J. Miner. Process. 2003, 72, 443–453.
40. Kvithyld, A.; Meskers, C.E.M.; Gaal, S.; Reuter, M.; Engh, T.A. Recycling light metals: Optimal thermal de-coating. JOM 2008, 60, 47–51.
41. Utigard, T.A.; Friesen, K.; Roy, R.R.; Lim, J.; Silny, A.; Dupuis, C. The Properties and Uses of Fluxes in Molten Aluminum Processing. JOM 1998, 50, 38–43.
42. Velasco, E.; Nino, J. Recycling of aluminium scrap for secondary Al-Si alloys. Waste Manag. Res. 2011, 29, 686–693.
43. Wallace, G. Production of secondary aluminium. In Fundamentals of Aluminium Metallurgy; Woodhead Publishing: Sawston, UK, 2011; pp. 70–82.
44. Wallace, G. Production of secondary aluminium. In Fundamentals of Aluminium Metallurgy; Woodhead Publishing: Sawston, UK, 2011; pp. 70–82.
45. Blomberg, J.; Söderholm, P. The economics of secondary aluminium supply: An econometric analysis based on European data. Resour. Conserv. Recycl. 2009, 53, 455–463.
46. Green, J.A. Aluminum Recycling and Processing for Energy Conservationa and Sustainability; Green, J.P., Ed.; ASM International: Novelty, OH, USA, 2007; p. 220.
47. Katarzyna, B., Le, C. H., Louda, P., Michał, S., Bakalova, T., Tadeusz, P., & Prałat, K. The Fabrication of Geopolymer Foam Composites Incorporating Coke Dust Waste. Processes, 2020, 8(9), 1052.
48. Available online: http://www.geopolymer.org/ (accessed on 10 March 2021).
49. Sheppard, L.M., Geopolymer Composites: A Ceramics Alternative to Polymer Matrices, 2005. Available online: http://composite.about.com/ (accessed on 10 March 2021).
50. Kiran Kumar Poloju. Geopolymer Concrete. I n book: Advanced Materials and Sustainability in Civil Engineering, 2022. DOI: 10.1007/978-981-16-5949-2_9.
51. Gustavo Arcones-Pascual; Francisco Hernández Olivares; Alberto Sepulcre Aguilar. Old Kingdom Pyramids, constructive hypothesis with geopolymers: a brief review. Conference: Vitrogeowastes. Vitrification and Geopolymerization of Wastes for Immobilization or Recycling, 2017.
52. Daher Sayfeddine. Realization of Davidovits theory on pyramid construction using mobile laser robot. November 2018 IOP Conference Series Earth and Environmental Science 194(2):022030. DOI: 10.1088/1755-1315/194/2/022030.
53. Joseph Davidovits. Why the pharaohs built the Pyramids with fake stones. Edition: 2009 (hard cover), revised edition 2017 (soft cover) Publisher: Institut Géopolymère, Geopolymer Institute, Saint-Quentin, France.
54. Joseph Davidovits; Luis E. Huaman; Ralph Davidovits. Ancient geopolymer in south-American monument. SEM and petrographic evidence, 2018. Materials Letters 235((2019)):120-124. DOI: 10.1016/j.matlet.2018.10.033.
55. Joseph Davidovits; Luis E. Huaman; Ralph Davidovits. Ancient organo-mineral geopolymer in South-American Monuments: Organic matter in andesite stone. SEM and petrographic evidence. April 2019, Ceramics International 45:7385-7389. DOI: 10.1016/j.ceramint.2019.01.024.
56. Joseph Davidovits. SYNTHESIS OF NEW HIGH-TEMPERATURE GEO-POLYMERS FOR REINFORCED PLASTICS/COMPOSITES. Conference: PACTEC '79 Society of Plastics Engineers At: Costa Mesa, California, USA. Volume: Proceedings, pp. 151-154.

57. Joseph Davidovits; Luis E. Huaman; Ralph Davidovits. Tiahuanaco monuments (Tiwanaku / Pumapunku) in Bolivia are made of geopolymer artificial stones created 1400 years ago. Conference: Geopolymer Camp 2018. At: Campus Universitaire, Saint-Quentin, France. DOI: 10.13140/RG.2.2.31223.16800.
58. Joseph Davidovits. Geopolymers: Inorganic Polymeric New Materials. August 1991Journal of Thermal Analysis and Calorimetry 37(8):1633-1656. DOI: 10.1007/BF01912193.
59. Joseph Davidovits. Geopolymer cement to minimize carbon-dioxde greenhouse-warming. April 1993, Ceramic Transactions 37(1):165-182.
60. Cecílie Mizerová; Ivo Kusák; Pavel Rovnanik; Patrik Bayer. Conductive Metakaolin Geopolymer with Steel Microfibres. July 2021, Diffusion and Defect Data Pt.B: Solid State Phenomena 321:59-64. DOI: 10.4028/www.scientific.net/SSP.321.59.
61. John Provis; S.L. Yong; Peter Duxson. Nanostructure/microstructure of metakaolin geopolymers. In book: Geopolymers, 2009. DOI: 10.1533/9781845696382.1.72.
62. Alexey Manaenkov; Michaela Steinerova; Ekaterina Kukleva. Effect of Kaolin Addition into Metakaolin Geopolymer Composite. January 2021, Journal of Materials in Civil Engineering 33(1):06020022. DOI: 10.1061/(ASCE)MT.1943-5533.0003498.
63. Xu Chen; Andre Sutrisno; Lingyang Zhu; Leslie J. Struble. Setting and nanostructural evolution of metakaolin geopolymer. March 2017, Journal of the American Ceramic Society 100(9). DOI: 10.1111/jace.14641.
64. Alexey Manaenkov; Michaela Steinerova; Ekaterina Kukleva; Jiri Litos. EFFECT OF KAOLIN ADDITION INTO METAKAOLIN GEOPOLYMER COMPOSITE. April 2020, Stavební obzor - Civil Engineering Journal 29(1):1-9. DOI: 10.14311/CEJ.2020.01.0001.
65. Nur Ain Jaya; Liew Yun Ming; Mohd Mustafa Al Bakri Abdullah; Heah Cheng Yong. Porous Metakaolin Geopolymers with Tailored Thermal Conductivity. August 2019, IOP Conference Series Materials Science and Engineering 551(1):012088. DOI: 10.1088/1757-899X/551/1/012088.
66. ARR., Kalaiyarrasi; P., Partheeban. Mechanical and Micro Structural Properties of Metakaolin Geopolymer. June 2019, Emerging Materials Research 8(2):1-11. DOI: 10.1680/jemmr.17.00019.
67. A. Buchwald; Mónica Vicent Cabedo; Ralf Kriegel; Christian Kaps; Maria Monzó ; ; Antonio Barba. Geopolymeric binders with different fine fillers — Phase transformations at high temperatures. September 2009, Applied Clay Science 46(2):190-195. DOI: 10.1016/j.clay.2009.08.002.
68. A. Elimbi; Herve Tchakoute Kouamo; Daniel Njopwouo. Effects of calcination temperature of kaolinite clays on the properties of geopolymer cements. June 2011, Construction and Building Materials 25(6):2805-2812. DOI: 10.1016/j.conbuildmat.2010.12.055.
69. Yanru Wang; Yubin Cao; Zuhua Zhang; Jizhong Huang; Peng Zhang; Yuwei Ma; Hao Wang. Study of acidic degradation of alkali-activated materials using synthetic C-(N)-A-S-H and N-A-S-H gels. November 2021, Composites Part B Engineering 230(10):109510. November 2021, Composites Part B Engineering 230(10):109510. DOI: 10.1016/j.compositesb.2021.109510.
70. Min Yang; Yanjin Zheng; Xing Li; Xiaojun Yang; Feng Rao; Lele Zhong. Durability of alkali-activated materials with different C-S-H and N-A-S-H gels in acid and alkaline environment. December 2021, Journal of Materials Research and Technology 16. DOI: 10.1016/j.jmrt.2021.12.031.
71. Rupert J. Myers; Susan A. Bernal; John Provis. A thermodynamic model for C-(N-)A-S-H gel: CNASH_ss. Derivation and validation. August 2014, Cement and Concrete Research 66:27-47. DOI: 10.1016/j.cemconres.2014.07.005.
72. Lauren Y Gómez-Zamorano; Magdalena Balonis; Bartu Erdemli; Narayanan Neithalath; Gaurav Sant. C-(N)-S-H and N-A-S-H gels: Compositions and solubility data at 25°C and 50°C. March 2017, Journal of the American Ceramic Society 100(6). DOI: 10.1111/jace.14715.
73. José Alexandre Linhares Junior; Afonso Rangel Garcez de Azevedo; Markssuel Teixeira Marvila; Silvio Rainho Teixeira; Roman Fediuk; Carlos Maurício Fontes Vieira. Influence of processing parameters variation on the development of geopolymeric ceramic blocks with calcined kaolinite clay. January 2022, Case Studies in Construction Materials 16(n. 3):e00897. DOI: 10.1016/j.cscm.2022.e00897.
74. Dechang Jia; Peigang He; Meirong Wang; Shu Yan. Geopolymerization Mechanism of Geopolymers. December 2020. In book: Geopolymer and Geopolymer Matrix Composites. DOI: 10.1007/978-981-15-9536-3_3.
75. Sevgi Özen; Burak Uzal. Effect of Characteristics of Natural Zeolites on their Geopolymerization. September 2021, Case Studies in Construction Materials 15(4):e00715. DOI: 10.1016/j.cscm.2021.e00715.
76. Andrzej Kolezynski; Magdalena Król; Mikołaj Żychowicz. The structure of geopolymers – Theoretical studies. March 2018, Journal of Molecular Structure 1163:465–471. DOI: 10.1016/j.molstruc.2018.03.033.
77. Zuhua Zhang; Xiao Yao; Huajun Zhu; Sudong Hua; Yue Chen. Activating process of geopolymer source material: Kaolinite. February 2009, Journal of Wuhan University of Technology-Mater Sci Ed 24(1):132-136. DOI: 10.1007/s11595-009-1132-6.

78. H. Shi; Xiaolu Guo; Ming Xia. Geopolymerization process during early age and its characterization. February 2015, Kuei Suan Jen Hsueh Pao/ Journal of the Chinese Ceramic Society 43(2):174-183. DOI: 10.14062/j.issn.0454-5648.2015.02.07.
79. Xiao Yao; Zuhua Zhang; Huajun Zhu; Yue Chen. Geopolymerization Process of Alkali-Metakaolinite Characterized by Isothermal Calorimetry. September 2009, Thermochimica Acta 493(1-2):49-54. DOI: 10.1016/j.tca.2009.04.002.
80. Natalija Janošević; Djoric-Veljkovic Snezana; Gordana A. Toplicic-Curcic; Jugoslav Karamarkovic. Properties of geopolymers. January 2018, Facta universitatis - series Architecture and Civil Engineering 16(1):45 – 56. DOI: 10.2298/FUACE161226004J.
81. Mohammad A Al-Ghouti; Mariam Khan; Mustafa S. Nasser; Khalid A Al-Saad; OON Ee Heng. Application of geopolymers synthesized from incinerated municipal solid waste ashes for the removal of cationic dye from water. November 2020, PLoS ONE 15(11):e0239095. DOI: 10.1371/journal.pone.0239095.
82. Markssuel Teixeira Marvila; Afonso Rangel Garcez de Azevedo; Carlos Maurício Fontes Vieira. Reaction mechanisms of alkali-activated materials Mecanismos de reação de materiais álcali ativados. April 2021, Revista IBRACON de Estruturas e Materiais 14(3):2021. DOI: 10.1590/S1983-41952021000300009.
83. Joseph Davidovits. Geopolymer chemistry and sustainable development. July 2005, Conference: Geopolymer Green Chemistry and Sustainable Development Solutions, Geopolymer 2005 Conference At: Saint-Quentin, France. Institut Géopolymère / Geopolymer Institute. Volume: Session 1, pp. 9-17.
84. Nikita Barik; Jyotirmoy Mishra. Geopolymer concrete for sustainable development: A brief review. March 2020, Conference: TEQIP-III Sponsored- National Conference on Recent Innovations in Science, Engineering and Management (RISEM-2K20) At: TempleCity Institute of Technology and Engineering (TITE), Barunei, Khurda, Odisha.
85. Lateef Assi; Kealy Carter; Edward W Deaver; Paul Ziehl. Review of availability of source materials for geopolymer/sustainable concrete. April 2020, Journal of Cleaner Production 263:121477. DOI: 10.1016/j.jclepro.2020.121477.
86. Antonella Petrillo; Ilenia Farina; Marta Travaglioni; Cinzia Salzano; Salvatore Puca; Antonio Ramondo; Renato Olivares; Luigi Cossentino; Raffaele Cioffi. Opportunities and future challenges of geopolymer mortars for sustainable development. Woodhead Publishing Series in Civil and Structural Engineering. 2022, Pages 661-686. DOI: 10.1016/b978-0-12-821730-6.00013-9.
87. Srividya Thiyagarajan; P.R. Kannan Rajkumar; Sivasakthi Murugesan; Sujitha Arumugam; Jeyalakshmi Ramaswamy. A state-of-the-art on development of geopolymer concrete and its field applications. November 2021, Case Studies in Construction Materials 16(1):e00812. DOI: 10.1016/j.cscm.2021.e00812.
88. Joseph Davidovits; Michel Davidovics. "Geopolymer: Ultra-High Temperature Tooling Material for the Manufacture of Advanced Composites". April 1991, Conference: 36th International SAMPE Symposium, SAMPE 1991 At: San Diego, USA, Volume: 36, Vol. 2, pp. 1939-1949.
89. Joseph Davidovits; L. Buzzi; P. Rocher; Domingo Gimeno; C. Marini; S. Tocco. Geopolymeric cement based on low cost geologic material, results from the European Research project GEOCISTEM. June 1999, Conference: 2nd International Conference GEOPOLYMERE '99 At: Saint-Quentin, France. Institut Géopolymère / Geopolymer Institute, Volume: Geopolymer '99 Proceedings, pp. 83-96.
90. Caijun Shi; Ana Fernández-Jiménez. Stabilization/Solidification of Hazardous and Radioactive Wastes with Alkali-Activated Cements. November 2006, Journal of Hazardous Materials 137(3):1656-63. DOI: 10.1016/j.jhazmat.2006.05.008.
91. Jannie S J Van Deventer; G. C. Lukey. A comparative study of kaolinite versus metakaolinite in fly ash based geopolymers containing immobilized metals. August 2010, Chemical Engineering Communications April 2004(4):531-549. DOI: 10.1080/00986440490277974.
92. Marzieh Hassanpour; Mehdi Hassanpour; Mohammadreza Rezaie; Eysa Salajegheh; Mohammad Rashed; Iqbal Faruque; Mayeen Uddin Khandaker; D.A.Bradley. Studies of the mechanical and neutron shielding features of concrete by incorporation of green additive materials: Experimental and numerical study. Radiation Physics and Chemistry Volume 191, February 2022, 109846. DOI: https://doi.org/10.1016/j.radphyschem.2021.109846.
93. Mauro Mitsuuchi Tashima; Lourdes Soriano; Jorge LUIS Akasaki; Vinicius N. Castaldelli; J. Monzo; Jordi Payá; M. V. Borrachero. Spent FCC Catalyst for Preparing Alkali-Activated Binders: An Opportunity for a High-Degree Valorization. March 2014, Key Engineering Materials 600:709-716. DOI: 10.4028/www.scientific.net/KEM.600.709.
94. Peter Duxson; S. W. Mallicoat; G. C. Lukey; Waltraud M. Kriven; Jannie S J Van Deventer. The Effect of Alkali and Si/Al Ratio on the Development of Mechanical Properties of Metakaolin-Based Geopolymers. January 2007, Colloids and Surfaces A Physicochemical and Engineering Aspects 292(1):8-20. DOI: 10.1016/j.colsurfa.2006.05.044.

95. Daniel Kong; Jay G. Sanjayan; Kwesi Sagoe-Crentsil. Comparative Performance of Geopolymers Made with Metakaolin and Fly Ash After Exposure to Elevated Temperatures. December 2007, Cement and Concrete Research 37(12):1583-1589. DOI: 10.1016/j.cemconres.2007.08.021.
96. Joseph Davidovits. Why Alkali-Activated Materials (AAM) are NOT Geopolymers?. November 2018, Conference: GEOPOLYMER-CAMP 2014, 2015, 2016, 2017.At: Saint-Quentin, France. Geopolymer Institute, Institut Géopolymère.
97. Parham Shoaei; Farshad Ameri; Misagh Karimzadeh; Erfan Atabakhsh; Seyed Alireza Zareei; Babak Behforouz. Difference between geopolymers and alkali-activated materials. Handbook of Sustainable Concrete and Industrial Waste Management Recycled and Artificial Aggregate, Innovative Eco-Friendly Binders, and Life Cycle Assessment Woodhead Publishing Series in Civil and Structural Engineering 2022, Pages 421-435. DOI: 10.1016/b978-0-12-821730-6.00018-8.
98. Aaron Richard Sakulich. Reinforced Geopolymer Composites for Enhanced Material Greenness and Durability. December 2011, Sustainable Cities and Society 1(4):195-210. DOI: 10.1016/j.scs.2011.07.009.
99. IEA. Available online: https://www.iea.org/reports/cement (accessed on 31 January 2022).
100. Bas J van Ruijven; Detlef P. van Vuuren; Willem Boskaljon; Maarten L. Neelis; Deger Saygin; Martin Kumar Patel. Long-term model-based projections of energy use and CO_2 emissions from the global steel and cement industries. September 2016, Resources Conservation and Recycling 112:15-36. DOI: 10.1016/j.resconrec.2016.04.016.
101. Zhu Liu; Philippe Ciais; Zhu Deng; Steven Joseph Davis; Bo Zheng; Yilong Wang; Duo Cui; Biqing Zhu; Xinyu Dou; Piyu Ke; Taochun Sun; Rui Guo; Haiwang Zhong; Olivier Boucher; François-Marie Bréon; Chenxi Lu; Runtao Guo; Jinjun Xue; Eulalie Boucher; Katsumasa Tanaka; Frédéric Chevallier. Carbon Monitor, a near-real-time daily dataset of global CO_2 emission from fossil fuel and cement production. Nature research, 2020. Scientific Data 7(1). DOI: 10.1038/s41597-020-00708-7.
102. S. Swaddiwudhipong; D. Chen; Min-Hong Zhang. Simulation of the exothermic hydration process of Portland cement. January 2002, Advances in Cement Research 14(2):61-69. DOI: 10.1680/adcr.2002.14.2.61.
103. Ying Ma; Jueshi Qian. Influence of alkali sulfates in clinker on the hydration and hardening of Portland cement. August 2018, Construction and Building Materials 180:351-363. DOI: 10.1016/j.conbuildmat.2018.05.196.
104. Delic Dejan; Stojadinović Stojanka. Examination of the System: "Clinker + Gypsum + Water" through the Method of Differential Thermal Analysis. January 1972, In book: Thermal Analysis DOI: 10.1007/978-3-0348-5775-8_51.
105. Neville, A.M. Properties-of-Concrete-AM 149. 1995, 4th Edition, Addison Wesley Longman Ltd., Essex.
106. I. G Richardson; G. W Groves. The structure of the calcium silicate hydrate phases present in hardened pastes of white Portland cement/blast-furnace slag blends. 1997, Journal of Materials Science volume 32, pages 4793–4802.
107. Birat, J.P. Origins, basics, resource and energy needs. In Sustainable Materials Science-Environmental Metallurgy; De Gruyter: Berlin, Germany, 2021. https://doi.org/10.1051/978-2-7598-2443-4.
108. Shkolnikov, E.I.; Zhuk, A.Z.; Vlaskin, M.S. Aluminum as energy carrier: Feasibility analysis and current technologies overview. Renew. Sustain. Energy Rev. 2011, 15, 4611–4623.
109. UNI. Available online: https://store.uni.com/catalogo/uni-en-14039-2005 (accessed on 31 January 2022).
110. EPA. Available online: https://www.epa.gov/sites/default/files/2015-12/documents/3580a.pdf (accessed on 31 January 2022).
111. EPA. https://www.epa.gov/sites/default/files/2015-12/documents/8015c.pdf (accessed on 31 January 2022).
112. Katharina Walbrück; Felicitas Maeting; Steffen Witzleben; Dietmar Stephan.Natural Fiber-Stabilized Geopolymer Foams-A Review. Materials 2020, 1(1):3198.
113. Ju Hak Lee; Suthee Wattanasiriwech; Darunee Wattanasiriwech. Preparation of Carbon Fiber Reinforced Metakaolin Based-Geopolymer Foams. Key Engineering Materials 2018, 766:19-27.
114. EUR-Lex. Available online: https://eur-lex.europa.eu/legal-content/EN/TXT/?uri=celex%3A32010L0075 (accessed on 31 January 2022).
115. European Parliament. Available online: https://www.europarl.europa.eu/RegData/etudes/etudes/join/2006/375865/IPOL-ENVI_ET(2006)375865_EN.pdf (accessed on 31 January 2022).
116. EUR-Lex. Available online: https://eur-lex.europa.eu/legal-content/en/TXT/?uri=CELEX%3A32008R1272 (accessed on 31 January 2022).
117. EUR-Lex. Available online: https://eur-lex.europa.eu/legal-content/IT/TXT/PDF/?uri=CELEX:32014R1357&from=DA (accessed on 31 January 2022).
118. Gazzetta Ufficiale. Available online: https://www.gazzettaufficiale.it/eli/id/2010/12/01/10A14538/sg (accessed on 31 January 2022).
119. Tuttocamere. Available online: https://www.tuttocamere.it/files/ambiente/2015_06_24.pdf (accessed on 31 January 2022).
120. Padamata, S.K.; Yasinskiy, A.; Poliakov, P.A. Review of Secondary Aluminum Production and its Byproducts. JOM 2021, 73, 9. https://doi.org/10.1007/s11837-021-04802-y.

121. Gasparini E., Tarantino S.C., Conti M., Beisuz R., Chigna P., Auricchio F., Riccardi M.P., Zema M. Geopolymers from low-T activated kaolin: Implications for the use of alunite-bearing raw materials. App. Clay Sci., 2015, 114, 530-539.
122. Clausi M., Tarantino S.C., Magnani L.L, Riccardi M.P., Tedeschi C., Zema M. Metakaolin as a precursor of materials for applications in Cultural Heritage: Geopolymer-based mortars with ornamental stone aggregates. App. Clay Sci., 2016, 132, 589-599.
123. Duxson P., Lukey G.C., Van De Venter, J.S.J., Mallicoat S.W., M.Kriven W. Microstructural Characterization of Metakaolin-based Geopolymers, Ceram. Trans., 2005, 165, 71-85.
124. "BAUCIS LK: ČLUZ a.s." https://www.cluz.cz/en/baucis-lk (accessed on 31 January 2022).
125. "Sklopísek Střeleč, a.s." https://glassand.eu/celkova-produkce/podle-druhu/technicke-pisky (accessed on 08 Janauary 2021) .
126. Kinga Korniejenko; Beata Figiela; Krzysztof Miernik; Celina Ziejewska; Joanna Marczyk; Marek Hebda; An Cheng; Wei-Ting Lin. Mechanical and Fracture Properties of Long Fiber Reinforced Geopolymer Composites. Materials 2021, 14(18):5183.
127. Katharina Walbrück; Felicitas Maeting; Steffen Witzleben; Dietmar Stephan.Natural Fiber-Stabilized Geopolymer Foams-A Review. Materials 2020, 1(1):3198.
128. Ju Hak Lee; Suthee Wattanasiriwech; Darunee Wattanasiriwech. Preparation of Carbon Fiber Reinforced Metakaolin Based-Geopolymer Foams. Key Engineering Materials 2018, 766:19-27.
129. V., Nguyen; S. Van; Louda, P.; Katarzyna, B.; Roberto, E.; Piotr, L. Enhancing geopolymer composites by recycled fibers. Geopolymer Institute: Saint-Quentin, France, 2021.
130. Dudek, E., Mosiadz, M., and Orzepowski, M. (2007). Uncertainties of resistors temperature coefficients. Meas. Sci. Rev., 7(3), 23–26. [35] Glinicki, M. A., Jaskulski, R., Pichór, W., Dąbrowski, M., and Sobczak, M. (2015). Investigation of thermal properties of shielding concrete., Proc. Int. Symp. Brittle Matrix Composites 9, Editors: Brandt A. M., Olek J., Gl.
131. Kušnerová, M., Valíček, J., Harničárová, M., Hryniewicz, T., Rokosz, K., Palková, Z., Václavík, V., Řepka, M., and Bendová, M. (2013). A proposal for simplifying the method of evaluation of uncertainties in measurement results. Meas. Sci. Rev., 13(1), 1–6.
132. Karol Prałat, Justyna Ciemnicka, Artur Koper, Katarzyna Buczkowska and Piotr Łoś, Comparison of the thermal properties of geopolymer and modified gypsum, Polym. J., – manuscript in reviews.
133. Prałat, K., Jaskulski, R., Ciemnicka, J., & Makomaski, G. Analysis of the thermal properties and structure of gypsum modified with cellulose based polymer and aerogels. Arch. Civ. Eng., 2020, 66(4).
134. Wang, C.-C.; Chou, Y.-C.; Yen, C.-Y. Hydrogen Generation from Aluminum and Aluminum Alloys Powder. Procedia Eng. 2012, 36, 105–113.
135. Hiraki, T.; Takeuchi, M.; Hisa, M.; Akiyama, T. Hydrogen Production from Waste Aluminum at Different Temperatures, with LCA. Mater. Trans. 2005, 46, 1052–1057.
136. Van Deventer, J.S.; Provis, J.L. Geopolymers: Structures, Processing, Properties and Industrial Applications; Woodhead Publishing: Sawston, UK, 2009.
137. Žibret, G.; Teran, K.; Žibret, L.; Šter, K.; Dolenec, S. Building of the Al-Containing Secondary Raw Materials Registry for the Production of Low CO_2 Mineral Binders in South-Eastern European Region. Sustainability 2021, 13, 1535.
138. Bureau of International Recycling (BIR). Available online: www.bir.org (accessed on 30 July 2021).
139. Koper, A., Prałat, K., Ciemnicka, J., & Buczkowska, K. Influence of the Calcination Temperature of Synthetic Gypsum on the Particle Size Distribution and Setting Time of Modified Building Materials. Energies, 2020, 13(21), 5759.
140. Prałat, K., & Krymarys, E. A particle size distribution measurements of selected building materials using laser diffraction method. Technical Transactions, 2018, 11(5), 95-108.
141. Katharina Walbrück; Lisabeth Drewler; Steffen Witzleben; Dietmar Stephan. Factors influencing thermal conductivity and compressive strength of natural fiber-reinforced geopolymer foams. Open ceramics 2021, (5).
142. Zehua Ji; Meng Li; Liya Su; Yuansheng Pei. Porosity, mechanical strength and structure of waste-based geopolymer foams by different stabilizing agents. Construction and Building Materials 2020, 258(14):119555.
143. Zuhua Zhang; Hao Wang. The Pore Characteristics of Geopolymer Foam Concrete and Their Impact on the Compressive Strength and Modulus. Frontiers in Materials 2016, 3.
144. Chengying Bai; Giorgia Franchin; Hamada Elsayed; Alessandro Zaggia; Lino Conte; Hongqiang Li; Paolo Colombo. High-porosity geopolymer foams with tailored porosity for thermal insulation and wastewater treatment. Journal of Materials Research 2017, 32(17):1-9.
145. Nur Ain Jaya; Liew Yun Ming; Heah Cheng Yong; Mohd Mustafa Al Bakri Abdullah; H. Kamarudin. Correlation between pore structure, compressive strength and thermal conductivity of porous metakaolin geopolymer. Construction and Building Materials 2020, 247:118641.

146. Prałat, K., M. Łukasiewicz, and P. Miczko. Experimental study of the basic mechanical properties of hardened gypsum paste modified with addition of polyoxymethylene micrograins. Arch. Civ. Eng., 2020, 66, no. 2.
147. Yusrina mat daud; Mohammad Firdaus Abu hashim; A.R. Rozyanty. Mechanical Properties of Geopolymer Filler in Polymer Composites. Mineral-Filled Polymer Composites 2021.
148. Sujitra Onutai; Sirithan Jiemsirilers; Shigetaka Wada; P. Thavorniti. Preparation and Characterization of Fly Ash and Aluminium Waste Geopolymer. April 2014; Key Engineering Materials 608:108-113; DOI: 10.4028/www.scientific.net/KEM.608.108.
149. Natalia Wielgus; Małgorzata Safuta. Numerical simulation of mechanical properties tests of tungsten mud waste geopolymer. 2018, Journal of Civil Engineering 13(s1):87-94. DOI: 10.1515/sspjce-2018-0008.
150. Obaid Mahmoodi; Hocine Siad; M. Lachemi; Sina Dadsetan; M. Sahmaran. Development of ceramic tile waste geopolymer binders based on pre-targeted chemical ratios and ambient curing. October 2020, Construction and Building Materials 258:120297. DOI: 10.1016/j.conbuildmat.2020.120297.
151. Dilan Polat; Mustafa Guden. Processing and characterization of geopolymer and sintered geopolymer foams of waste glass powders. September 2021, Construction and Building Materials 300(8):124259. DOI: 10.1016/j.conbuildmat.2021.124259.
152. Byoungkwan Kim; Juhyeok Lee; Jaehyuk Kang; Wooyong Um. Development of geopolymer waste form for immobilization of radioactive borate waste. October 2021, Journal of Hazardous Materials 419:126402. DOI: 10.1016/j.jhazmat.2021.126402.
153. Zhiyuan Shao; Jiaqing Wang; Yongheng Jiang; Jun Zang; Tiejun Wu; Fei Ma; Binbin Qian; Luming Wang; Yueyang Hu; Bing Ma.The performance of micropore-foamed geopolymers produced from industrial wastes. October 2021, Construction and Building Materials 304:124636. DOI: 10.1016/j.conbuildmat.2021.124636.
154. Eng-Rasha Al-husseiny; Shahlaa Ebrahim. Synthesis of geopolymer for the removal of hazardous waste: a review. June 2021, IOP Conference Series Earth and Environmental Science 779(1):012102. DOI: 10.1088/1755-1315/779/1/012102.
155. Barbara Kozub; Patrycja Bazan; Rihards Gailitis; Kinga Korniejenko; Dariusz Mierzwiński. Foamed Geopolymer Composites with the Addition of Glass Wool Waste. August 2021; Materials 14(17):4978. DOI: 10.3390/ma14174978.
156. Suresh Kumar; Muthiah Muthukannan; Kadarkarai Arunkumar; Arunasankar Chithambar Ganesh; Rangaswamy Kanniga Devi; Utilisation of waste glass powder to improve the performance of hazardous incinerated biomedical waste ash geopolymer concrete. February 2022, Innovative Infrastructure Solutions 7(1). DOI: 10.1007/s41062-021-00694-8.
157. Aissa Bouaissi; Boudaoud Mohamed; Aribi Chouaib Chouaib; Ammar yahia; Mohammed Saidi. Study of mechanical properties of geopolymer mortar based on metallurgical industrial waste. December 2021, Conference: First National Virtual Conference on Chemical Process and Environmental Engineering NVCCPEE 2021.
158. Ismail Luhar; Salmabanu Luhar. Valorization of geopolymer paste containing wastes glass. January 2021, Research on Engineering Structures and Materials. DOI: 10.17515/resm2020.240st1213.
159. Daniela Carolina Paz Gómez; Ines Vilarinho; Silvia M. Pérez-Moreno; João Carvalheiras; José Luis Guerrero Márquez; Rui M. Novais; Maria Paula Seabra; Guillermos Ríos; Juan Pedro Bolívar; J.A. Labrincha. Immobilization of Hazardous Wastes on One-Part Blast Furnace Slag-Based Geopolymers. December 2021, Sustainability 13(23):13455. DOI: 10.3390/su132313455.
160. Richa Singh; Sarwani Budarayavalasa. Solidification and stabilization of hazardous wastes using geopolymers as sustainable binders. June 2021, Journal of Material Cycles and Waste Management 23(3). DOI: 10.1007/s10163-021-01245-0.
161. Isabella Lancellotti; Chiara Ponzoni; Luisa Barbieri; Cristina Leonelli. Wastes materials in geopolymers. September 2015, In book: WASTES 2015 – Solutions, Treatments and Opportunities. DOI: 10.1201/b18853-21.
162. Wu-Jian Long; Lin Can; Taohua Ye; Biqin Dong; Feng Xing. Stabilization/solidification of hazardous lead glass by geopolymers. August 2021, Construction and Building Materials 294(21):123574. DOI: 10.1016/j.conbuildmat.2021.123574.
163. Sneha Sen; Purna Saha. The Performance of Geopolymer Concrete Utilizing Wastes as Binder. July 2020, In book: Recent Developments in Sustainable Infrastructure, Select Proceedings of ICRDSI 2019. DOI: 10.1007/978-981-15-4577-1_67.
164. Mahmoud Zawrah; H.A. Badr; Reham Khattab; Heba El-sayed Sadek; S.E. Abo Sawan; A.A. El-Kheshen. Fabrication and characterization of non-foamed and foamed geopolymers from industrial waste clays. July 2021, Ceramics International 47(10). DOI: 10.1016/j.ceramint.2021.07.097.
165. Abbas Mohajerani; David Suter; Tristan Jeffrey-Bailey; Tianyang Song; Arul Arulrajah; Suksun Horpibulsuk; David W. Law. Recycling waste materials in geopolymer concrete. April 2019, Clean Technologies and Environmental Policy 21(3). DOI: 10.1007/s10098-018-01660-2.

166. Elsa Paul. Performance assessment of geopolymer concrete using various industrial wastes. February 2021; Materials Today: Proceedings 45(62). DOI: 10.1016/j.matpr.2021.01.660.
167. Bernal, S.A., Rodriguez, E.D., Kirchheim, A.P.; John L. Provis. Management and valorisation of wastes through use in producing alkali-activated cement materials. 2016, Journal of Chemical Technology and Biotechnology, 91 (9). pp. 2365-2388. DOI: https://doi.org/10.1002/jctb.4927.
168. Ercoli, R.; Orlando, A; Borrini, D.; Tassi, F.; Bicocchi, G., Renzulli, A. Hydrogen-Rich Gas Produced by the Chemical Neutralization of Reactive By-Products from the Screening Processes of the Secondary Aluminum Industry. Sustainability 2021, 13,(31). DOI: 10.3390/su132112261.
169. Vu Nguyen; Le Van Su; Petr Louda; Michał Marek Szczypi ´nski; Roberto Ercoli; Ružek Vojtech; Piotr Łoś; Karol Prałat; Przemyslaw Plaskota; Tadeusz Pacyniak; Katarzyna Buczkowska. Low-Density Geopolymer Composites for the Construction Industry. 2022 Polymers 14(304). DOI: 10.3390/polym14020304.
170. Roberto Ercoli; Dorota Laskowska; Nguyen Vu Van; Le Van Su; Petr Louda; Piotr Ło´s; Justyna Ciemnicka; Karol Prałat; Alberto Renzulli; Eleonora Paris; Matteo Basilici; Cezary Rapiejko; Katarzyna Buczkowska. Mechanical and Thermal Properties of Geopolymer Foams (GFs) Doped with By-Products of the Secondary Aluminum Industry. 2022 Polymers 14(4):703. DOI: 10.3390/polym14040703.